C6 glioma neuronal interactions and their moderation by the tryptophan-kynurenine metabolism pathway

Trinity College Dublin
Coláiste na Tríonóide, Baile Átha Cliath
The University of Dublin

A dissertation submitted to The University of Dublin in the fulfilment of the requirement for the degree of
Master in Science in School of Pharmacy and Pharmaceutical Sciences

By

Yuliia Rakovets

Supervisor: Prof. Andrew Harkin

School of Pharmacy and Pharmaceutical Sciences – Faculty of Health Sciences, Trinity College Dublin,

Dublin, Ireland

Date of submission: 31/01/2021

Declaration

I declare that this thesis has not been submitted as an exercise for a degree at this or any other university and it is entirely my own work.

I agree to deposit this thesis in the University's open access institutional repository or allow the library to do so on my behalf, subject to Irish Copyright Legislation and Trinity College Library conditions of use and acknowledgement.

Signed	**Date**
Yuliia Rakovets	31/01/2021

Acknowledgements

First of all, I would like to thank my supervisor, Prof. Andrew Harkin, for giving me the opportunity to carry out my postgraduate research project in his lab. Your guidance and support in the past 18 months were invaluable for me.
I would also like to thank Prof. Mani Ramaswami for kindly allowing me to use his epifluorescent microscope. I am grateful to Kate O'Reilly, who patiently trained me when I started. You are always very helpful. I want to thank Luiza Dos Santos and Eduardo Ruiz-Hernandez for the passage of C6 cell line they provided.

Thanks to all of my colleagues at TCIN - Caoimhe, Sarah, Teresa, Guillaume, Aline and Sudharshana. I am fortunate to have had such a fantastic company.

I am eternally grateful to my parents Eduard and Iryna for taking that hard decision in November 2013. This would never have been possible without you.
I am very thankful to Prof. Ales Stuchlik from Czech Academy of Sciences for his continuous support. The experience I gained during my internship under your supervision shaped me as a person.
I also want to thank my dear friends – Nelia, Laura, Juraj, Enrico and Chiara, I miss you a lot.

I want to thank my fiancé Arda for his sincere support, encouragement, inspiration, love and understanding. This thesis is dedicated to you, our Bono and Efe.

Finally, I want to thank me for believing in me, being me and never giving up.

Abstract

Brain glia possess the rate limiting enzyme indoleamine 2, 3-dioxygenase (IDO) which catalyses the conversion of tryptophan to kynurenine. Microglia also express kynurenine monooxygenase (KMO) and kynureninase (KYNU) which lead to the production of the excitotoxin quinolinic acid and other free radical producing metabolites. Conversely astrocytic glia express kynurenine aminotransferase (KAT) which leads to the production of kynurenic acid (KYNA), which acts as an NMDA receptor antagonist and is reported to have neuroprotective properties. Previous investigations have confirmed that IFNγ-stimulated kynurenine pathway (KP) induction in microglia reduces neurite outgrowth and complexity, and that these alterations may be abrogated using pharmacological inhibitors of the KP. In this investigation these findings were extended by assessing a role for the KP in mediating changes associated with C6 glioma cells, a rat glioma cell line. Conditioned media (CM) from C6 cells was placed on mature primary cortical neurons for 24h. Neurons were fixed, and neurite outgrowth and complexity were assessed using fluorescent immunocytochemistry followed by Sholl analysis. Furthermore, the co-localised expression of synaptic proteins synaptophysin and the post synaptic density 95 (PSD-95) were determined. Results show increased mRNA expression of IDO in C6 cells compared to rat primary mixed glial cells. Conditioned media from C6 cells reduced neurite outgrowth and complexity and co-localised expression of synaptic markers with reductions in these parameters prevented when C6 cells were pre-treated with the IDO inhibitor, 1-methyltryptophan (1-MT) (L) (0.5mM) or when KYNA (0.3 µM) was co-applied directly to neurons. Furthermore, conditioned media from C6 glioma cells had no effect on neuronal viability yet altered microglial and astroglial morphology towards an activated state as observed by ionized calcium-binding adapter molecule 1 and glial fibrillary acidic protein immunoreactivity respectively; effects which were also partially rescued by prior treatment of C6 cells with 1-MT. Overall, this study indicates that inhibition of the KP in C6 cells may be targeted to protect against C6 glioma cell associated neuronal atrophy. Alternatively activating the neuroprotective branch of the KP by raising KYNA concentration may also provide protection from glioma-associated neuronal atrophy.

Table of contents

List of figures

List of tables

Abbreviations

CNS	Central Nervous system
IFNγ	Interferon gamma
BBB	Blood-brain barrier
ROS	Reactive oxygen species
AD	Alzheimer's disease
PD	Parkinson's disease
MS	Multiple sclerosis
ALS	Amyotrophic lateral sclerosis
TNFα	Tumor necrosis factor alpha
IL-1	Interleukin-1
IL-1β	Interleukin-1- β
STAT3	Signal transducer and activator of transcription 3
IL-6	Interleukin-6
IL-12	Interleukin-12
IL-23	Interleukin-23
MHC	Major histocompatibility complex
IFNγ-R	Interferon gamma receptor
NF-κB	Nuclear factor kappa B
JAK	Janus kinase
TLRs	Toll-like receptors
MYD88	Myeloid differentiation primary response 88
TIR	Toll/interleukin-1 receptor
TIRF	Toll/interleukin-1 receptor-domain-containing adapter-inducing interferon-β
IKK	IκB kinase
MAPK	Mitogen-activated protein kinase
AP-1	Activator protein 1
iNOS	Inducible nitric oxide synthase
COX-2	Cyclooxygenase-2
SH2	Src homology 2
NO	Nitric oxide
Tyr-705	Tyrosine-705
TGF-β	Transformig growth factor β
CM	Conditioned medium
GAM	Glioma associated macrophages
MCP	Monocyte chemoattractant protein
M-CSF	Macrophage colony-stimulating factor
GM-CSF	Granulocyte macrophage colony-stimulating factor
GBM	Glioblastoma
WHO	World Health Organization
NK	Natural killer
NKT	Natural killer T cell
APC	Antigen presenting cell
DC	Dendritic cell
TME	Tumor microenvironment
MRI	Magnetic resonance imaging
MRA	Magnetic resonance angiography
Rb	Retinoblastoma
EGFR	Epidermal growth factor receptor

IDH	Isocitrate dehydrogenase
PDX	Patient-derived xenografts
RT	Radiotherapy
PDMS	Polydimethylsiloxane
TMZ	Temozolomide
TRYP	Tryptophan
BCNU	Bis-chloroethylnitrosourea
NAD^+	Nicotinamide adenine dinucleotide
KP	Kynurenine pathway
IDO	Indoleamine-2,3-dioxygenase
TDO	Tryptophan-2,3-dioxygenase
L-KYN	L-Kynurenine
KYNA	Kynurenic acid
3HK	3-hydroxy-l-kynurenine
KAT	Kynurenine aminotransferase
KMO	Kynurenine-3-monooxygenase
KYNU	Kynureninase
3HAA	3-hydroxyanthranilic acid
QUIN	Quinolinic acid
NMDA	N-methyl-D-aspartate
AMPA	α-amino-3-hydroxy-5-methyl-4-isoxazolepropionic acid
1-MT	1-Methyltryptophan
dH_2O	Distilled water
EtOH	Ethanol
UV	Ultraviolet
NBM	Neurobasal medium
cNBM	Complete neurobasal medium
DMEM	Dulbecco's modified Eagle's medium
cDMEM	Complete dulbecco's modified Eagle's medium
PBS	Phosphate buffer saline
FBS	Fetal bovine serum
RPM	Rotations per minute
DIV	*Days in vitro*
P	Postnatal
CCK-8	Cell Counting Kit-8
WST-8	(5-(2,4-disulfophenyl)-3-(2-methoxy-4-nitrophenyl)-2-(4-nitrophenyl)-2H-tetrazolium)
PFA	Paraformaldehyde
NGS	Normal goat serum
BSA	Bovine serum albumin
PBS-T	PBS containing 0.1% Triton-X
MAP2	Microtubule-associated protein 2
DAPI	4´,6-Diamidino-2-phenylindole dihydrochloride
PSD-95	Post-synaptic density protein 95
Iba1	Ionized calcium binding adaptor molecule **1**
GFAP	Glial fibrillary acidic protein
CTCF	Corrected total cell fluorescence
qPCR	Quantitative polymerase chain reaction
RNA	Ribonucleic acid
MDB	Membrane desalting buffer
rDNase	Recombinant deoxyribonuclease

cDNA	Complementary deoxyribonucleic acid
RT	Reverse transcriptase
RT-PCR	Real-time polymerase chain reaction
MGB	Minor groove binding
GAPDH	Glyceraldehyde-3-phosphate dehydrogenase
ANOVA	Analyses of variance
IRF	Interferon regulatory factor

1 General Introduction

1.1 Cellular composition of the central nervous system (CNS)

The central nervous system (CNS) is a complex system, consisting of the brain and spinal cord that coordinates all bodily functions by receiving and combining information from the whole organism. Two main types of cells that are found in the CNS are called neurons and glia. Neurons are excitable cells that are specialized to transmit and communicate information throughout the body by both chemical and electrical means, while glia, being non-excitable cells, maintain homeostasis, and provide immunological protection and support to neurons overall.

1.1.1 Neurons

Neurons were first recognized as a principal structural and functional unit of the CNS in the late 19th century when the Spanish anatomist Santiago Ramón y Cajal described neuronal anatomy through a silver staining process [1].

Our brain is made up of 86 billion neurons [2], and the structure they configure is highly specialized to fulfil a wide range of functions. Although the anatomy of various types of neurons differs, they all share common features, including a distinctive cell body, dendrites, axon, and axon terminals [3]. Short though numerous dendritic branches serve to receive and integrate electrical signals, while the single axon is responsible for transmitting the information to other neurons [4]. Each neuron is linked with thousands of others at the specialized sites called synapses, allowing the formation of neural networks [5]. The synapse is composed of the presynaptic cleft, where the conversion of action potential to neurotransmitter release takes place, and the postsynaptic cleft, with specialized receptors that recognize the released transmitters that initiate new signals in the dendrites of adjacent neurons.

The main component of the neural cell body is the nucleus – the center of genetic expression of nearly all neural proteins. Some proteins can be synthesized in dendrites as well; however, proteo-synthesis cannot be found in axons. Followed by post-translational modifications, proteins are transported along the axon using cytoskeletal “tracks”. The three components of the neural cytoskeleton are microtubules, actin filaments and neurofilaments, and these play a key role in forming and maintaining neural morphology, polarity and function overall [4]. Since some of the axons can reach more than a meter in length, microtubule-associated transport of

proteins, organelles and vesicles down these axons is critical for neural growth, function and survival [6].

1.1.2 Microglia

Microglia are the resident innate immune cells of the CNS that represent 5-10% of the adult brain cell population [7]. They were first described by Pío del Río-Hortega in 1919, who recognized that ramified cells transform into an amoeboid form under certain conditions. While small in size, as the name *microglia* suggests, these cells have the ability to migrate and recognize sites of injury. They follow a multistage activation process. Microglia mediate active immune response, acting as macrophages scavenging within the CNS and clearing cellular debris, including damaged or dead neurons and infectious agents through phagocytosis [8,9].

There are two types of microglia in the normal brain: so-called ''resting'' microglia, although serving as fast sensor in the CNS [10], and ''activated'' microglia, that display inflammatory and phagocytic features [11]. Microglia in the resting state have a small cell body and occupy their own territory 15-30 µm wide. They scan the microenvironment, sense disturbance and elaborate further responses to maintain brain parenchyma homeostasis, which eventually triggers microglial activation [12]. In the resting condition, microglia have relatively low expression of receptors involved in immune response and show a minimal release of immunological factors such as cytokines [13].

Upon detection of injury/pathogen, microglia start a complex process of transformation to the amoeboid form. This modification involves a clear change in their ramified morphology to a round-shaped full phagocyte with two possible phenotypes: classically activated M1 state that produces pro-inflammatory mediators and alternatively activated M2 state that triggers an anti-inflammatory response [14–17] [Figure 1].

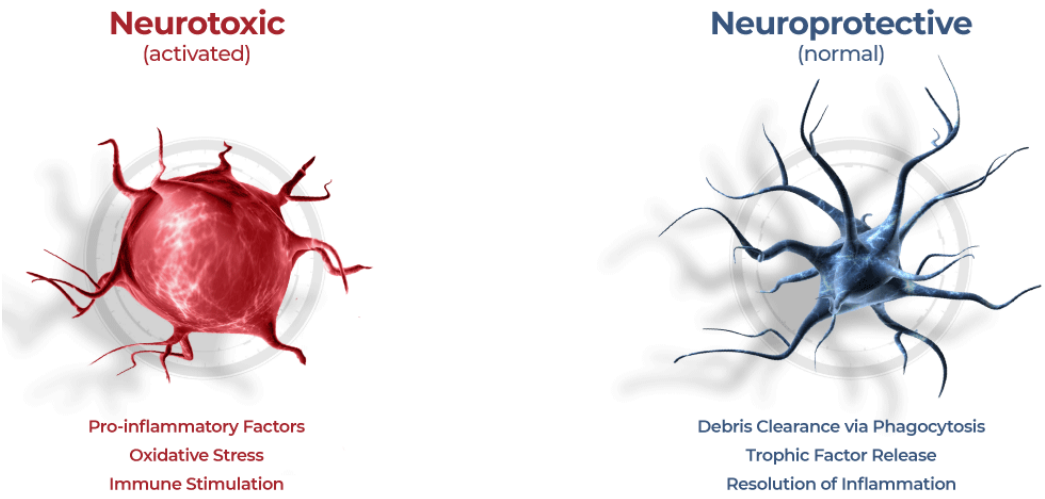

Figure 1: Difference in the morphology of neurotoxic (M1) and neuroprotective (M2) microglial activation states (from ospheris.com)

Functions of microglial cells in the CNS appear to be complex as they exhibit both neuroprotective and neurotoxic effects. The activation of microglia is overall beneficial for neural tissue if it proceeds in a controlled manner and for a short period of time. However dysregulated or excessive activation in the brain can induce neurotoxicity due to the sustained release of pro-inflammatory factors, chemokines, reactive oxygen and nitrogen species, glutamate and neurotoxic mediators that set off cycles of microglial-mediated neurodegeneration [18,19]. There is experimental evidence indicating that overactivated microglia are detrimental in a number of neuroinflammatory and degenerative brain disorders [20–22].

1.1.3 Astrocytes

Astrocytes are the most numerous specialized multifunctional neuroglial cells of the CNS. They play an important role in information processing as they have multiple contacts with neurons at synapses and are located near other CNS-resident cells (microglia, oligodendrocytes and other astrocytes) and blood vessels [23,24]. Astrocytes also provide trophic support to neural cells, establish the CNS boundaries and maintain the blood-brain barrier (BBB). Numerous studies also indicate that astroglial cells support extracellular homeostasis in coordination with microglia [25–27]. Astrocytes are active players in neuroinflammation and regulation of innate and adaptive immune response to neural tissue damage and are strategically located and capable of becoming reactive for this purpose. Their response can be beneficial by immunosuppression and

tissue repair or detrimental by inflammation and tissue damage, depending on the timing and the kind of inflammatory and/or damage signals present [24,28]. There are two different reactive states of astrocytes proposed. The A1 phenotype occurs following exposure to an inflammatory stimulus, exhibits upregulation of pathways related to antigen presentation, complement activation and increased neurotoxicity [29,30]. The A2 phenotype, also called alternative activated astrocytes, release neuroprotective and neurotrophic factors, thrombospondins, and participate in scar formation [29,30]. Followed by local environment change, activated astrocytes go through a morphological transformation, increase their metabolic activity and start to produce pro-inflammatory cytokines, chemokines, reactive oxygen species (ROS), growth and trophic factors [31]. Together with microglia, factors produced by astrocytes target neighbouring cells and, depending on the context, can have neuroprotective or neurotoxic effects.

1.2 Glia activation and neuroinflammation

Inflammation is a complex biologically regulated response of body tissues to an infection or injury in order to eliminate the cause of it and effect repair. Neuroinflammation, in turn, is known to be a biochemical and cellular response of the brain and spinal cord tissue, that leads to morphological, anatomical and functional changes in the CNS. The inflammatory response involves a cascade of reactions and signals, which leads to activation of innate immune cells and adaptive immunity. Inflammation in CNS also includes activation of astrocytes and microglia. Although acute neuroinflammation plays a neuroprotective role in the brain [32], chronic neuroinflammation is always considered damaging and neurotoxic to nervous tissue [33] and is an important factor associated with cognitive impairment and progression of neurodegenerative diseases, such as Alzheimer's disease (AD), Parkinson's disease (PD), Multiple sclerosis (MS), amyotrophic lateral sclerosis (ALS) and many others [34].

The neuroinflammatory response is primarily an integral protective mechanism of the CNS that results in repair and regeneration of neurons, eliminating invading pathogens, initiating angiogenesis and normal resolution. However, the excessive and chronic inflammatory response can lead to the production of neurotoxic factors, such as tumor necrosis factor alpha (TNFα), interleukin-1 (IL-1) and IFNγ [32,33,35,36], and cause an adverse effect on neural parenchyma. There are various neuroinflammatory pathways that are activated by different stimuli which result in the release of pro-inflammatory cytokines from these innate immune cells of the CNS.

1.2.1 IFNγ mediated immune response

IFNγ is known to be a multifunctional cytokine and inducer of TNFα, interleukin-1- β (IL-1β), signal transducer and activator of transcription 3 (STAT3), interleukin-6 (IL-6), interleukin-12 (IL-12) and interleukin-23 (IL-23)[37,38]. The predominant source of IFNγ is T- and NK-cells, but it can be produced by other cells, including microglia, astrocytes and neurons. It upregulates the expression of adhesion/costimulatory molecules, like the major histocompatibility complex (MHC) class II molecules to sustain antigen-dependent T-cell activation [39]. Surprisingly, a recent study has shown that astrocytes, but not microglia, express IFNγ receptors (IFNγ-R) at immunohistochemically detectable levels in human AD hippocampus, PD substantia nigra, ALS spinal cord as well as corresponding areas of non-neurological cases [40]; on the other hand, cultured human microglia and astrocytes show constitutive expression of IFNγ-R at mRNA and protein levels [40]. These major findings suggest that in the human CNS, microglial expression of IFNγ-R protein is much lower than astrocytic expression level regardless of whether the CNS is affected with neurological disease. Nevertheless, microglia and oligodendrocytes acquire IFN-γ-R expression at comparable levels to astrocytes in cell culture.

After IFNγ gamma is released and bound to its specific receptor IFNγ-R, signalling cascade is initiated through nuclear factor kappa B (NF-κB) or Janus Kinase/STAT (JAK/STAT) signalling pathways [41].

1.2.1.1 NF-κB signalling pathway

The inactive NF-κB resides in the cytoplasm associated with the natural biological inhibitor IκB. IFNγ-Rs are coupled to myeloid differentiation primary response 88 (MYD88) and Toll/interleukin-1 receptor (TIR)-domain-containing adapter-inducing interferon-β (TRIF) adaptor proteins and recognition of pathogen leads to the activation of IκB kinases (IKK) and mitogen-activated protein kinase (MAPK) [42]. Phosphorylation events result in the release and nuclear translocation of NF-κB [43]. IkB and MAPKs also control activator protein 1 (AP-1), and interferon regulator factor families; as a result, they activate production of several pro-inflammatory cytokines and chemokines, such as IL-1β, IL-6, TNF-α and IFNγ, inducible nitric oxide synthase (iNOS) and cyclooxygenase-2 (COX-2) which promote neuroinflammation [44]. Inducible NF-κB in glia regulates inflammatory processes that worsen inflammatory-mediated neurodegeneration.

NF-κB has also been demonstrated as a major signal transducer affecting cellular permeability, endocytosis, and intracellular trafficking at the level of the blood-brain barrier [45]. NF-κB transcription factors are known to be abundant in the brain where they have diverse functions in neurons, glia, and cerebral blood vessels.

Activation of NF-κB signalling is essential for acute and chronic inflammatory responses and can be initiated by various receptors on the surface of glial cells, including receptors for IL1, TNFα and IFNγ [46].

1.2.1.2 JAK/STAT signalling pathway

Signalling through the JAK/STAT pathway plays critical roles in the initiation and regulation of innate immune responses and adaptive immunity. Moreover, over seventy different cytokines and interferons use this pathway to mediate innate and adaptive immunity [47]. When a cytokine binds to its specific receptor on the cell membrane, the kinase activity of cytoplasmic, receptor-associated JAKs is activated. The activated JAKs phosphorylate a tyrosine residue in the cytoplasmic domain of the cytokine receptor to provide a docking site for STATs. STATs bind the cytokine receptor via their Src homology 2 (SH2) domains and are phosphorylated on tyrosine residues by JAKs, leading to the formation of homo- or hetero-dimers via SH2-phosphate interactions. Dimerized STATs then translocate from the cytoplasm into the nucleus, where they modulate the expression of cytokine-responsive genes by binding to specific DNA elements [48]. In mammals, four JAKs (JAK1, JAK2, JAK3, TYK2) and seven STATs (STAT1, 2, 3, 4, 5a, 5b, 6) have been identified, and each cytokine utilizes a specific combination of JAK and STAT members to transduce a unique signal [41].

The main consequence of the activation of this pathway is to promote inflammation-associated gene expression but also to regulate survival-associated gene expression. Depending on the STAT isoform activated it is possible to have different effects on inflammation, survival, proliferation or differentiation of the cells on the CNS. The role of STAT3 during brain inflammation is still controversial. It can either promote cell death and contribute to brain damage or be implicated in neuronal survival [49]. The role of STAT1 is more consensual as it promotes cell death [50], while activation of STAT1 and NF-κB transcription factors leads to polarization of microglia/macrophages toward a neurotoxic phenotype [51].

1.2.2 IFNγ induced glial activation

IFNγ is crucial during the complex activation process of microglia and astrocytes. Under quiescent conditions *in vitro*, glial cells feature ramified morphology, low expression of activation markers and minimal release of pro-inflammatory cytokines and nitric oxide (NO) [52].

Activation of microglia by IFNγ involves elevated expression of cell membrane molecules and translation of pro-inflammatory cytokines which facilitate infiltration of immune cells [37,53]. IFNγ causes changes in microglial morphology, surface receptors and cytokine release profile. It induces hypertrophy that is characterized by short and flat cellular processes, MHC-II and CD86 upregulation, and increased levels of IL-6 and TNF-α [54]. Activation of the IFNγ signalling pathways also plays an essential role in neuronal atrophy, synapse loss, and subsequently, severe cellular dysfunction and death [55].

Similar to microglia, astrocytes also release inflammatory cytokines [56], glutamate [57], reactive oxygen species [58] and NO [59] in response to IFNγ, which are all potentially neurotoxic. Human astrocytes were shown to be neurotoxic via regulation by STAT3 following stimulation with IFNγ [60].

1.3 Glioblastoma

Glioblastoma multiforme (GBM) is the most common and aggressive high grade (cancerous) brain tumor that remains largely incurable with an incidence 3.2/100 000 adults per year [61]. The disease has been clinicopathologically categorized into primary GBM, which arises de novo – a grade IV tumor [Word Health Organization (WHO)]; in contrast, secondary glioblastomas develop through progression from diffuse astrocytoma (WHO grade II) or anaplastic astrocytoma (WHO grade III)[62,63] (Figure 2). These

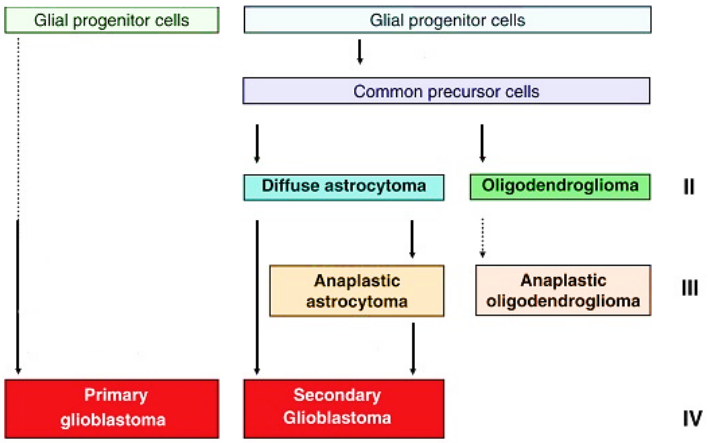

Figure 2: Schematic development of two types of GBM (from Ohgaki et al., 2011).

tumors are graded according to the presence of anaplastic features, tumor's growth potential and aggressiveness in low-grade (or WHO grade II) and high-grade tumors (either WHO grade III or anaplastic and WHO grade IV or glioblastoma).

85-90% glioblastoma patients typically present with de novo grade IV lesions delineating primary glioblastoma [64]. Survival time is extremely poor for patients diagnosed with GBM ranging typically between 8 to 15 months. The tumor can occur at any age but tends to occur more often in older adults. First symptoms are commonly present as headaches, seizures, vomiting, changes in mood and personality and blurred vision [65].

GBM is a type of astrocytoma, cancer arising from astrocytes. The disease is considered to be initiated by genetic mutations in ''common'' cancer genes as well as by immunological dysfunction.

1.3.1 Immune response to GBM

Cancer cells are visible to the immune system, as they are the origin of processes like mutations, aberrant processing of proteins, chronic stress and constant cell death. This would naturally cause immune surveillance if the tumor didn't evolve mechanisms to suppress immune response. Immune cells such as natural killer (NK) cells, natural killer T (NKT) cells, cytotoxic T-cell (CD8+ T-cell) and gamma delta T cells provide the first line of defence against tumor cells by exerting direct cytotoxic effects and secreting high levels of IFNγ, IL-6 and TNF-α/β to promote tumor cell destruction [66].

The most effective immune response against tumoral cells is the cytotoxic response, with CD8+ T-cell being the main component. T-cell activation requires two distinct signals: the first signal is delivered by the engagement of T-cell receptor with antigenic peptides presented on MHC class 1 molecules expressed on tumor cell membrane, or MHC class 2 molecules expressed on antigen presenting cells (APCs); second signal is provided by one of several non-specific molecules such as the binding CD28 receptors on T cells with B7 ligand on activated APCs. NKT cells, a subpopulation of T lymphocytes, are considered tumor cell killers; they produce antitumor molecules, such as Fas ligand, IL-4, IFNγ, IL-13, perforin, and granzyme, that also promote lysis of tumor cells [67,68]. As a result, the immune system is active, and tumor can be eventually destroyed. Main types of effective APCs are dendritic cells (DC), macrophages and B cells.

Microglia are also a part of the tumor microenvironment (TME) and play an important role in angiogenesis and tumorigenesis of gliomas [69,70]. It is known, that immunoprotective ability of microglia is inhibited in tumors; moreover, microglia and macrophages secrete various cytokines and growth factors that contribute to successful immune evasion, growth, and invasion of brain neoplasms.

1.3.2 The effect of glioma on healthy brain cells

In order to improve the patients' condition, astroglioma must be treated aggressively. To this end, it is important to understand the effect of tumor cells and their microenvironment and likely impact of treatments on healthy brain cells. These treatments may eventually lead to the restoration of structure and physiological functions of the neuroparenchyma.

1.3.2.1 The effect of glioma on neurons

Rapid growth and expansion of astrocytoma (especially high-grade gliomas) lead to the inclusion of additional glial cells, extracellular toxicity, hypoxia and neuronal damage [71]. Under physiological conditions, oxygen and glucose levels in the brain are tightly regulated to ensure an adequate oxygen supply to support the function of neurons. In fact, a decrease in oxygen level in the brain causes cellular metabolic changes and stimulates an immediate increase in oxygen supply by regulating flow and promoting glycolysis, angiogenesis and, as a result, cell survival [72].

Multiple studies also revealed the active release of the excitatory amino acid glutamate *in vitro* in human glioma cells, and the extracellular levels of glutamate are increased both in and around experimental glioma implants *in vivo* [73,74]. The reported glutamate secretion by glioma cells evidently contributes to hyperexcitability of neural network that consequently leads to seizure activity in the TME [75,76].

Evidence also indicates synaptogenic properties of tumor cells, as the subpopulation of glioma cells *in vivo* increase synaptogenesis and promote cortical hyperexcitability [77]. This correlates with the onset of seizure activity in tumor-bearing mice and from other studies in a transgenic mouse model of glioma [75].

1.3.2.2 The effect of glioma on microglia

As mentioned above, microglia can transform into M1 or M2 phenotype under different circumstances, and the tumor environment is not an exception. In particular, their immune marker profile is strongly influenced by glioma released factors. M1-associated pro-inflammatory cytokines such as IFNγ, TNF-α, IL-2, and IL-12 are significantly downregulated, while high amounts of M2-associated anti-inflammatory cytokines such as transforming growth factor beta (TGF-β), IL-6, and IL-10 are found in the gliomas, indicating an immunosuppressive TME [78]. Furthermore, it has been demonstrated that glioma cell-derived conditioned medium (CM) is able to increase STAT3 activity in microglia cells, indicative of the increased activity of the anti-inflammatory M2-like cytokines IL-6 and IL-10 [79].

A positive correlation between the number of microglia/macrophages in peritumoral tissue and glioma malignancy was demonstrated in several studies [80,81]. One of the most important recruiters of glioma-associated microglia/macrophages (GAM) is the monocyte chemoattractant protein (MCP)-1 that is secreted by astrocytoma and glioblastoma cells *in vitro* and *in vivo* [78,82].

Recruitment and the subsequent pro-tumorigenic M2-like phenotype polarization of GAMs have been shown to be mediated by macrophage colony-stimulating factor (M-CSF), granulocyte M-CSF (GM-CSF) secreted by glioma cells [83,84].

1.3.2.3 The effect of glioma on astrocytes

Reactive astrogliosis within the TME is poorly explored. However, some studies state the polarization of tumor-associated astrocytes towards an alternative activation state [85,86]. Recent data also imply that inflammatory astrocyte subtype is induced through microglia signalling, and by the astrocyte-microglia crosstalk [85]. If the same mechanisms apply to glioma cells remains to be investigated.

1.3.3 *In vitro* models of glioblastoma

1.3.3.1 Rat C6 glioma cell line

The employment of cell culture is one of the effective ways to study human cancer biology. The ideal glioma model should be similar to human GBM in terms of morphological characteristics, invasive pattern, vascular behaviour, and immune microenvironment.

C6 glioma cell line was chemically induced in Wistar rats by repetitive exposure to *N*-Nitroso-*N*-methylurea in the late 1960s [87]. Rapidly proliferating C6 cells are reported to be morphologically close to GBM cells when injected into the brain of neonatal rats [88]. This glioma model also exhibits histological features such as foci of tumor necrosis, high mitotic index and nuclear polymorphism, which are characteristic of human GBM [88–90]. The injection of C6 cells into the rodent brain result in intracranial growth and formation of malignant solid tumors surrounded by reactive astrocytes [91,92]. Moreover, a study of the tumor-immune microenvironment shows C6 resembles human GBM immune infiltrates [90]. Magnetic resonance imaging (MRI) and magnetic resonance angiography (MRA) *in vivo* show that C6 resembles human GBM most accurate between other rodent glioma models [89,93]. The C6 rat glioma model is, therefore, the most common experimental model used in the research of growth and invasion of high-grade gliomas. Regarding genetical profile, cells are reported to have a wild type p53 gene, with overexpression of retinoblastoma (Rb) and epidermal growth factor receptor (EGFR) genes [94–96].

In general, the C6 rat glioma model has been used in different studies to investigate tumor invasion, migration and growth, tumor-related angiogenesis, blood-brain barrier disruption and regulation and production of growth factors [97–101]. It is widely used both as an *in vitro* glioblastoma cell model and *in vivo* glioma model, following intracerebral transplantation in Wistar rats, to investigate effects of targeted therapy and radiotherapy (RT).

C6 cell line and primary cells were chosen to determine the effect of C6 CM in vitro prior to in vivo experiments. The results of this work present a solid foundation for the future animal work, for instance, transplantation of C6 cells into rat brain through stereotactic surgery.

1.3.3.2 Human-derived U87 glioma cell line

U87 is a human primary cell line that is widely used not only for glioblastoma research but also in other brain cancer studies [102]. It was derived from a human grade IV glioma almost 50 years ago [103] and is reported to be isocitrate dehydrogenase (IDH)-wild type O6-methylguanine-DNA methyltransferase promoter methylated [104]. A recent study using a polydimethylsiloxane (PDMS) -based microfluidics device reported that, following the injection into the device, U87 cells exhibited fast migration (0.50 ± 0.07 μm/min), rapid proliferation, the formation of neurosphere-like structures with the highest invasion capability between the types of GBM cell models tested [105]. U87 implantation was also reported to cause large defined masses in the brain parenchyma, that resembled glioblastoma tumors[106]. However, in 2016 the commonly used version of U87MG (from the American type culture collection) was found to be non-identical to its patient of origin and therefore cannot be relied on in glioblastoma research [107].

1.3.4 In vivo models of glioblastoma

1.3.4.1 Mice transplantation modelling

Mice are undoubtedly the most accessible mammalian models because of the simplicity of their genetic manipulation and short reproductive times. Transplantation of tumor-initiating cells into mice brain presents relatively low-cost model of GBM, enabling investigation of tumor biology, including tumor-host interactions and immune control. Transplanted cells can be either transformed/engineered cells (i.e., C6 cells), or cells from primary tumors. Transplants can be allografts, in which the implanted cancer cells are from the same species as the recipient, e.g., mouse into mouse, or xenografts, where implanted cells are from a different species, e.g., human into mouse.

Patient-derived xenografts (PDX) are used extensively in translational research and are the main recent focus of GBM research [108,109]. The PDX model has the advantage of retaining both the genetic and histological features of the primary tumor from which it was derived. There is some controversy as to whether PDX models are best established by injecting freshly biopsied tumor tissue [110,111] or cultured tumor spheres into mice [112], and whether orthotopic or subcutaneous xenograft is preferable. PDX models are generally established by injecting glioblastoma tumor spheres produced under serum-free neurosphere-culture conditions, into immunodeficient

mice. Tumor spheres have several advantages over serum-cultured glioblastoma cell lines: the tumor spheres retain a molecular profile similar to that of the patient's original tumor, thus maintaining tumor heterogeneity [113,114]; their molecular profile is stable over time, and they are both tumorigenic and phenotypically similar to the patient's original tumor, even in aspects such as single-cell invasion and tumor angiogenesis [115,116]. However, not all human gliomas are successfully cultured as tumor spheres; reported success rates vary from 10 to 20%. At present, there is little molecular evidence for preferring adherent culture over sphere culture. The generation of tumorigenic cell populations from human glioblastomas using neurosphere culture has significantly advanced our knowledge of specific subpopulations within human primary tumors. Even though their phenotypes *in vivo* are not necessarily predictable, these cell populations are an important tool for studying the tumorigenicity and progression of glioblastoma *in vivo*.

1.3.4 Standard glioblastoma chemotherapy

There are several ways to treat brain tumors such as GBM, including surgery, RT, chemotherapy, or the combination of all. However, glioblastoma multiforme has only a few clinically approved therapeutic regimens.

Chemotherapeutic drugs destroy cancer cells and inhibit their growth. Current ''gold standard'' and most commonly prescribed glioblastoma chemotherapy medication is Temozolomide (TMZ). This treatment is, by far, the most effective as it increases the median overall survival from 12 months (with RT alone) to 14.6 months, and the percentage of patients alive at 2 years after treatment increases from 10.4% to 26.5% [117,118]. TMZ is an alkylating agent: it has an ability to alkylate/methylate DNA which damages it and causes cell cycle arrest and eventually apoptosis. Due to its short half-life, TMZ has been administered at relatively high doses with resultant side effects [119].

Carmustine (bis-chloroethylnitrosourea - BCNU) is an FDA approved chemotherapy drug that acts based on the same mechanism as TMZ. Nonetheless, several studies reported TMZ to be more effective and prolonging patients' survival [120]. A novel method of GBM treatment delivery is Gliadel® wafer - a biodegradable polymer loaded with BCNU and implanted into the tumor bed at the time of its surgical removal [121]. Being directly inserted into the brain and releasing the chemotherapeutic agent directly at the site of tumor, the compound does not have to cross

blood-brain barrier and therefore rescues the patients from adverse side effects. A meta-analysis reported a 37% reduction in risk of mortality of newly diagnosed GBM patients treated with BCNU wafers [122]. Risk of mortality, or the death risk, provides a medical classification to estimate the likelihood of in-hospital death for a patient and is calculated by analyzing the survival curves.

Considering the significant clinical benefit of Gliadel®, scientists hypothesized there to be similar benefits with wafers releasing TMZ on glioma cells. In fact, a recent study reports an improved median survival in an animal gliosarcoma model treated with BCNU wafer compared to TMZ wafer of 15 compared to 19 days, respectively [121]. Moreover, the combination of two drugs in a single wafer resulted in median survival of 28 days, with 25% of the group surviving for more than 120 days [121].

Combinational local chemotherapy is a promising method in which to treat GBM. Yet still, there are many complications involved in the chemotherapeutic approach, and this, in addition to its ineffectiveness, forces patients to discontinue tumor treatment. Only 5% of glioblastoma patients survive for more than five years after the initial diagnosis. This fact highlights the crucial role and importance of the ongoing development of new innovative strategies for treatment.

1.4 The kynurenine pathway

In the brain, the important factor of neuromodulation and inflammation is the kynurenine pathway – a metabolic pathway of degradation of the essential amino acid tryptophan [123]. Activation of the kynurenine pathway has been associated with neurodegeneration as well as immunosuppression in cancer models, namely glioblastoma [124, 125]. It had also been reported that glioblastoma patients have an imbalance between tryptophan metabolites, suggesting that activation of the kynurenine pathway is present during glioblastoma progression thus may be related to tumor progression [126].

1.4.1 Tryptophan metabolism along the kynurenine pathway

Tryptophan (TRYP) is an α-amino acid and an important precursor in the biosynthesis of serotonin, melatonin and nicotinamide adenine dinucleotide (NAD^+). The catabolism of L-

tryptophan is precisely regulated by a number of metabolic pathways. One of them is the kynurenine pathway (KP) - an immune-mediated tryptophan catabolism [127]. KP is induced in times of stress and inflammation [128] and results in the production of neuroactive metabolites that are implicated in wide range of neurodegenerative and other disorders, including glioblastoma [129]. It can be stimulated by various pro-inflammatory cytokines, such as TNFα, IFNγ, IL-1 and LPS [130].

First, tryptophan is metabolized by either of the rate-limiting enzymes, indoleamine-2,3-dioxygenase (IDO) 1/2 or tryptophan-2,3-dioxygenase (TDO) into N-Formyl-L-Kynurenine that is further degraded into L-kynurenine (L-KYN) by the enzyme formamidase. L-kynurenine (L-KYN) is a key metabolite and plays a central role in the KP [131]. 40% of L-kynurenine in the brain is generated locally, and the remaining 60% is transported from the blood by the neutral amino acid carrier. It can be metabolized through three distinct pathways to form kynurenic acid (KYNA), 3-hydroxy-l-kynurenine (3HK) and anthranilic acid by the action of kynurenine aminotransferase (KAT), kynurenine-3-monooxygenase (KMO) and kynureninase (KYNU) enzymes, respectively. 3HK can be further transformed into xanthurenic acid, and both 3HK and anthranilic acid can be enzymatically converted to 3-hydroxyanthranilic acid (3HAA) by KYNU. 3HAA is then transformed through several metabolic into picolinic acid and non-enzymatically converted to quinolinic acid (QUIN) — the precursor of NAD^+ and $NADP^+$ synthesis. The metabolites of this pathway are collectively called kynurenines [Figure 3].

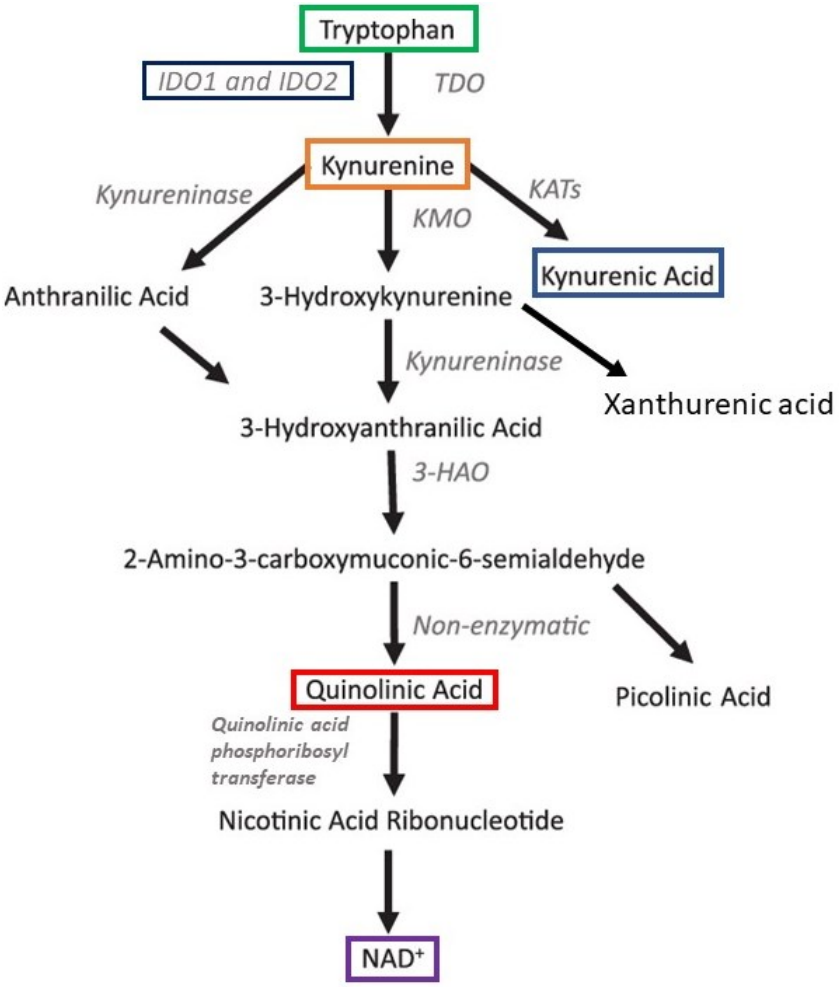

Figure 3: A schematic diagram of the KP

The neurotoxic branch of the KP produces N-methyl-D-aspartate (NMDA) receptor agonist QUIN, while the neuroprotective part results in the synthesis of KYNA, which is an NMDA and α-amino-3-hydroxy-5-methyl-4-isoxazolepropionic acid (AMPA) receptor antagonist [128]. QUIN and 3HK also mediate neurotoxicity through free radical production, while KYNA exerts neuroprotective effects by acting as a free radical scavenger [129]. Activation of the NMDA receptor has been shown to permeate cells to Ca^{2+}, Na^{+} and K^{+} ions. Increased intracellular Ca^{2+} influx activates several secondary messenger signalling pathways leading to synaptic alterations. Moreover, increased intracellular Ca^{2+} influx due to excessive NMDA receptor activation can induce excitotoxicity and neuronal cell death in several neurodegenerative diseases[132]. QUIN and other toxic metabolites are predominantly synthesized by infiltrating macrophages and microglia, which associate the neurodegenerative effects of kynurenine pathway activation with neuroinflammation [131].

1.4.2 KP involvement in GBM progression

There is evidence that KP enzymes are overexpressed in various tumor types, including GBM [129]. During GBM formation, while the host immune system plays a role in eliminating recognized tumor cells, cytotoxic T lymphocytes secrete IFNγ, TNFα and other pro-inflammatory cytokines that strongly induce IDO expression and KP activation. Glioblastoma IDO expressing cells and L-KYN production promotes tumor resistance to genomic instability and tumor growth: L-KYN regulates DNA repairing enzyme DNA polymerase kappa [133]. TRYP depletion caused by high TRYP uptake by IDO expressing cells enhances the KP effect against T cell activation and proliferation. QUIN production by microglial cells supports tumor tolerance to oxidative stress by NAD+ production and promotes cell proliferation by the regulation of fibroblast growth factor-1 release [134,135]. Elevated IDO levels and increased concentration of other KP enzymes and metabolites promote cancer development by immunosuppression and immunoinhibition.

These facts contribute to the idea that KP activation enhance an immunosuppressive environment by tryptophan depletion or via direct effects of the KP intermediates on immune and other cells in TME.

1.4.3 Inhibition of the KP protects against reactive microglial-associated reductions in the complexity of primary cortical neurons

Previous studies on elucidating the role of the KP in glial cells leading to neuroinflammatory related changes and associated reductions in neuronal complexity which utilized the BV-2 cell line have been undertaken. BV-2 is a murine microglial cell line, immortalized after injection of mice with a v-raf/v-myc recombinant retrovirus [102]. BV-2 cells express these oncogene products intracellularly and gp70 (murine leukemia virus) antigen on the cell surface. This cell line exhibit characteristics similar to microglia in culture and, therefore, are used as a model of activated microglia.

O'Farrell et al. (2017) showed that stimulation of BV-2 microglia with IFNγ for 24 hours activates the KP in these cells. IFNγ was used as an inflammatory stimulus based on its capability to induce IDO gene expression and enzymatic activity [136]. Indeed, exposure to IFNγ also induced the expression of IDO and other KP enzymes, such as KMO and KYNU, and raised the concentration of KYN and 3-HK in the conditioned media of BV-2 microglia [128]. Transfer of conditioned media

from the IFNγ-stimulated BV-2 microglia to primary cortical neurons reduced all measures of neurite outgrowth and complexity. Pre-treatment of BV-2 cells with the 1-methyltryptophan (1-MT, 0.5 mM), an IDO inhibitor, prevented the IFNγ-induced changes in metabolite concentrations in the conditioned and reversed the reductions in the complexity of primary cortical neurons induced by conditioned media from IFNγ treated mixed glia [128].
Direct treatment of primary cortical neurons with IFNγ (10 ng/ml) had no effect on the neuronal complexity; therefore, the reductions in the neurite outgrowth and complexity following IFNγ stimulation of BV-2 microglia are likely due to the release of factors from the BV-2 microglia into the media that are then transferred to neurons.

Taking into consideration these previous findings, this project sets out to determine how glioma may influence microglia, astrocytes and neurons, using C6 cells as an *in vitro* glioma model with IFNγ stimulation of mixed glia added as a comparator set of experiments.

1.4.4 IDO inhibition as an effective strategy in GBM treatment

IDO is an inducible enzyme that catalyzes the first step in tryptophan catabolism. IDO1 is a monomeric heme-containing protein that plays a vital role in the mechanisms of tolerance and immunosuppression [137]. Many malignancies can overexpress IDO1 when exposed to IFNγ or other inflammatory cytokines [138]. Tumor-induced immunosuppressive mechanisms contribute to poor prognosis, as was shown by an inverse correlation between IDO1 expression and patient survival [139,140]. IDO elevation is considered to be an early event in the formation of neoplasms as it is elevated in the tumor-promoting inflammatory environment, even in the absence of tumor initiation [141]. Once malignancy has developed, IDO overexpression supports the proliferation of malignant cells and angiogenesis by contributing to escape from immune surveillance via different mechanisms.

Glioma cells were also reported to overexpress IDO1 and IDO2 mRNA when compared to human astrocyte cultures and also showed to have a decreased mRNA expression of KAT [142]. The same study also showed an increased KYN/TRYP and decreased KYNA/KYN ratios in the plasma of GBM patients when compared to the plasma of healthy controls [142]. The significantly elevated expression of IDO enzyme in cancer and other cells in the TME is clearly a promising target for GBM treatment, and the inhibition of IDO is regarded as a potential strategy for glioblastoma

patients. It is also important to consider if KP inhibition might influence healthy neuronal and glial cells in the brain affected by the presence of a glioblastoma.

1.5 Aims and objectives

In order to extend our knowledge of the role of the KP in driving reactive glia-associated reductions in the complexity of primary cortical neurons, this project aims

1. to assess the effects of IFNγ stimulation of primary mixed glial cultures, followed by transfer of conditioned media from these cells to mature primary cortical neurons in order to determine any effects on the complexity and co-localized expression of synaptic markers indicative of synapse formation.

The focus is then

2. to determine the effect of transfer of the conditioned media from C6 glioma cells to healthy primary cortical neurons, microglia and astrocytes.

In particular, the effect of conditioned media from C6 glioma cells on (a) neuronal viability, complexity, and co-localized expression of synaptic markers (ability to form synapses) and (b) microglial and astrocytic cell activation and transformation are assessed.

Finally, the project aims

3. to assess a role for the KP in mediating conditioned media from C6 cells associated changes in the viability, morphology and complexity of neuronal and glial cells *in vitro*. In this regard, the effect of the IDO inhibitor, 1-MT, is used.

If KP is involved in C6 CM-induced reductions in the neuronal complexity and co-localized expression of neuronal synaptic proteins, activation and transformation of glial cells *in vitro*, then IDO inhibitor 1-MT can attenuate these changes.

2 Methods

2.1 Materials

2.1.1 Animals

Wistar rats (male/female)	TCD Comparative medicine, Ireland

2.1.2 General equipment

Autoclave	Sanyo, Ireland
Axio Imager Z1	Carl Zeiss, Germany
Biosafety cabinet	ADS Laminaire, France
Centrifuge: Legend RT+	Sorvall, Ireland
Gyro rocker	Stuart, Ireland
Haemocytometer	VWR, Ireland
Laminar flow hood	ADS Laminaire, France
Microscope: CKX41	Olympus, UK
Nanodrop® ND1000 Spectrophotometer	Thermo Fisher Scientific, US
Plate reader	Biotek, US
StepOnePlus™ Real-Time PCR System	Applied Biosystems, US
Thermal Cycler (PTC-200 Peltier)	MJ Research, US
Thermo Steri Cycle CO_2 Incubator Hepa Class 100	Bio-Sciences Limited, Ireland
Vortex	Ika, Ireland

2.1.3 General consumables

24-well plates	Sarstedt, Ireland
Biosphere filter tips (10, 20, 100, 200, 1000 µL)	Sarstedt, Ireland
Cell culture flasks (T-75 cm2)	Corning, Ireland
Cell scrapers	Sarstedt, Ireland
Cell strainers (40 µm),	BD Falcon VWR, Ireland
Falcon tubes (15 mL, 50 mL),	Sterile Sarstedt, Ireland
Filter units (0.22 µm), single-use (Millex)	Millipore, Ireland
Glass coverslips (13 mm)	VWR, Ireland

Haemocytometer	VWR, Ireland
Laboratory tissue rolls	VWR Int., Ireland
Microscope slides 76 mm x 26 mm	Fisher Scientific, Ireland
Microtubes (0.5 mL, 1.5 ml, 2 mL)	Sarstedt, Ireland
Parafilm	Fisher Scientific, Ireland
Microscope slides 76 mm x 26 mm	Thermo Fisher Scientific, Ireland
Microtubes (0.5 mL, 1.5 mL, 2 mL)	Sarstedt, Ireland
Pasteur pipettes (3.5 mL)	Sarstedt, Ireland
Petri dishes (90 mm)	Fisher Scientific, Ireland
Pipettes (manual and automated)	Gilson Inc., US
Pipette tips (200 µL, 1000 µL)	Sarstedt, Ireland
Pipettes (5 mL, 10 mL, 25 mL), sterile	Sarstedt, Ireland
Scalpels, disposable, sterile (Swann-Morton)	Fisher Scientific, Ireland
Serological pipette (10, 25 mL)	Sarstedt, Ireland
Syringes (20 mL, 50 mL)	Fisher Scientific, Ireland
Syringe filters (0.2 µm)	Pall Corporation, USA
Transfer pipettes (sterile; 3 ml)	Sarstedt, Ireland

2.1.4 General laboratory chemicals

Absolute Ethanol	Hazmat, TCD, Ireland
β-mercaptoethanol	Sigma Aldrich, UK
Biocidal ZFTM	WAK-Chemie Medical, Germany
Dimethyl sulfoxide	Sigma Aldrich, UK
HEPES	Sigma Aldrich, UK
Triton X-100	Sigma Aldrich, UK
Trypan Blue (0.4%)	Sigma Aldrich, UK
Trypsin-EDTA solution (0.25%)	Sigma Aldrich, UK
Virkon	Antec Int., USA

2.1.5 Cell Culture reagents

B-27 Supplement	Gibco, UK
Bovine serum albumin	Sigma Aldrich, Ireland

Biocidal ZFTM	WAK-Chemie Medical, Germany
Donkey serum	Sigma Aldrich, Ireland
Dulbecco's modified Eagle medium: F12	Labtech Int., UK
Dulbecco's phosphate buffered saline (10X)	Sigma Aldrich, UK
Foetal Bovine Serum- heat inactivated	Invitrogen, UK
Fungizone	Invitrogen Life Technologies, UK
Glutamax	Gibco, UK
Horse serum	Sigma Aldrich, Ireland
Neurobasal A medium	Invitrogen, UK
Normal goat serum	Sigma-Aldrich, Ireland
Penicillin-streptomycin	Invitrogen, UK
Poly-D-lysine hydrobromide	Sigma Aldrich, UK
Poly-L-lysine hydrobromide	Sigma Aldrich, UK
Trypan Blue (0.4%)	Sigma Aldrich, UK
Trypsin-EDTA solution (0.25%)	Sigma Aldrich, UK
Vectashield mounting medium with DAPI	Vector Laboratories, UK

2.1.6 Experimental treatments

KYNA	Sigma Aldrich, UK
Recombinant rat IFNγ	Peprotech, Ireland
1-MT	Sigma Aldrich, UK

2.1.7 Assay Kits

CCK-8 Assay Kit	Dojindi labs, Kumamoto, Japan

2.1.8 Molecular materials and reagents

Biosphere filter tips (10, 20, 200, 1000 µL)	Sparks Labs supplies Ltd, Ireland
Molecular grade ethanol	Sigma Aldrich, UK
High capacity cDNA archive kit	Applied Biosystems, UK

Microamp 96-well reaction plate	Applied Biosystems, UK
Nucleospin* RNA II Isolation kit	Macherney-Nagel, Germany
Nunc-Immuno™ MicroWell™ 96 well	Sigma Aldrich, UK
Optical adhesive covers	Applied Biosystems, UK
Paraformaldehyde	Sigma Aldrich, UK
PCR minitubes	Sarstedt, Ireland
RNase-free microtubes (1.5 mL)	Ambicon Inc., US
RNase-free water	Macherney-Nagel, Germany
RNaseZap* wipes	Ambicon Inc., US
TaqMan* Gene Expression Assays	Applied Biosystems, UK
TaqMan* Universal PCR Master Mix	Applied Biosystems, UK

2.2 *In vitro* experiments

2.2.1 Ethics statement

All animal procedures were carried out in accordance with the European Council Directive 2010/63/EU and were approved by the Animal Research Ethics Committee in Trinity College Dublin (AE19136).

2.2.2 Aseptic techniques

Aseptic techniques were imperative throughout all cell culture work, including preparation of the cell culture reagents and culture plates to ensure the maintenance of a sterile environment, free from fungi, bacteria and viruses, that could otherwise affect cell function and viability. Aseptic technique included the use of sterile disposable plastics and sterilization of all glassware, plastics and distilled water (dH_2O) by autoclaving at 121°C for 30-60 min prior to use. Dissection kit instruments were cleaned with Virkon, sterilized by baking for a minimum of 2 hours. All cell culture work was carried out in a laminar flow hood, which prevents contamination with airborne pathogens by allowing only filtered air to come into contact with cells. The interior of the laminar hood was wiped down with 70% ethanol (EtOH) before and after use; hood surface was also exposed to ultraviolet (UV) light for 30 min after use. All items transferred into the flow hood were sprayed and wiped down with 70% EtOh to prevent contamination of the culture work area with external pathogens. Disposable latex gloves were worn at all times while working in the laminar flow hood and were sprayed with 70% EtOH before use. Gloves were also changed regularly during the process of cell culture preparation. Cells were maintained at 37°C in a 5% CO_2 humidified atmosphere provided by a Thermo Steri Cycle CO_2 Hepa Class 100 Incubator. Both the incubator and laminar flow hood were cleaned regularly with Biocidal ZF and a steri-cycle was run to maintain a sterile environment when not in use.

2.2.3 Preparation of culture media

2.2.3.1 Primary neuronal cultures:

Neurobasal media (NBM) was utilised for maintenance of primary neuronal cultures and was supplemented with 1% (v/v) penicillin-streptomycin, 0.1% (v/v) fungizone and 1% (v/v) glutaMax. Briefly, 5 ml of penicillin-streptomycin, 500 µl of fungizone and 5 ml of glutaMax were filter-sterilized using 0,2 µm syringe filter and added to a 500 ml bottle of NBM. NBM was then aliquoted to 50 ml falcon tubes, parafilmed and stored in the fridge until further use. Prior to use NBM was supplemented with 1% B-27 (referred to as complete NBM (cNBM) hereafter).

2.2.3.2 Primary mixed glial cultures:

Dulbecco's modified Eagle's medium (DMEM) F12 was utilised for maintenance of primary mixed glial cultures and was supplemented with 10% (v/v) heat-inactivated fetal bovine serum (FBS), 1% (v/v) penicillin-streptomycin and 0.1% (v/v) fungizone [referred to as complete DMEM (cDMEM)]. cDMEM was aliquoted into 50 ml falcon tubes, parafilmed and refrigerated until further use.

2.2.3.3 Primary enriched microglial cultures:

cDMEM was utilized for maintenance of primary enriched microglial cultures and was supplemented with GM-CSF (10 ng/ml) and M-CSF (5 ng/ml) immediately before use to give a final concentration of 10 ng/ml each.

2.2.3.4 Primary astrocytic cultures, C6 cell line cultures:

cDMEM was utilized for maintenance of primary astrocytic cultures. It was prepared as described above for mixed glial cultures. cDMEM was aliquoted into 50 ml falcon tubes, parafilmed and refrigerated until further use.

2.2.3.5 Phosphate buffer saline (PBS):

10X PBS was diluted to 1X PBS by adding 5 ml 10X PBS to 45 ml of distilled H_2O (dH_2O) prior to use.

2.2.4 Preparation of experimental treatments

Following preparation, stock solutions were filter-sterilized using 0.2 µm syringe filter. They were then aliquoted and stored at -20/-80°C for future use. Experimental compounds were prepared fresh each time immediately prior to treatment by diluting stock solution to working concentration in the appropriate pre-heated media (Table 1).

Compound name	**Molecular weight (g/mol)**	**Stock Concentration**	**Pre-heated solvent**
1-MT	218.25	20 mM	cNBM[1], cDMEM[2]
KYNA	189.97	1 mM	cNBM
IFNγ	n/a	100 µg/ml	0.1% BSA[3] in PBS

Table 1: Table of compounds, molecular weights, and solvents

[1] Complete neurobasal media
[2] Complete Dulbecco's modified Eagle's medium
[3] Bovine serum albumin

2.2.5 Maintenance of the C6 glioma cell line

2.2.5.1 Resuscitation

A cryovial containing frozen down C6 glioma cells was removed from liquid nitrogen storage and thawed in the water bath as rapidly as possible to prevent the formation of intracellular ice crystals and cell death. Once defrosted, the cells were added to a new falcon tube in the laminar flow hood and 10 ml pre-warmed cDMEM was slowly added to the cells to dilute out the DMSO. The cell suspension was then centrifuged at 1,000 rotations per minute (rpm) for 5 min at 21°C.

The supernatant was removed, and the cells were resuspended in 1 ml cDMEM. Cells were counted using the trypan blue exclusion method as described above. C6 cells were subsequently seeded onto a T75 cm^2 flask at 1 x 10^6 cells/flask. The day of seeding is the days *in vitro* (DIV) 1.

2.2.5.2 Conservation

C6 glioma cells were incubated at 37°C in a 5% CO2 humidified atmosphere in cDMEM. Media was changed every other day due to their high proliferation potential. When the C6 cells became confluent, which occurred on DIV 3-4, they were split into subcultures. First, the trypsin and cDMEM were pre-warmed in the incubator. The media from the flask was aspirated, and 5 ml of trypsin was added. The flask was incubated for 5 min at 37°C. After the incubation, cells were quickly examined under the light microscope (Olympus CKX41); fully trypsinized cells should appear rounded up and no longer attached to the flask surface. 15 ml of cDMEM was added to the flask to deactivate trypsin. The cell suspension was collected, spun at 1,000 rpm for 5 min at 21°C. The supernatant was removed, and cells were resuspended in 1 ml cDMEM. The cells were counted using trypan blue exclusion method and a haemocytometer and then reseeded on T75 cm^2 flasks at 1 x 10^6 cells/flask.

2.2.5.3 Cryopreservation

C6 cells were trypsinized off T75 cm^2 flasks as described above, spun at 1,000 rpm for 5 min at 21°C. The supernatant was removed, and cells were resuspended in 1 ml cDMEM. The cells were counted using trypan blue exclusion method and a haemocytometer and frozen at a concentration of 1 x 10^6 cells/ml in a freezing solution of cDMEM supplemented with 40% FBS and 10% DMSO. The cryovials were frozen overnight in a Nalgene Mr. Frosty freezing container at -80°C. After 24 hr, cryovials were quickly transferred to liquid nitrogen for long-term storage.

2.2.5.4 Harvest of conditioned media form C6 cell culture

The C6 cells were grown to confluence which occurred on DIV 3-4. Cells were then treated for 24 hours with appropriate compound.

To obtain conditioned media for assessment of neuronal complexity and co-localized expression of synaptic markers in primary neuronal cells, C6 cells were treated with cNBM. After 24 hours treatment, CM was collected, filter-sterilized into 50 ml falcon tube using a 0.2 µm syringe filter and supplemented with 1% B-27. C6 CM was subsequently parafilmed and stored at -20^{o}C until further use.

To obtain conditioned media for assessment of microglial and astrocytic immunoreactivity, C6 cells were treated with cDMEM. After 24 hours treatment, the CM was collected and filter-sterilized into 50 ml falcon tube using a 0.2 µm syringe filter. C6 CM was subsequently parafilmed and stored at -20^{o}C until further use.

To test the effect of 1-MT on various immunocytochemical parameters, C6 cells were treated with 0.5 mM 1-MT (in cNBM for neurons or cDMEM for glia), conditioned media was collected, parafilmed and stored at -20^{o}C until further use.

To test the effect of KYNA on various immunocytochemical parameters, C6 cells were treated with 0.3 µM KYNA (in cNBM for neurons and cDMEM for glia), conditioned media was collected and transferred to neurons.

2.2.6 Preparation of Poly-D-Lysine coverslips for neurons

Poly-D-lysine was prepared by reconstituting 5 mg with 50 mL sterile dH_2O to obtain a stock concentration of 0.1 mg/ml. This solution was then filter-sterilized using a 0.2 µm syringe filter and frozen at -20°C in 5 mL aliquots until further use. Each Poly-D-lysine aliquot was diluted prior to use by adding 5 mL sterile tissue culture grade water giving a working concentration of 50 µg/mL.

Glass coverslips (13 mm) were carefully placed in the wells of a 24-well plate followed by sterilization under UV light for 60 min in a laminar flow hood. Coverslips were aseptically coated by placing a drop of Poly-D-lysine solution (75 µL) on the centre of each coverslip and incubating for 45 min. This facilitate the adhesion of neurons to the coverslip. The poly-D-lysine was then removed by aspiration and stored again at 4°C for reuse up to 3 times. Coverslips were washed twice with sterile tissue culture grade water and left to dry fully for approximately 2 hours in a laminar flow hood. Any remaining droplets were removed by aspiration with a pasteur pipette

and micropipette. Once dry, plates were either directly used for the cell culture or parafilmed and stored in the fridge for up to two weeks or at -80°C for up to two months.

2.2.7 Preparation of Poly-L-Lysine coverslips for glia

Poly-L-lysine was prepared by reconstituting 5 mg with 50 mL sterile dH_2O to obtain a stock concentration of 0.1 mg/ml. This solution was then filter-sterilized using a 0.2 µm syringe filter and frozen at -20°C in 5 mL aliquots until further use.

Glass coverslips (13 mm) were carefully placed in the wells of a 24-well plate followed by sterilization under UV light for 60 min in a laminar flow hood. Coverslips were aseptically coated by placing a drop of Poly-L-lysine solution (100 µL) on the centre of each coverslip and incubating for 10 min. The rest of the procedure was carried out as previously described.

2.2.8 Preparation of primary cortical neuronal cultures

Primary cortical neuronal cultures were prepared as previously described [143,144] from postnatal day 1-2 (P1-2) neonate Wistar rat pups under sterile conditions in a laminar flow hood. Trypsin-EDTA, B-27, NBM, DMEM and plates were pre-warmed in the CO_2 incubator prior to dissection. Neonates were decapitated using a large, sharp scissors. The skin was cut along the midline using a small scissors to reveal the skull. The skull was cut along the midline as well taking care to avoid placing pressure on the brain. Curved forceps were used to carefully remove the brain from the skull. The brain was subsequently placed onto a sterile petri dish. Straight forceps were used to remove the obvious blood vessels and surrounding meninges. The olfactory bulbs and the cerebellum were removed from the brain, and the cortical tissue from both hemispheres was placed in a drop of pre-warmed cNBM to prevent it from drying out. The cortical tissue was cross chopped using a scalpel and then transferred into 5 ml of Trypsin-EDTA for 4 min at 37°C. Following this, 5 ml of DMEM was added to deactivate trypsin. This solution was gently triturated and spun for 3 min at 2,000 rpm, 21°C. After removing the supernatant, the cell pellet was resuspended in 5 ml DMEM and quickly triturated to a homogenous suspension. The cell suspension was then passed through a cell strainer with a 40 µm filter into a new sterile falcon tube and centrifuged at 2,000 rpm for 4 min at 21°C. The supernatant was discarded. The pellet

was then resuspended in 1 ml of pre-warmed cNBM and gently triturated until a homogenous cellular suspension was obtained. The resulting neuronal cell suspension was counted using the trypan blue exclusion method.

2.2.8.1 Neuronal cell counting and plating

The trypan blue exclusion method for cell counting is based on the ability of viable cells with intact cellular membrane to exclude trypan blue dye, unlike dead cells. 1 ml of cell suspension was first diluted 1:50 in cNBM and again 1:2 with trypan blue dye, resulting in a final dilution being 1:100. A glass haemocytometer was used to count the cells under a light microscope (Olympus CKX41). The cell suspension was then diluted using cNBM to give a final concentration of 3 x 10^5 cells/ml. For Sholl analysis and synaptic protein co-localization experiments, 100 µl of this cell suspension was gently pipetted onto the centre of a poly-D-lysine coated coverslip in 24-well plates. The concentrated cells were then incubated at 37°C in a humidified, 5% CO_2 atmosphere for a minimum of 2 hours to allow adherence of neurons before being topped up with 200 µL of pre-warmed cNBM. The day of plating was referred to as *day in vitro* 0 (DIV 0). Media was replaced with fresh cNBM every 5-7 days. Neurons were left to grow on the coverslip for at least 14 days to mature. Mature neurons used for Sholl analysis and synaptic protein colocalization studies were treated with compounds at DIV 18-21 and fixed for immunocytochemistry.

2.2.9 Preparation of mixed glial cultures

Primary cortical mixed glial cultures were prepared as previously described [143] from P2-3 Wistar rat neonates under sterile conditions in a laminar flow hood. These cultures consist of approximately 70% astrocytes and 30% microglia [144]. DMEM and plates were pre-warmed in the CO_2 incubator prior to dissection. Neonates were decapitated using a large, sharp scissors. The skin was cut along the midline using a smaller scissors to reveal the skull. The skull was cut along the midline as well to avoid placing pressure on the brain. Curved forceps were used to carefully remove the brain from the skull. The brain was subsequently placed onto a sterile petri dish. Straight forceps were used to remove the obvious blood vessels and surrounding meninges. The olfactory bulbs and the cerebellum were removed from the brain, and the cortical tissue from

both hemispheres was placed in a drop of pre-warmed cDMEM to prevent it from drying out. The cortical tissue was then cross chopped and placed in 6 ml of cDMEM, followed by 20 min incubation. The tissue was subsequently triturated until the homogenous suspension, passed through sterile 40 µm cell strainer into a 50 ml falcon tube and centrifuged at 2,000 rpm for 3 min at 21°C. Depending on the assay planned to be carried out on mixed glial cultures (i.e. harvesting of conditioned media or immunohistochemistry assay), the protocol differs as outlined in sections 2.2.9.1 and 2.2.9.2.

2.2.9.1 Culturing mixed glial for the harvesting of conditioned media and primary enriched astrocytic cultures

After the removal of the supernatant, cell pellet was resuspended in 1ml cDMEM, and then added to the bottom of a T75 cm^2 flask together with 5 ml cDMEM. Flasks were placed into an incubator at 37°C, 5% CO_2 for 2 hours to allow adherence of cells to the bottom of the flask. After 2 hours, flasks were topped up by adding an additional 4 mL cDMEM. The day of plating was referred to as DIV 0. Media was replaced every 2-4 days by removing and discarding old media and pipetting 10 mL fresh, pre-warmed cDMEM down along the sides of the flask to prevent disturbing cells.

2.2.9.2 Culturing mixed glia for immunocytochemistry assay

After the tissue was centrifuged, the supernatant was removed, and the cell pellet was resuspended in 2.4 ml cDMEM. 100 µL of the cell suspension was added to each well and left to incubate for 2 hours to allow adherence. Wells were topped up with 200 µl cDMEM after 2 hours. Mixed glia were treated when confluent (DIV 8-12).

2.2.10 Preparation of enriched primary astrocytic cultures

Primary astrocytic cultures were prepared from primary mixed glial cultures as described above [144]. Once 90% confluent, the mixed glia were separated by placing the T75 cm^2 flasks in an orbital cell shaker at 200 rpm for 2 hours at 37°C to remove microglia from the astrocytic

monolayer. Flasks were tapped 10 times on the culture hood surface to encourage the separation of microglial cells. Cells were scraped and the cell suspension was collected and centrifuged at 2,000 rpm for 5 minutes at 21°C. The supernatant was discarded, and the pellet was resuspended in 2.4 ml cDMEM. 100 µl of cell suspension was added to each well and left to incubate for 2 hours to allow adherence. Wells were topped up with 200 µl cDMEM after 2 hours. Astrocytes were treated approximately 24-48 hours after plating.

2.2.11 Analysis of cell viability using the CCK-8 assay

The Cell Counting Kit-8 (CCK-8) assay (Dojindi labs, Kumamoto, Japan) was used to measure neuronal viability in accordance with the manufacturer's protocol. Mature neurons (DIV21) were treated, and after the appropriate number of hours the treatment was removed and replaced with 6.25% CCK-8 solution in media. 320 µL of fresh CCK-8 solution was added per well. The plate was subsequently incubated at 37°C for 1 hour and 100 µL sample from each well was then transferred to individual wells of a 96-well plate. The plate was read using a microplate reader at an absorbance λ of 450 nm.

CCK-8 allows very convenient sensitive colorimetric assay for determination of viable cell numbers and can be used for cell proliferation assays as well as cytotoxicity assays. It uses Dojindo's highly water-soluble tetrazolium salt WST-8 (5-(2,4-disulfophenyl)-3-(2-methoxy-4-nitrophenyl)-2-(4-nitrophenyl)-2H-tetrazolium) and produces a water-soluble formazan dye WST-8 formazan upon reduction in presence of an electron mediator. WST-8 is reduced by dehydrogenases in cells to give an orange coloured product WST-8 formazan. The amount of the formazan dye generated by dehydrogenases in cells is directly proportional to the number of living cells [145–147].

2.2.12 Neuronal immunocytochemistry

2.2.12.1 Neuron staining with MAP2 for the Sholl analysis

Following treatment, media was removed from each well and the cells were fixed in 4% paraformaldehyde (PFA) by adding 400 µL 4% PFA in PBS to each well for 20 min at room

temperature. PFA was then removed, and the coverslips were washed 3 times with PBS. After 3 washes, non-specific interactions were blocked by adding 300 µL blocking buffer containing 2% normal goat serum (NGS), and 2% bovine serum albumin (BSA) in PBS containing 0.1% Triton-X (PBS-T) to each well and the plate was left on a rocker (Stuart Scientific 3D Gyratory Rocker) at room temperature for 2 hours. The blocking buffer was subsequently discarded. 200 µl of primary antibody containing microtubule-associated protein 2 (MAP2, [mouse; M1406]) in blocking buffer (1:1000) was added to each well and left refrigerated overnight. The primary antibody was removed, and the cells were washed three times in PBS, each wash for 5 min on the rocker. Secondary antibody containing Alexa Fluor 546 [goat anti-mouse; A11003] in PBS-T (1:500) was added and left for 2 hours on a rocker at room temperature in a light-protected environment by wrapping in tinfoil. Secondary antibody was removed, and cells were washed three times with PBS, each wash for 5 min on the rocker. Glass coverslips were then removed and mounted onto glass slides for imaging and Sholl analysis. A small drop of Vectashield fluorescent mounting media containing DAPI (4´,6-Diamidino-2-phenylindole dihydrochloride), which is a counterstain for DNA, was placed on the microscope slides (1-1.2 mm). Coverslips were lifted from the plate using forceps and a needle and placed inverted onto the drop of mounting medium. Any excess of the Vectashield was gently removed using tissue paper. Coverslips were left to dry for approximately 2 hours in a light-protected environment. The edges of the coverslips were then sealed using nail varnish and the slides were left to dry before storage in the dark at 4°C.

Coverslips were visualized using an AxioImager Z1 epifluorescent microscope with a Zeiss AxioCam HR camera and AxioVision 4.8.2 software at 20X magnification. In order to be included in the analysis, coverslips had to display a healthy neuronal network throughout the visual field. 7 individual images were taken per coverslip and 6 coverslips (replicates) per experimental condition were typically collected for analysis. Where possible, experimenter was blind to treatment, and cells were selected in the DAPI channel to avoid bias.

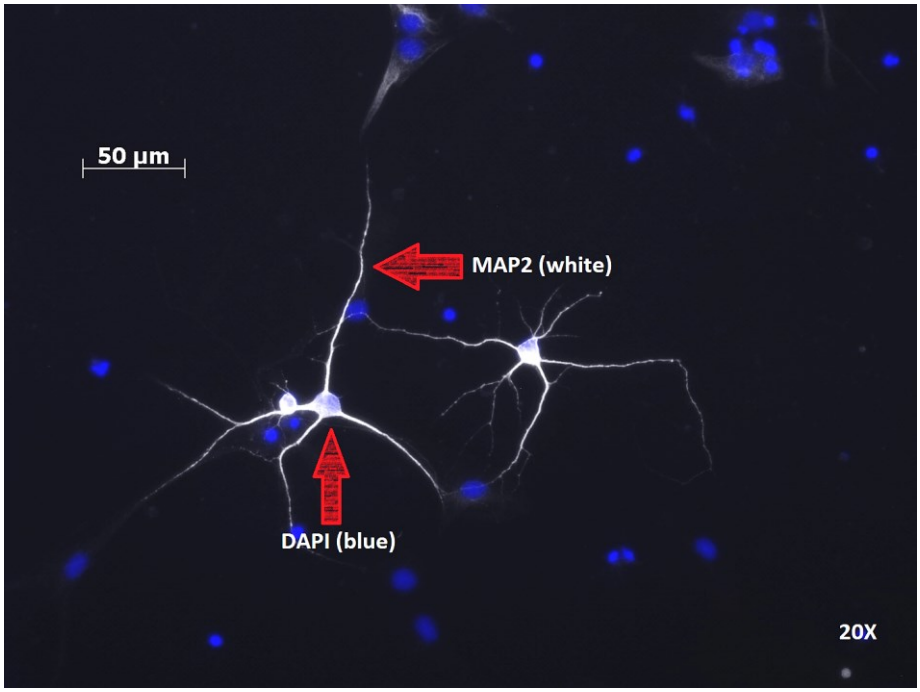

Figure 4: Representative image of MAP2 stained neurons

Representative cultures of mature (DIV 21) primary cortical neurons stained with anti-MAP2 (white) and DAPI (blue) followed by fluorescent microscopy (20X magnification).

2.2.12.2 Sholl analysis

Sholl analysis is a widely used method for quantifying and graphically representing various parameters of neuronal complexity following treatment. The simplified version of this protocol (Fast Sholl) was adapted from Sholl [148] and Gutierrez and Davies [149]. This analysis involves placing 25 concentric rings with regular 10 µm radial increments around the neuron and quantifying the number of neurites intersecting each ring using the following equation: xi = xi-1 + bi – ti, where "xi" is the number of neurites for the "ith" segment, "bi" is the number of branches occurring in the "ith" segment and "ti" the number of terminations in that segment. This equation was programmed into Matrix Laboratory (MATLAB, R2012b) to follow a semi-automated procedure. The number of neuritic branches, relative neuritic length, number of primary neurites and Sholl profile were determined for each neuron. The Sholl profile represents the number of neuritic branches at each radial distance from the cell soma.

A

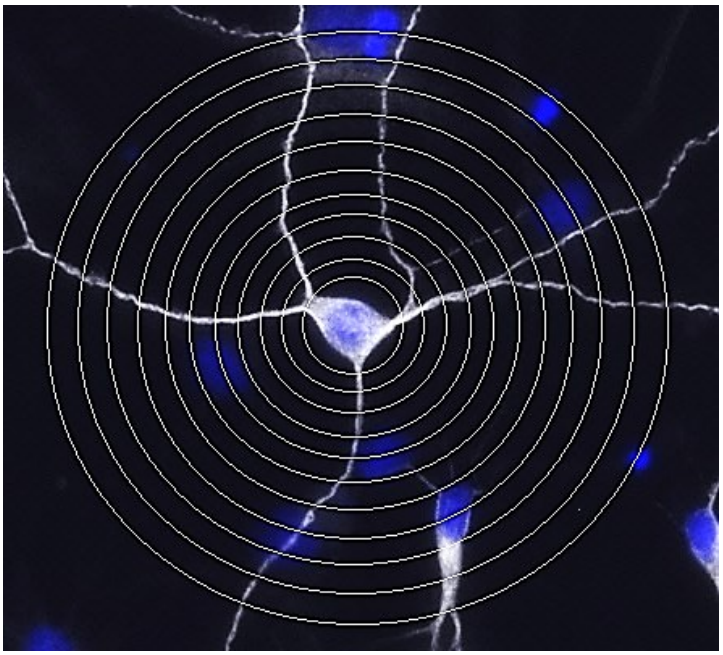

B

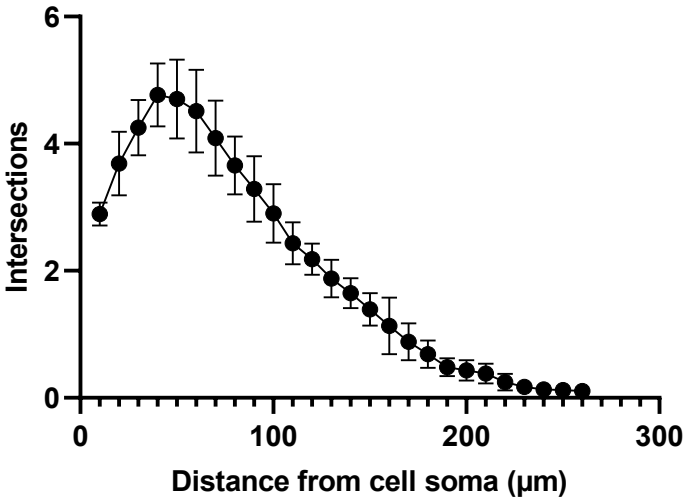

Figure 5: Sholl analysis

Fluorescent image of a rat cortical neuron stained with MAP2 (white) and DAPI (blue) with overlaying concentric rings (A) and a typical Sholl profile (B).

2.2.12.3 Neuron staining with synaptic markers and analysis of their co-localization

Mature neurons (DIV 18-21) were treated for the appropriate number of hours and fixed in ice-cold methanol. The cells were permeabilized and blocked using a blocking buffer consisting of 50% NGS + 0.2% Triton-X in PBS for 30 min at room temperature on a rocker. The blocking buffer was then removed, and cells were washed with PBS. 200 µl of primary antibody cocktail raised against the pre-synaptic marker synaptophysin [rabbit; PA1-1043] and the post-synaptic marker post-synaptic density protein 95 (PSD95) [mouse; MA1-046] diluted in PBS (1:500) was added to each well and left refrigerated overnight. 200 µl of secondary antibody cocktail containing Alexa Fluor secondary antibody 546 [goat anti-rabbit; A11010] and Alexa Fluor 488 secondary antibody [goat anti-mouse; A11001] diluted in PBS (1:1000) was added to the wells and left for 2 hours on a rocker at room temperature in a light-protected environment by wrapping in tinfoil. Secondary antibody was removed, and cells were washed three times with PBS. Each wash was performed for 5 min on a rocker. Glass coverslips were then removed and mounted onto glass slides as described above.

Coverslips were visualized at 40X magnification using an AxioImager Z1 epifluorescent microscope with a Zeiss AxioCam HR camera and AxioVision 4.8.2 software. In order to be included in the analysis, coverslips had to display a healthy neuronal network throughout all its area. 7 individual images were taken per coverslip and 6 coverslips (replicates) per experimental condition were typically collected for analysis. Where possible, the experimenter was blinded to treatment, and cells were selected in the DAPI channel to avoid bias. The optimum exposure intensity for both synaptophysin and PSD95 channels was determined using a control coverslip that was maintained throughout.

2.2.12.4 Analysis of co-localization of synaptic markers in mature neurons

The analysis was adapted from Ippolito and Eroglu [150], using the ImageJ analysis programme (NIH) and the Puncta Analyser plug-in written by Barry Wark. For image analysis, individual images were opened in ImageJ and a region of interest was outlined using a free hand selection. The Puncta Analyser was used to adjust the thresholds of the red channel (synaptophysin) and green channel (PSD95) so that the intensity corresponded to discrete individual puncta. Minimum puncta size was set at a value of 4 pixels for this experiment. Threshold values were

standardized based on control-treated neurons in order to maintain a consistent approach for comparison between groups. For the purpose of this analysis, synapses were defined as 'puncta', or co-localized puncta resulting from the signal generated with the pre-synaptic synaptophysin and post-synaptic PSD95. The number of co-localized puncta were quantified using the ImageJ ''Puncta Analyser'' plugin.

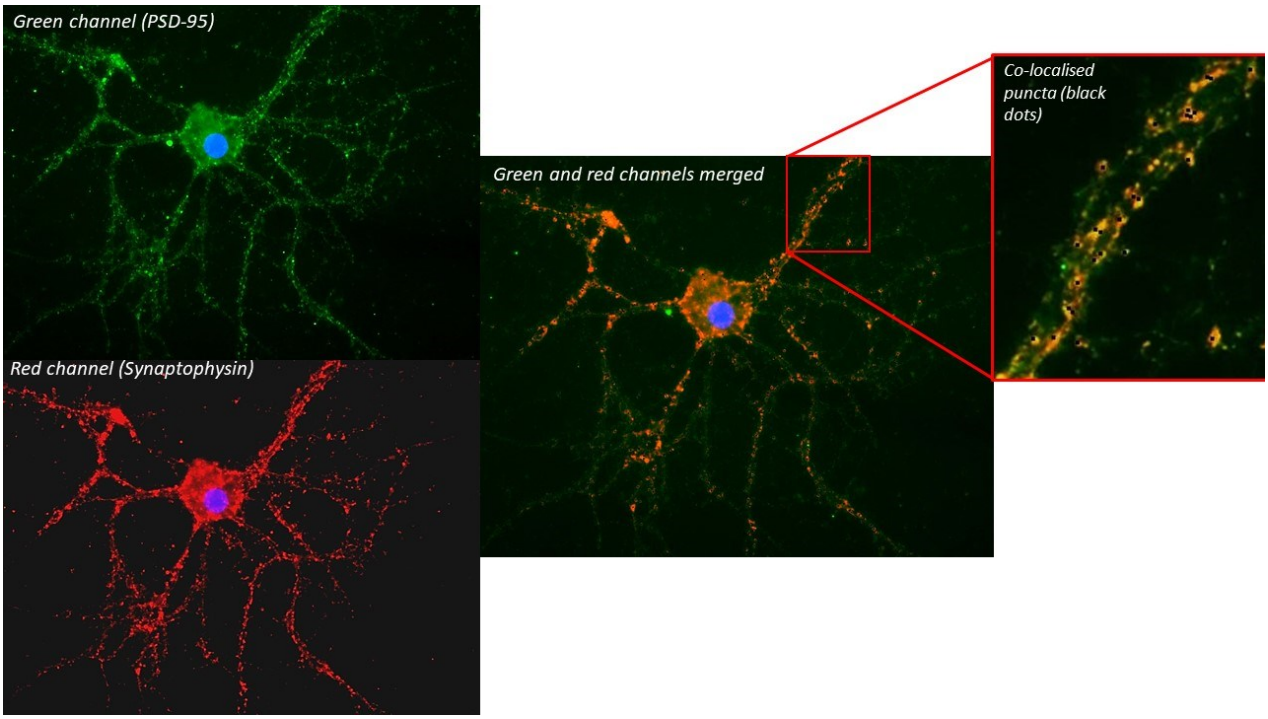

Figure 6: Flourescent image of mature neurons stained with anti-synaptophysin and anti-PSD95

Neurons stained with the presynaptic marker, synaptophysin (red channel image) and the post-synaptic marker, PSD95 (green channel image). Merged image (and inset) displays points of co-localization (black dots).

2.2.13 Glial immunocytochemistry

2.2.13.1 Iba1 staining for microglia

For microglia complexity and immunofluorescence cells were fixed with 4% PFA for 30 min in a fume hood. Cells were then washed 3 times with PBS. Non-specific binding sites were blocked by

applying a blocking buffer containing 5% horse serum and 2% donkey serum in PBS-T for 30 min on a rocker. After 30 min the blocking buffer was removed and 200 µL anti-Ionized calcium binding adaptor molecule 1 (Iba1) primary antibody [polyclonal goat; ab5076] in blocking buffer (1:1000) was added to each well and left refrigerated overnight. After 3 x 5 min washes, cells were stained with 200 µL Alexa Fluor 488 secondary antibody [mouse anti-goat; A27012] diluted in PBS (1:500) and left for 2 hours on a rocker at room temperature in a light-protected environment by wrapping in tinfoil. Secondary antibody was removed, and cells were washed three times (3 x 5 min washes) with PBS before adding dH_2O to each well. The glass coverslips were subsequently removed and mounted onto glass slides as described above.

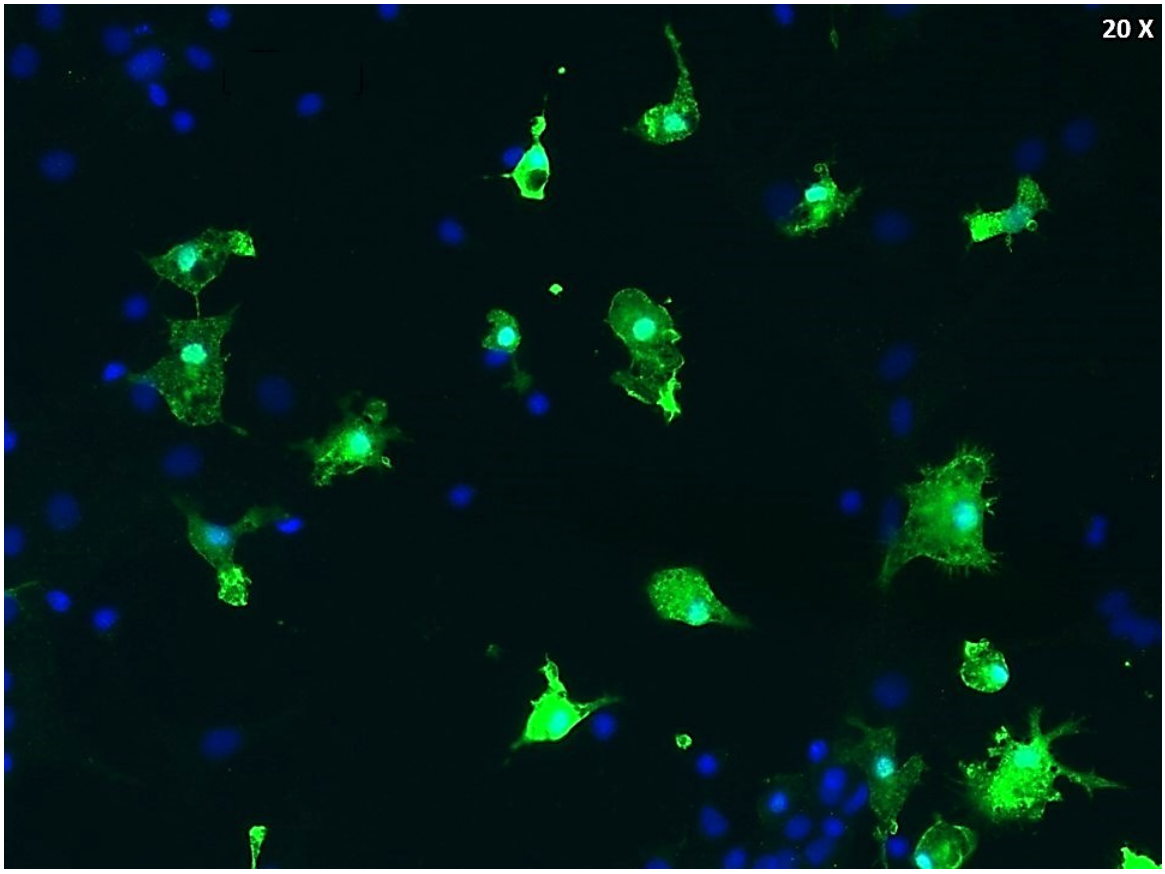

Figure 7: Fluorescent image of mixed glial cultures stained for IBA1

Representative cultures of primary microglia cultures stained with anti-Iba1 (green) and DAPI (blue).

2.2.13.2 GFAP staining for astrocytes

Enriched astrocyte cultures were fixed with 4% PFA for 30 min in a fume hood. Cells were then washed 3 times with PBS. Non-specific binding sites were blocked by applying a blocking buffer (5% horse serum and 2% donkey serum in PBS-T) for 30 min on a rocker. After 30 min the blocking buffer was removed and 200 µL anti-glial fibrillary acidic protein (GFAP) primary antibody [rabbit; Z0334] diluted in blocking buffer (1:500) was added to each well and left refrigerated overnight. After 3 x 5 min washes, cells were stained with 200 µL Alexa Fluor 488 secondary antibody [goat anti-rabbit; A11008] diluted in PBS (1:500) and left for 2 hours on a rocker at room temperature in a light-protected environment provided by wrapping in tinfoil. Secondary antibody was removed, and cells were washed three times for 5 min with PBS. Glass coverslips were then removed and mounted onto glass slides as described above.

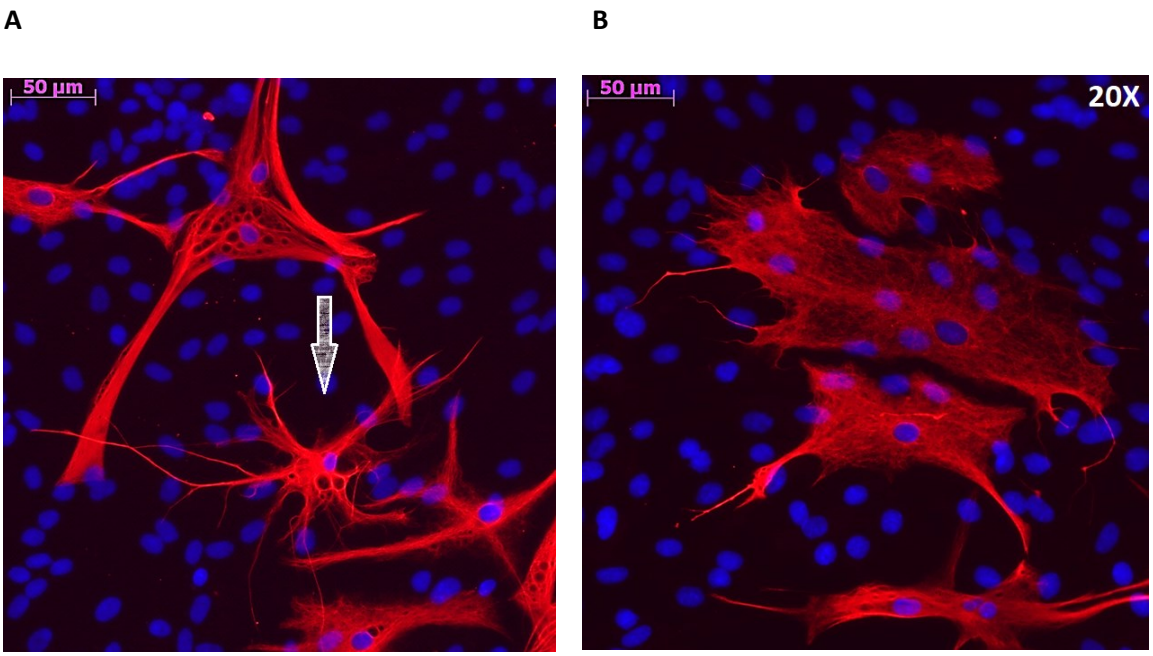

Figure 8: Fluorescent image of mixed glial culture stained for GFAP

Representative images of mixed glial culture stained with anti-GFAP (red) and DAPI (blue); A – white arrow indicates a nonreactive astrocyte, B – activated astrocytes.

2.2.13.3 Analysis of microglial complexity and immunofluorescence

Coverslips were visualised at 20X magnification using an AxioImager Z1 epifluorescent microscope with a Zeiss AxioCam HR camera and AxioVision 4.8.2 software. 7 images were taken per coverslip and, where possible, 5 cells were analysed per image. A constant exposure was maintained throughout all images. Mean cell area and perimeter were quantified using the particle measurement feature on ImageJ (1.51s, USA). Iba1 immunoreactivity was quantified by calculating the corrected total cell fluorescence (CTCF) using the ImageJ integrated density feature. A total of 5 microglia cells was analysed per treatment group per experiment where possible (the experiment was repeated three times). The following formula was applied to account for non-fluorescent background regions:

CTCF = [integrated density – (area of selected cell x mean fluorescence of background readings)]

2.2.14 Quantitative polymerase chain reaction (qPCR)

2.2.14.1 Harvesting cells for mRNA analysis

Prior to carrying out ribonucleic acid (RNA) extraction all surfaces were wiped down with RNaseZap® wipes to prevent RNA breakdown or contamination. Following cell culture treatment, media was removed, and cells were lysed by adding 350 µl RA1 lysis buffer supplemented with 1% β-mercaptoethanol to each well. Cells were pooled where necessary. Cells were scraped from the base of wells using a 1000 µl filtered pipette tip and the lysate was transferred to a 2 ml RNase-free Eppendorf. Pipette tips were changed between treatment groups in order to prevent cross-contamination. Cell lysates were harvested and stored at -80°C for subsequent RNA extraction.

2.2.14.2 RNA extraction

RNA was extracted from samples using a NucleoSpin® RNA kit according to the procedure outlined in the manufacturer's instructions. Cell lysates were added to Nucleospin® filter columns in a collecting tube and filtered using a centrifuge for 1 minute at 11,000 x g. The filter column was discarded and 350 µl of 70% EtOH was added to the filtered lysate and mixed by pipetting up and down approximately five times to adjust RNA binding conditions. The mixture was then loaded into a NucleoSpin® RNA column and centrifuged for 30 seconds at 11,000 x g in order to let the RNA bind to the silica column. The silica membrane was placed in a new collecting tube (2 ml) and was desalted using 350 µl of Membrane Desalting Buffer (MDB) to allow the recombinant deoxyribonuclease (rDNase) digest more effectively and centrifuged for 1 minute at 13,000 rpm. 95 µl of the rDNase reaction mixture (10 µl reconstituted rDNase and 90 µl Reaction Buffer for rDNase) was added onto the centre of the silica membrane of the NucleoSpin® RNA column and left for 15 minutes at room temperature. Following incubation, the silica membrane was washed several times in order to digest any contaminating DNA. Firstly, the membrane was washed using 200 µl of Buffer RA2 to inactivate the rDNAse and centrifuged for 30 seconds at 11,000 x g. The column was then changed to a new 2 ml collection tube. The membrane was dried by washing two more times using 600 µl RA3 and centrifuging for 30 seconds at 13,000 rpm and then using 250 µl RA3 and centrifuging for 2 minutes at 11,000 x g. The column was then placed into a nuclease-free collection tube and the flow-through discarded. The pure RNA was eluted in 40 µl RNase free water by centrifuging for 1 minute at 11,000 x g into a new RNase-free collection Eppendorf. RNA samples were either equalised or stored at -80°C until required.

2.2.14.3 RNA equalization

RNA extraction samples prepared above were defrosted slowly on ice if they had been stored at -80°C. They were kept on ice throughout the RNA equalization procedure. A Nanodrop® ND1000 was the spectrophotometer used to quantify total RNA concentrations in each sample. 1 µl of RNase-free water was used to blank the Nanodrop. Samples were gently and quickly vortexed prior to reading. Two absorbance readings (ng/ml) were obtained for 1 µl of each RNA sample in duplicate and a final average concentration was recorded. Purity was demonstrated by the A260/280 ratio where a ratio of 2 indicates highly pure RNA. The sensor was cleaned with

absorbent paper between sample readings. The RNA samples were equalised using RNase-free H_2O to the lowest recorded concentration of RNA.

2.2.14.4 Complementary deoxyribonucleic acid (cDNA) synthesis

cDNA was reverse transcribed from equalised RNA using a High Capacity cDNA Reverse Transcription Kit according to the protocol provided. An equal volume of equalised RNA (10 µl) was mixed with an equal volume (10 µl) of cDNA Mastermix (containing RT Buffer (Reverse Transcriptase), dNTPs, random primers, multiscribe RT and RNase-free H_2O). The samples were mixed, briefly centrifuged and placed into a Thermal Cycler and set to the "AbCDNA" programme which ran at 25°C for 10 minutes, 37°C for 120 minutes and 85°C for 5 minutes. Upon completion of the programme, the samples were removed and frozen at -20°C until required for PCR analysis.

2.2.14.5 Real-time Polymerase Chain Reaction (RT-PCR)

Assessment of target genes was carried out using Taqman® Gene Expression Assays, containing specific target primers and a FAM® dye labelled MGB (minor groove binding) target probe. Glyceraldehyde-3-phosphate dehydrogenase (GAPDH) was used as an endogenous control to normalise gene expression between samples and was quantified using a VIC-labelled probe for rat GAPDH.

4 µl of each cDNA sample was added to an individual well in a PCR plate. Primer mixes were made up using TaqMan® Fast Advanced Master Mix, the primer of interest and GAPDH as the endogenous control. Primers were gently vortexed and 6 µl was added to each well making up a final volume of 10 µl. The plate was sealed with an optically clear plastic cover and centrifuged at 800 rpm, 4^{o} for 30 seconds. The plate was analysed using the quantitative PCR thermocycler and Step One software. The Comparative CT method and fast run were chosen, and the target gene expression was assessed using a TaqMan gene expression assay. Target gene expression was assessed relative to the endogenous control GAPDH. Samples were assayed in one run (40 cycles), which consists of 2 stages: Holding stage [50°C for 2 minutes, and 95°C for 20 seconds] and a Cycling stage [95°C for 1 second, and 60°C for 20 seconds].

Target	TaqMan Gene Expression Assay ID
IDO1	Rn01482210_m1
KMO	Rn00665313_m1
KYNU	Rn00588108_m1
TDO2	Rn00574499_m1

Table 2: List of target probes used in PCR

2.2.14.6 Analysis of quantitative PCR data

The gene expression of all the quantitative PCR was assessed using the ΔΔCT method (Applied Biosystems RQ software). This method quantifies gene expression of treated samples to a control sample as 'fold change' i.e. the difference in the number of cycles (CT) between sample and control. It involves setting a fluorescence threshold when the PCR reaction is in the exponential phase i.e. when the PCR reaction is optimal or 100% efficient. It is this threshold against which CT is measured to provide a measure of gene expression. Samples demonstrating high fluorescence have low CT readings indicating greater amplification and hence, greater gene expression. When a PCR is 100% efficient a difference of one-cycle indicates a 2-fold difference in copy number, similarly a 5-fold difference indicates a 32-fold difference. Fold change is quantified by subtracting the CT of the endogenous control (GAPDH) from the CT of the target gene for each sample. This difference denoted as ΔCT indicates differences in cDNA quantity. The ΔCT of the control sample is then subtracted from itself and all the other samples giving the ΔΔCT (cycle difference corrected for endogenous control). The control sample always has a ΔΔCT value 70 of 0. ΔΔCT is converted into a fold difference which is used to determine related change in expression. qPCR data was exported into an Excel file and fold change values were visualised using GraphPad Prism 8.

2.3 Statistical analysis

All data were analysed using GraphPad Prism 8. Statistical tests including Unpaired *t*-test or analyses of variance (ANOVA) were performed where relevant. In cases where a statistically significant change was found following one- or two-way ANOVA, *post hoc* comparisons were performed to identify group differences using the Newman-Keuls test. Repeated measures ANOVA was used to analyse Sholl profile data. PCR data was normalised to express results as a fold change of control samples. Data were deemed significant when P <0.05 (*), P <0.01 (**), P <0.001 (***) or P<0.0001 (****).

2.4 Study design

Experiment	**Treatment time**	**Treatment groups**	**Method**
Effect of conditioned media from IFNγ exposed mixed glia on the complexity of mature primary cortical neurons	24 h	1. CM Mixed glia 2. CM IFNγ Mixed Glia	ICC (MAP2) Sholl analysis
Effect of conditioned media from IFNγ exposed mixed glia on the co-localized expression of synaptic markers in mature primary cortical neurons	24 h	1. CM Mixed glia 2. CM IFNγ Mixed Glia	ICC (Synaptophysin and PSD-95) Quantification of synaptic puncta
Effect of 1-MT on reductions in complexity of mature primary cortical neurons induced by conditioned media from IFNγ exposed mixed glia	24 h	1. CM Mixed Glia 2. CM Mixed Glia 1-MT 3. CM IFNγ Mixed Glia 4. CM IFNγ + 1-MT Mixed Glia	ICC (MAP2) Sholl analysis
Effect of 1-MT on reductions in on the co-localized expression of synaptic markers in mature primary cortical neurons induced by conditioned media from IFNγ exposed mixed glia	24 h	1. CM Mixed Glia 2. CM Mixed Glia 1-MT 3. CM IFNγ Mixed Glia 4. CM IFNγ + 1-MT Mixed Glia	ICC (Synaptophysin and PSD-95) Quantification of synaptic puncta
mRNA expression of KP enzymes in primary cortical astrocytes, mixed glia, IFNγ exposed mixed glia and C6 cells	24 h	1. Primary cortical astrocytes 2. Mixed Glia 3. IFNγ exposed Mixed Glia 4. C6 cells	qRT-PCR
Effect of C6 CM on the viability of mature primary cortical neurons	24 h, 48 h	1. CM Mixed Glia 2. C6 CM	CCK-8 viability assay

Effect of C6 CM on the complexity of mature primary cortical neurons	24 h	1. CM Mixed Glia 2. C6 CM	ICC (MAP2) Sholl analysis
Effect of C6 CM on the co-localized expression of synaptic proteins in mature primary cortical neurons	24 h	1. CM Mixed Glia 2. C6 CM	ICC (Synaptophysin and PSD-95) Quantification of synaptic puncta
Effect of C6 CM on microglial morphology and IBA1 immunoreactivity in mixed glial culture	24 h	1. Control (DMEM) 2. C6 CM	ICC (IBA1)
Effect of C6 CM on astrocyte morphology and GFAP immunoreactivity in mixed glial culture	24 h	1. Control (DMEM) 2. C6 CM	ICC (IBA1)
Effect of 1-MT on reductions in neuronal complexity induced by C6 CM	24 h	1. CM Mixed Glia 2. CM 1-MT Mixed Glia 3. C6 CM 4. 1-MT C6 CM	ICC (MAP2) Sholl analysis
Effect of 1-MT on reductions in co-localized expression of synaptic markers induced by C6 CM	24 h	1. CM Mixed Glia 2. CM 1-MT Mixed Glia 3. C6 CM 4. 1-MT C6 CM	ICC (Synaptophysin and PSD-95) Quantification of synaptic puncta
Effect of 1-MT on C6 CM induced changes in microglial morphology and IBA1 immunoreactivity in mixed glia culture	24 h	1. Control (DMEM) 2. 1-MT 3. C6 CM 4. 1-MT C6 CM	ICC (IBA1)
Effect of 1-MT on C6 CM induced changes in astrocyte morphology and GFAP immunoreactivity in mixed glia culture	24 h	Control (DMEM) 1-MT 0,5 mM (DMEM) C6 CM C6 CM+1-MT 0,5 mM	ICC (GFAP)
Effect of direct KYNA treatment on the co-localized expression of synaptic proteins in mature primary cortical neurons	24 h	Control (NBM) KYNA 0.03 µM KYNA 0.1 µM KYNA 0.3 µM	ICC (Synaptophysin and PSD-95) Quantification of synaptic puncta
Effect of KYNA on reductions in neuronal synaptic protein co-localization induced by C6 conditioned media	24 h	CM Mixed Glia C6 CM C6 CM + KYNA 0.3 µm	ICC (Synaptophysin and PSD-95) Quantification of synaptic puncta

Table 3: Table of experimental plan

2.4.1 The effect of conditioned media from IFNγ exposed mixed glia on the complexity and co-localized expression of synaptic proteins in mature primary cortical neuronal cultures

2.4.1.1 The effect of CM from IFNγ exposed mixed glia on complexity of primary cortical neurons

Mixed glia cultures (DIV14) were treated with IFNγ (10 ng/ml in cNBM) for 24 hours, and the resulting CM was collected and transferred to mature primary cortical neurons (DIV21) for 24 hours. For comparison, mixed glial culture was treated with cNBM for 24 hours, and the resulting CM was collected and transferred to mature primary cortical neurons (DIV21) for 24 hours. Cells were fixed, and MAP2 immunocytochemistry and Sholl analysis were performed to determine neuronal complexity.

The time point was chosen based on prior research in our lab which demonstrated that conditioned media from IFNγ (10 ng/mL) treated mixed glia reduced the complexity of immature neurons after 24 hr exposure *in vitro*.

2.4.1.2 The effect of CM from IFNγ exposed mixed glia on the synaptic protein co-localization

Mixed glial cultures (DIV14) were treated with IFNγ (10 ng/ml in cNBM) for 24 hours, and the resulting CM was collected and transferred to mature primary cortical neurons (DIV21) for 24 hours. For comparison, mixed glial cultures were treated with cNBM for 24 hours, and the resulting CM was collected and transferred to mature primary cortical neurons (DIV21) for 24 hours. Cells were fixed, and Synaptophysin/PSD-95 immunocytochemistry was performed to determine co-localization of these synaptic proteins.

2.4.2 The effect of 1-MT on reductions in complexity and co-localized expression of synaptic proteins induced by conditioned media from IFNγ treated mixed glia in mature primary cortical neuronal cultures

2.4.2.1 The effect of 1-MT on reductions in neuronal complexity induced by CM from IFNγ treated mixed glia

Mixed glial cultures (DIV14) were co-treated with 1-MT (0.5 mM) and IFNγ (10 ng/ml in cNBM) or vehicle (cNBM) for 24 hours and the resulting CM was collected and transferred to mature primary cortical neurons (DIV21) for 24 hours. Cells were fixed, and MAP2 immunocytochemistry and Sholl analysis were performed to determine neuronal complexity.

2.4.2.2 The effect of 1-MT on reductions in co-localized expression of synaptic proteins induced by CM from IFNγ treated mixed glia

Mixed glia culture (DIV14) was co-treated with 1-MT (0.5 mM) and IFNγ (10 ng/ml in cNBM) or vehicle (cNBM) for 24 hours and the resulting CM was collected and transferred to mature primary cortical neurons (DIV21) for 24 hours. Cells were fixed, and Synaptophysin/PSD-95 immunocytochemistry was performed to determine co-localization of these synaptic proteins.

2.4.3 mRNA expression of KP enzymes in primary cortical astrocytes, mixed glia, IFNγ exposed mixed glia and C6 cells

2.4.3.1 mRNA expression of KP enzymes in primary cortical astrocytes and C6 cells

To investigate the mRNA expression of KP enzymes, primary cortical astrocytes and C6 cells were treated with vehicle (cDMEM) for 24 hours. Cells were harvested for RNA extraction, followed by RT-PCR. mRNA expression of IDO1, KYNU, TDO2 and KMO enzymes was quantified.

2.4.3.2 mRNA expression of KP enzymes in mixed glia, IFNγ exposed mixed glia, and C6 cells

To investigate the mRNA expression of KP enzymes, mixed glial cultures were treated with IFNγ (10 ng/ml) for 24 hours. Mixed glia and C6 cells were treated with vehicle (cDMEM) for 24 hours. Cells were harvested for RNA extraction, followed by RT-PCR. mRNA expression of IDO1, KYNU, TDO2 and KMO enzymes was quantified.

2.4.4 The effect of conditioned media from C6 glioma cells on the viability, complexity and co-localized expression of synaptic proteins in mature primary cortical neuronal culture

2.4.4.1 The effect of CM from C6 glioma cell line on neuronal viability

C6 cell culture was treated with cNBM for 24 hours, and the resulting CM was collected and transferred to mature primary cortical neurons (DIV21) for 24 and 48 hours. CCK-8 viability assay was employed to determine the effect of C6 CM on neuronal viability.

2.4.4.2 The effect of CM from C6 glioma cell line on neuronal complexity

C6 cell culture was treated with cNBM for 24 hours, and the resulting CM was collected and transferred to mature primary cortical neurons (DIV21) for 24 hours. For comparison, mixed glial culture was treated with cNBM for 24 hours, and the resulting CM was collected and transferred to mature primary cortical neurons (DIV21) for 24 hours. Cells were fixed, and MAP2 immunocytochemistry and Sholl analysis was performed to determine neuronal complexity.

2.4.4.3 The effect of CM from C6 glioma cell line on co-localized expression of synaptic markers

C6 cell culture was treated with cNBM for 24 hours, and the resulting CM was collected and transferred to mature primary cortical neurons (DIV21) for 24 hours. For comparison, mixed glial culture was treated with cNBM for 24 hours, and the resulting CM was collected and transferred to mature primary cortical neurons (DIV21) for 24 hours. Cells were fixed, and Synaptophysin/PSD-95 immunocytochemistry was performed to determine co-localization of these synaptic proteins.

2.4.5 The effect of conditioned media from C6 glioma cells on the morphology of microglia and astrocytes in primary mixed glial cultures

2.4.5.1 The effect of CM from C6 glioma cell line on microglial morphology

C6 cell culture was treated with cDMEM for 24 hours, and the resulting CM was collected and transferred to mixed glial culture (DIV14). For comparison, mixed glial cultures were treated with cDMEM for 24 hours. Cells were fixed, and IBA1 immunocytochemistry was performed to determine the morphology of microglial cells.

2.4.5.2 The effect of CM from C6 glioma cell line on astrocytic morphology

C6 cell culture was treated with cDMEM for 24 hours, and the resulting CM was collected and transferred to mixed glial culture (DIV14). For comparison, mixed glial cultures were treated with cDMEM for 24 hours. Cells were fixed, and GFAP immunocytochemistry was performed to determine the morphology of astrocytic cells.

2.4.6 The effect of 1-MT on conditioned media from C6 cells induced reductions in complexity and co-localized expression of synaptic proteins in mature primary cortical neuronal cultures

2.4.6.1 The effect of 1-MT on C6 CM induced reductions in neuronal complexity

C6 cells and mixed glial cultures were treated with 1-MT (0.5 mM in cNBM) or vehicle (cNBM) for 24 hours, and the resulting CM were collected and transferred to mature primary cortical neurons (DIV21) for 24 hours. Cells were fixed, and MAP2 immunocytochemistry was performed to determine by Sholl analysis.

2.4.6.2 The effect of 1-MT on C6 CM induced reductions in co-localized expression of synaptic proteins in mature primary cortical neuronal cultures

C6 cells and mixed glial cultures were treated with 1-MT (0.5 mM in cNBM) or vehicle (cNBM) for 24 hours, and the resulting CM was collected and transferred to mature primary cortical

neurons (DIV21) for 24 hours. Cells were fixed, and synaptophysin and PSD-95 immunocytochemistry were performed to determine co-localized expression of synaptic proteins.

2.4.7 The effect of 1-MT on conditioned media from C6 cells induced changes in microglial and astrocytic morphology, IBA1 and GFAP immunoreactivity

2.4.7.1 The effect of 1-MT on C6 CM induced IBA1 and GFAP immunoreactivity and changes in microglial and astrocytic morphology respectively, in mixed glia culture

C6 cells were treated with 1-MT (0.5 mM in cDMEM) for 24 hours, and the resulting CM was collected and transferred to mixed glial culture (DIV14) for 24 hours. As a control group, mixed glial cultures were treated with DMEM for 24 hours (control group).

Mixed glial cultures were also treated with 1-MT (0.5 mM in cDMEM) for 24 hours.

Cells were fixed, and IBA1 and GFAP immunocytochemistry were performed to determine the effect of 1-MT on C6 CM induced IBA1/GFAP immunoreactivity and changes in microglial/astrocytic morphology.

2.4.8 The effect of KYNA on conditioned media from C6 cells induced reductions in co-localized expression of synaptic proteins in mature primary cortical neuronal cultures

2.4.8.1 The effect of direct KYNA treatment on the co-localized expression of synaptic proteins in mature primary cortical neurons

Mature primary cortical neurons (DIV21) were directly treated with 0.03 µM, 0.1 µM and 0.3 µM KYNA (in cNBM) for 24 hours. Cells were fixed, and Synaptophysin/PSD-95 immunocytochemistry was performed to determine co-localization of these synaptic proteins.

Concentrations of kynurenic acid were chosen based on previous work investigating its effect on primary neurons. Previous findings in the lab demonstrate that that KYNA (0.03 µM) increases neuronal viability, while having no effect on the viability of either immature or mature neurons

at any other concentration tested [151]. Additional findings have shown that KYNA has no effect on neuronal viability at concentrations ranging from 0.1-1000 µM [152].

2.4.8.2 The effect of KYNA on C6 CM related reductions in neuronal synaptic protein co-localization

C6 cells were treated with 0.3 µM KYNA (in cNBM) for 24 hours, and the resulting CM was collected and transferred to mature primary cortical neurons (DIV21) for 24 hours. For comparison, mixed glial cultures were treated with cNBM for 24 hours, and the resulting CM was collected and transferred to mature primary cortical neurons (DIV21) for 24 hours. Cells were fixed, and Synaptophysin/PSD-95 immunocytochemistry was performed to determine co-localization of these synaptic proteins.

3 Results

3.1 The effect of conditioned media from IFNγ exposed mixed glia on the complexity and co-localized expression of synaptic proteins in mature primary cortical neuronal cultures

3.1.1 The effect of conditioned media from IFNγ exposed mixed glia on complexity of primary cortical neurons

Transfer of CM from IFNγ treated mixed glia to primary cortical neurons provoked a reduction in the number of neuritic branches [P = 0.0001], neuritic length [P < 0.0001] but no effect on the number of primary neurites when compared to mixed glia CM control [Unpaired t-tests, Figure 9 A, B, C].

Two-way ANOVA of the number of neuritic branches at specific distances from the neuronal cell soma showed an effect of distance [F (1, 3160) = 206.8, P < 0.0001], an effect of treatment [F (19, 3160) = 134.4, P < 0.0001] and a treatment x distance interaction [F (19, 3160) = 4.265, P < 0.001]. Lower neuritic branching at the distances 50-140 µm from the cell soma were observed following transfer of CM from IFNγ treated mixed glia compared to CM from mixed glial cultures [Figure 9 D].

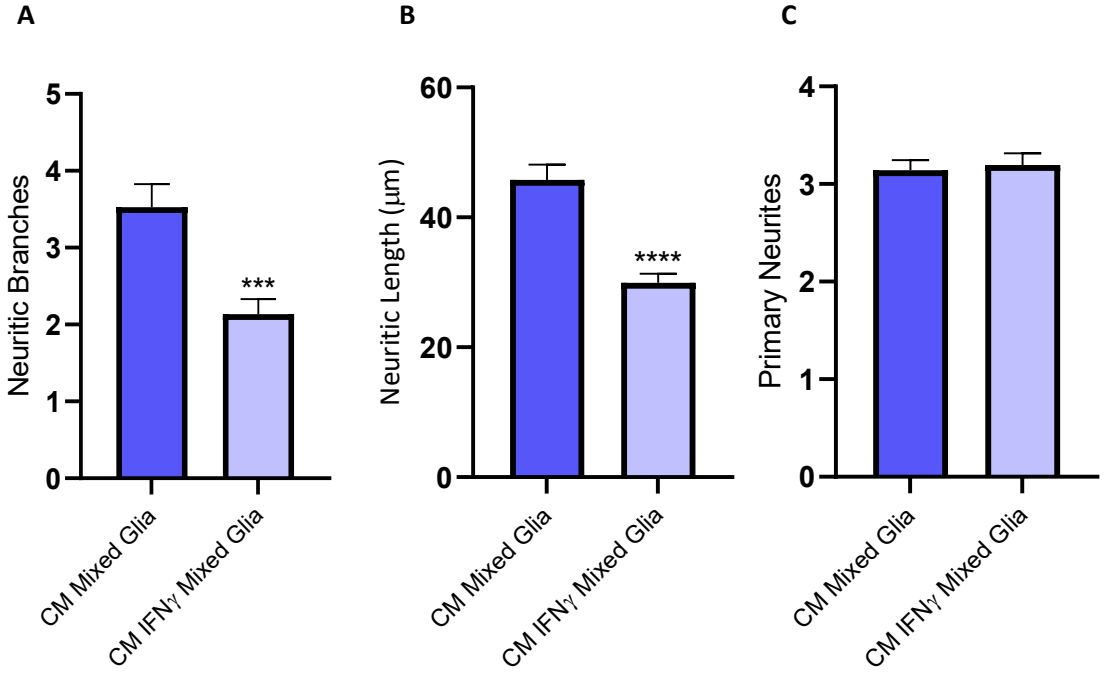

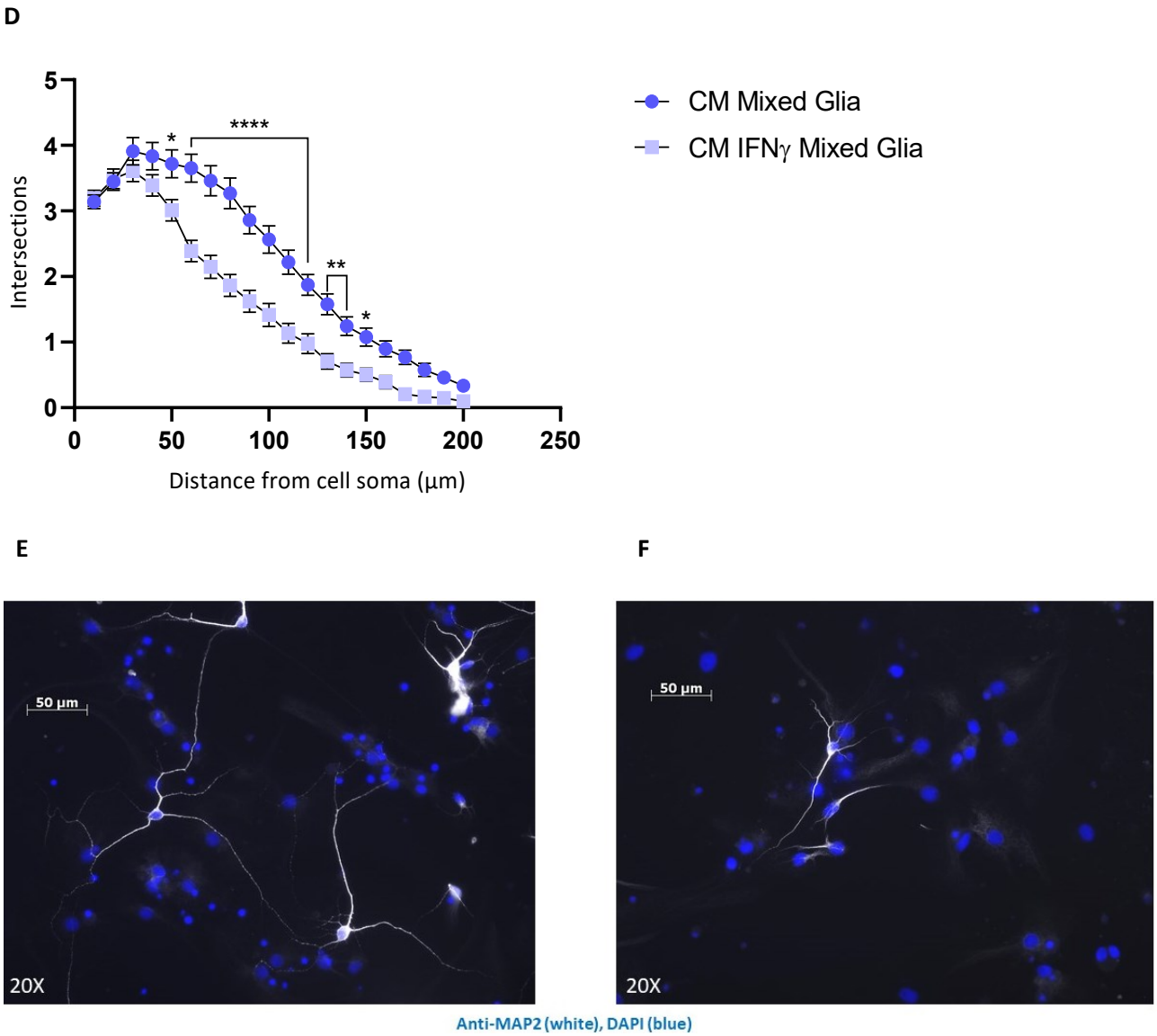

Figure 9: Conditioned media from IFNγ treated mixed glia reduces the complexity of mature primary cortical neurons
Sholl analysis was performed to determine the number of neuritic branches (A), neuritic length (B), number of primary neurites (C) and the Scholl profile (D). Data are expressed as mean ± SEM, n=6 coverslips per treatment group from 3 independent experiments. ****P<0.0001, **P<0.01, *P<0.05 vs control Mixed Glia CM (Unpaired t-test/Newman-Keuls post hoc test). Representative images of control (E) and CM IFNγ Mixed Glia (F) treatment group.

3.1.2 The effect of conditioned media from IFNγ exposed mixed glia on the synaptic protein co-localization

There was a reduction in the number of synaptophysin, PSD-95 and co-localized puncta following treatment with CM from IFNγ treated mixed glia compared to mixed glia CM control [P < 0.0001 Figure 10 A, B, C].

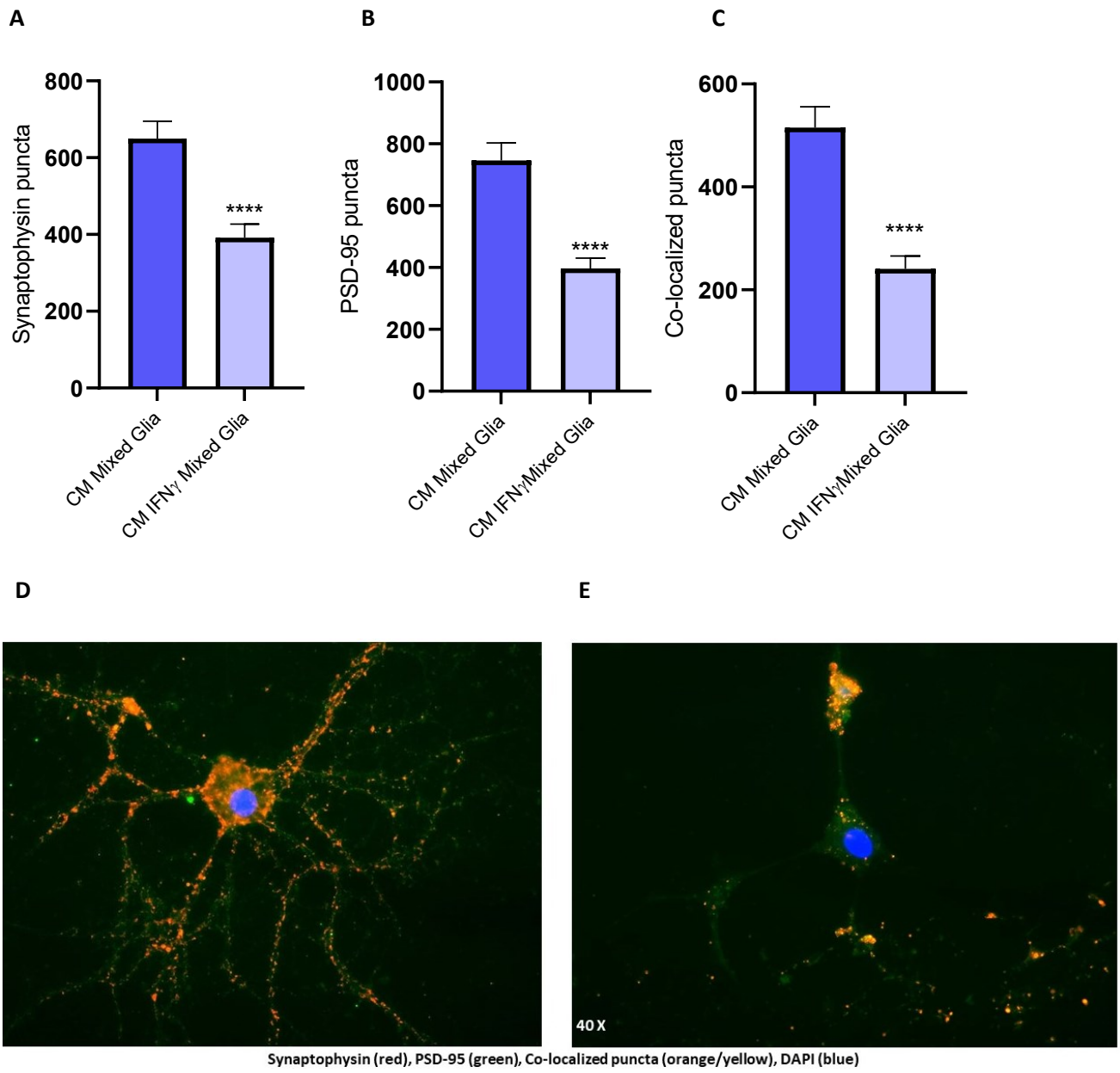

Figure 10: Conditioned media from IFNγ treated mixed glia reduces co-localized expression of synaptic proteins in mature primary cortical neurons

Synaptophysin puncta (A), PSD-95 puncta (B) and co-localized puncta (C). Data are expressed as mean ± SEM, n=6 coverslips per treatment group from 3 replicates of 1 experiment. ****P<0.0001 vs CM from mixed glial cultures (Unpaired t-test/Newman-Keuls post hoc test). Representative images of control (D) and CM IFNγ Mixed Glia (E) treatment group.

3.2 The effect of 1-MT on reductions in complexity and co-localized expression of synaptic proteins induced by conditioned media from IFNγ treated mixed glia in mature primary cortical neuronal cultures

3.2.1 The effect of 1-MT on reductions in neuronal complexity induced by conditioned media from IFNγ treated mixed glia

Two-way ANOVA of neuritic branches showed an effect of CM from IFNγ treated mixed glia [F (1, 299) = 16.02, P < 0.001], and CM from IFNγ treated mixed glia by 1-MT interaction [F (1, 299) = 7.091, P = 0.008]. Post hoc comparisons revealed a reduction in the number of neuritic branches following treatment with CM from IFNγ treated mixed glia compared to mixed glia CM control [P = 0.0002, Figure 11 A]. Co-treatment of mixed glia with 1-MT had no effect on CM from IFNγ treated mixed glia induced reductions in the number of neuritic branches compared to vehicle treated controls.

Two-way ANOVA of neuritic length showed an effect of CM from IFNγ treated mixed glia [F (1, 304) = 11.28, P < 0.001], 1-MT [F (1, 304) = 9.560, P = 0.002] and CM from IFNγ treated mixed glia x 1-MT interaction [F (1, 304) = 11.91, P < 0.001]. Post hoc comparisons revealed a reduction in the neuritic length following treatment with CM from IFNγ treated mixed glia compared to mixed glia CM control [P = 0.0002, Figure 11 B]. Co-treatment of mixed glia with 1-MT protected against CM from IFNγ treated mixed glia induced reductions in neuritic length compared to vehicle treated controls.

Two-way ANOVA of primary neurites showed a CM from IFNγ treated mixed glia x 1-MT interaction [F (1, 307) = 4.197, P = 0.04]. Post hoc comparisons revealed no difference between treatment groups [Figure 11 C].

Two-way ANOVA of the number of neuritic branches at specific distances from the neuronal cell soma showed an effect of distance [F (3.980, 1218) = 498.1, P < 0.001], an effect of treatment [F (3, 306) = 6.670, P < 0.001] and CM from IFNγ treated mixed glia x 1-MT interaction [F (57, 5814) = 2.870, P < 0.001]. Post hoc comparisons revealed that CM from IFNγ treated mixed glia reduced neuritic branching at the distances 20-80 µm and 120-140 µm from the cell soma compared to CM from mixed glia. 1-MT protected against these reductions when compared to vehicle treated controls [Figure 11 D].

A

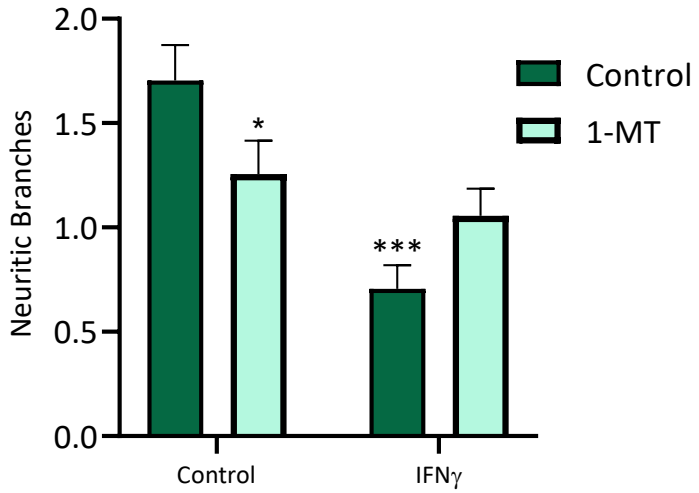
2.0
1.5
1.0
0.5
0.0
Neuritic Branches
*
***
Control
1-MT
Control
IFNγ

B

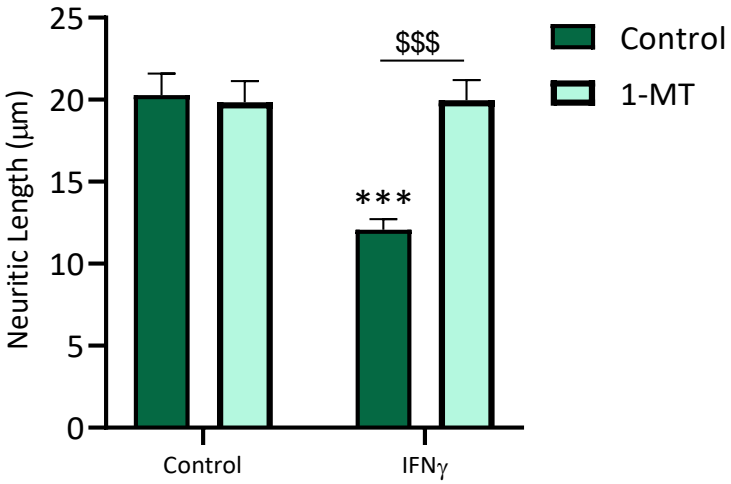
25
20
15
10
5
0
Neuritic Length (µm)
$$$
***
Control
1-MT
Control
IFNγ

C

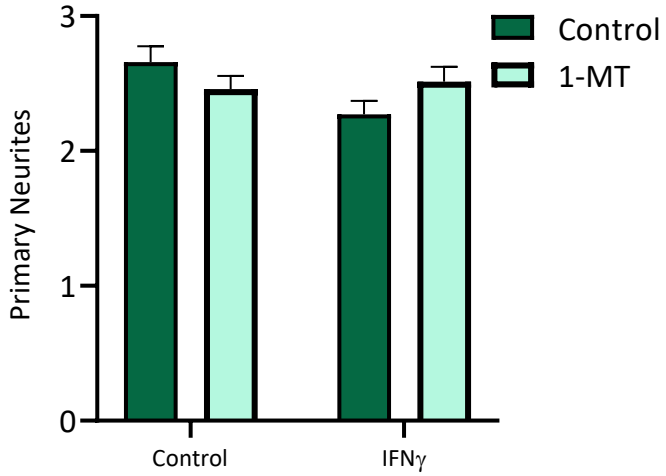
3
2
1
0
Primary Neurites
Control
1-MT
Control
IFNγ

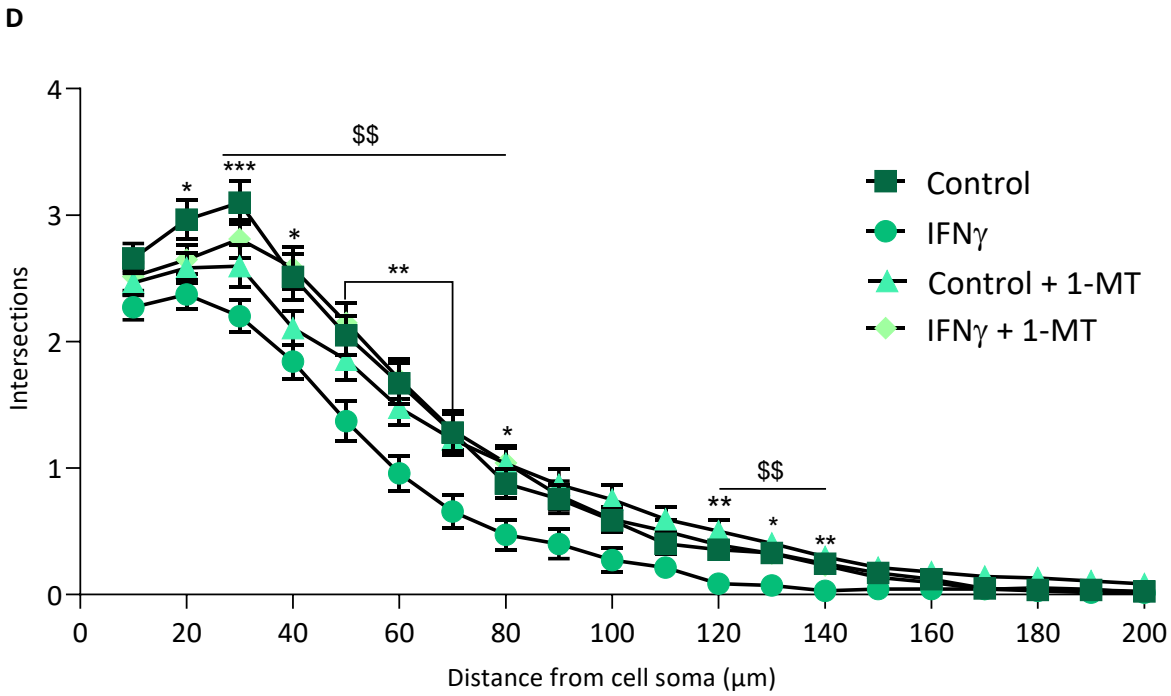

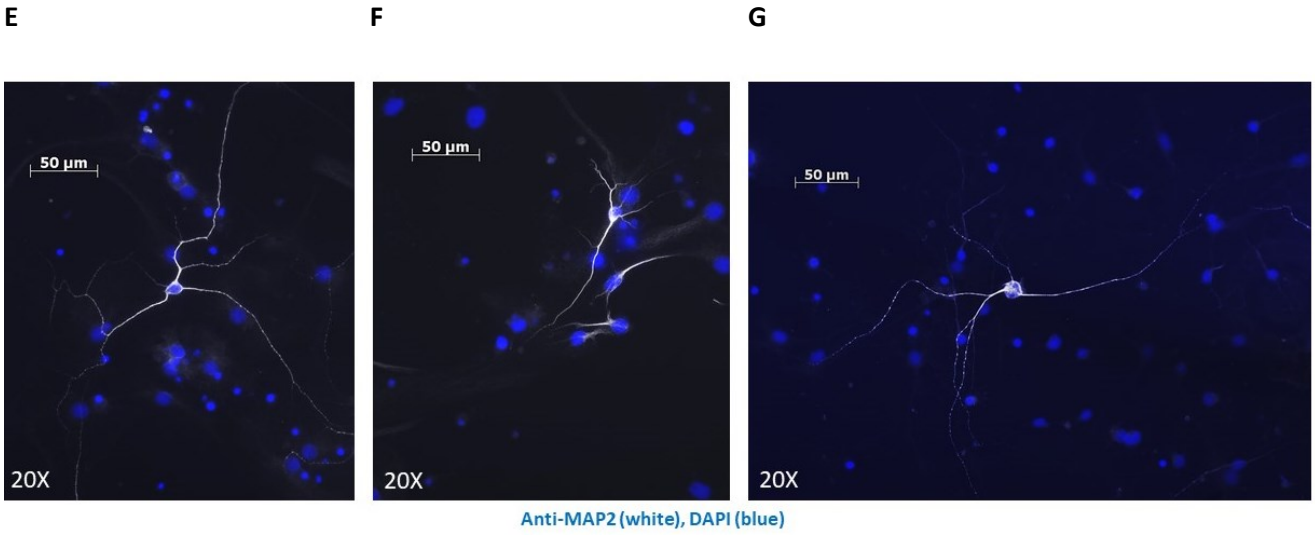

Figure 11: 1-MT protects against reductions in the complexity of mature primary cortical neurons induced by conditioned media from IFNγ treated mixed glia

Sholl analysis was performed to determine the number of neuritic branches (A), the neuritic length (B), the number of primary neurites (C) and the Scholl profile (D). Data are expressed as mean ± SEM, n=6 coverslips per treatment group from 3 independent experiments. ***P<0.001, **P<0.01, *P<0.05 vs control Mixed Glia CM (Newman-Keuls post hoc test). $$$ P<0.001, $$ P<0.01 vs C6 CM (Newman-Keuls post hoc test). Representative images of control (E), CM IFNγ Mixed Glia (F) and CM IFNγ Mixed Glia + 1-MT (G) treatment groups.

3.2.2 The effect of 1-MT on reductions in co-localized expression of synaptic proteins induced by conditioned media from IFNγ treated mixed glia

Two-way ANOVA of the number of synaptophysin puncta showed an effect of CM from IFNγ treated mixed glia [$F(1, 267) = 7.865$, $P = 0.0054$] and CM from IFNγ treated mixed glia with 1-MT interaction [$F(1, 267) = 8.115$, $P = 0.0047$]. Post hoc comparisons revealed a reduction in the number of puncta following treatment with CM from IFNγ treated mixed glia compared to CM from mixed glial cultures [$P = 0.0002$, Figure 12 A]. Co-treatment of mixed glia with 1-MT protected against CM from IFNγ treated mixed glia induced reductions in the number of synaptophysin puncta compared to vehicle treated controls [$P = 0.0021$].

Two-way ANOVA of the number of PSD-95 puncta showed an effect of CM from IFNγ treated mixed glia [$F(1, 267) = 11.88$, $P = 0.0007$] and CM from IFNγ treated mixed glia with 1-MT interaction [$F(1, 267) = 16.38$, $P < 0.0001$]. Post hoc comparisons revealed a reduction in the number of puncta following treatment with CM from IFNγ treated mixed glia compared to CM from mixed glia cultures [$P < 0.0001$, Figure 12 B]. Co-treatment of mixed glia with 1-MT protected against CM from IFNγ treated mixed glia induced reductions in the number of PSD-95 puncta compared to vehicle treated controls [$P = 0.0021$]. Treatment of mixed glia with 1-MT and transfer of CM to primary cortical neurons decreased the number of PSD-95 puncta when compared to vehicle treated controls [$P < 0.05$].

Two-way ANOVA of the number of co-localized puncta showed an effect of CM from IFNγ treated mixed glia [$F(1, 267) = 24.95$, $P < 0.0001$], and CM from IFNγ treated mixed glia x 1-MT interaction [$F(1, 267) = 8.312$, $P = 0.0043$]. Post hoc comparisons revealed a reduction in the number of puncta following treatment with CM from IFNγ treated mixed glia compared to CM from mixed glia cultures [$P < 0.0001$, Figure 12 C]. Co-treatment of mixed glia with 1-MT protected against CM from IFNγ treated mixed glia induced reductions in the number of co-localized puncta compared to vehicle treated control [$P = 0.0002$].

A

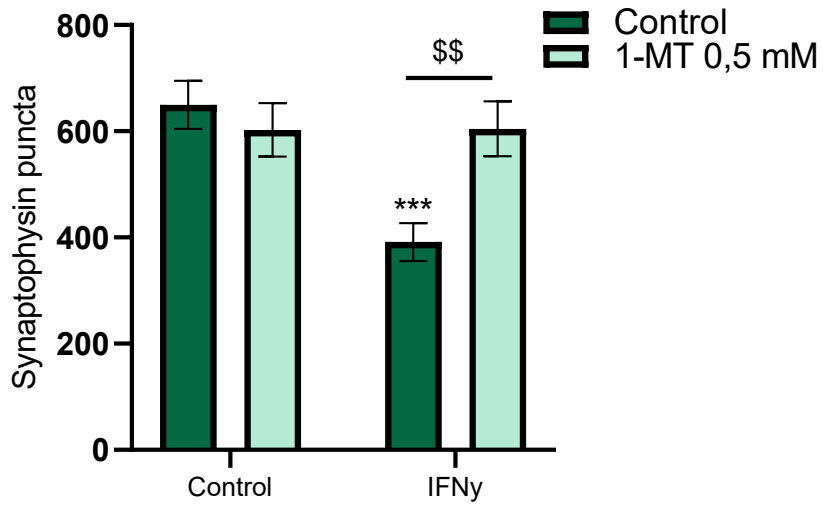
Control
1-MT 0,5 mM
Synaptophysin puncta
800
600
400
200
0
$$
***
Control
IFNy

B

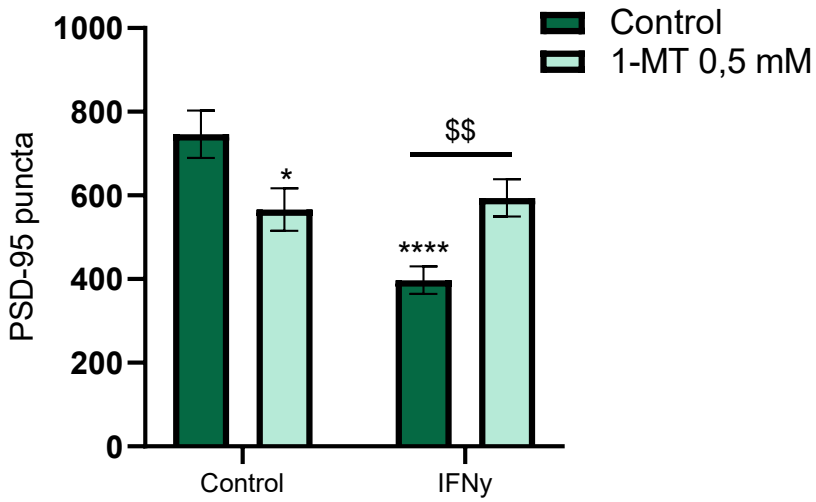
Control
1-MT 0,5 mM
PSD-95 puncta
1000
800
600
400
200
0
$$
*
****
Control
IFNy

C

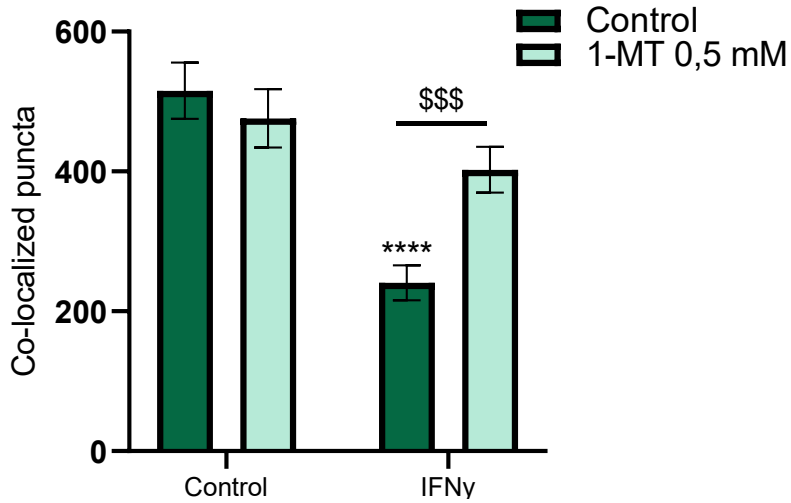
Control
1-MT 0,5 mM
Co-localized puncta
600
400
200
0
$$$
****
Control
IFNy

D

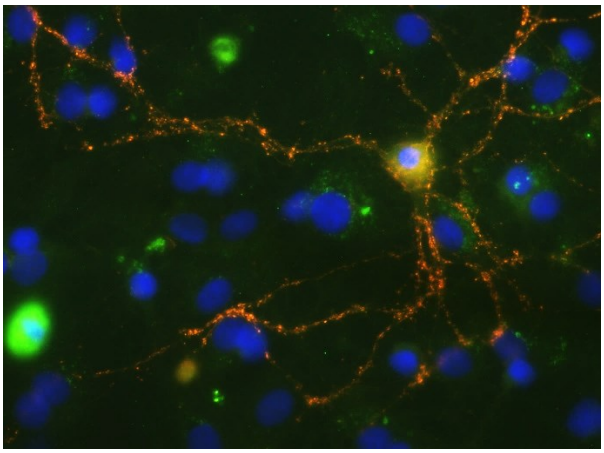

E

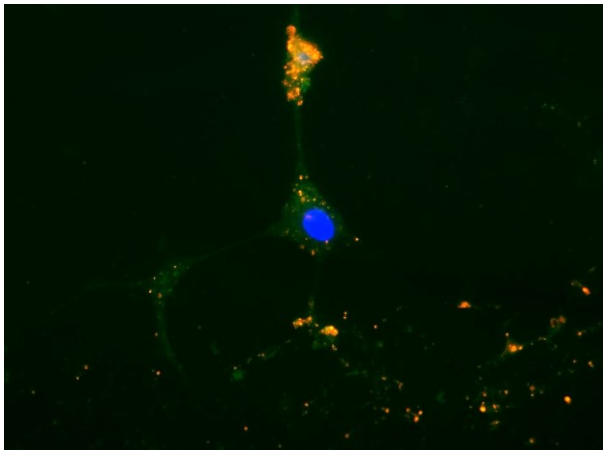

F

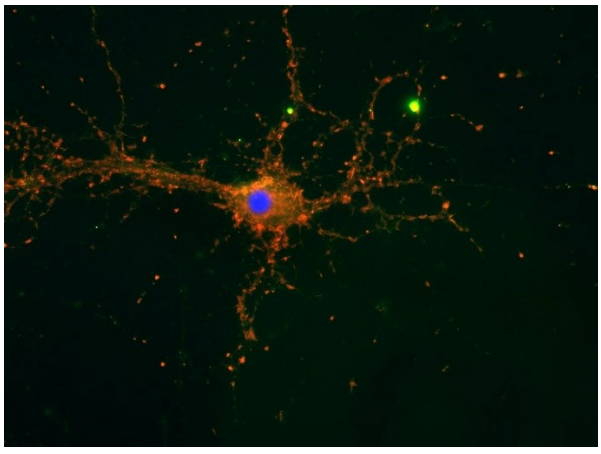

Figure 12: 1-MT protects against reductions in the co-localized expression of synaptic proteins induced by transfer of conditioned media from IFNγ treated mixed glia to mature primary cortical neurons

Synaptophysin puncta (A), PSD-95 puncta (B) and co-localized puncta (C). Treatment with 1-MT reduces the number of PSD-95 puncta [$P < 0.05$] compared to vehicle treated control but does

not affect the number of synaptophysin or co-localized puncta. Data are expressed as mean ± SEM, n=6 coverslips per treatment group from 3 replicates of 1 experiment. ****P<0.0001, ***P<0.001, **P<0.01, *P<0.05 vs control Mixed Glia CM (Newman-Keuls post hoc test). $$$ P<0.001, $$ P<0.01 vs C6 CM (Newman-Keuls post hoc test). Representative images of control (D), CM IFNγ Mixed Glia (E) and CM IFNγ Mixed Glia + 1-MT (F) treatment groups. Synaptophysin (red), PSD-95 (green), Co-localized puncta (orange/yellow), DAPI (blue), 40X.

3.3 mRNA expression of KP enzymes in primary cortical astrocytes, mixed glia, IFNγ exposed mixed glia and C6 cells

3.3.1 mRNA expression of KP enzymes in primary cortical astrocytes and C6 cells

mRNA expression of IDO1 was higher [T = 8.876, P < 0.05] and of KMO lower [T = 92.18, P = 0.0001] in C6 cells when compared to vehicle treated primary cortical astrocytes. There was no difference in mRNA expression of TDO2 and KYNU when compared to vehicle treated control (Unpaired t-test).

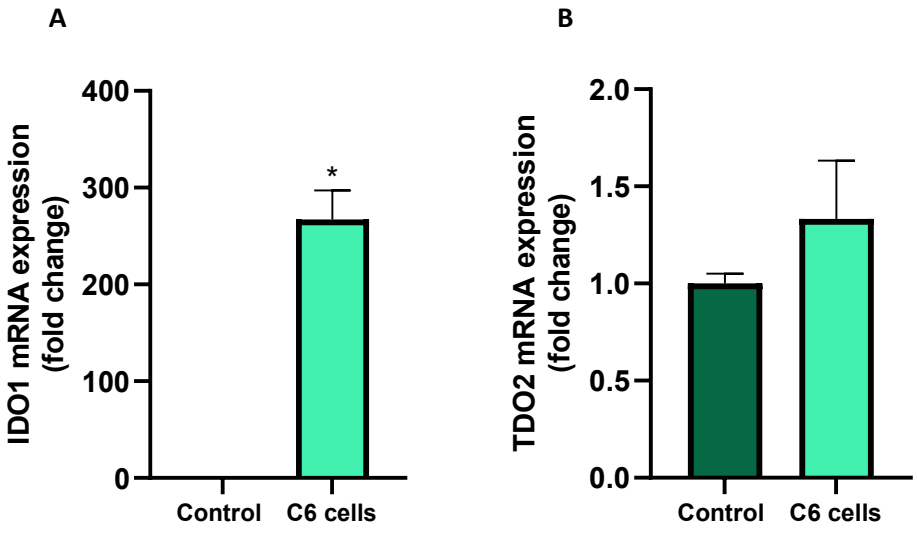

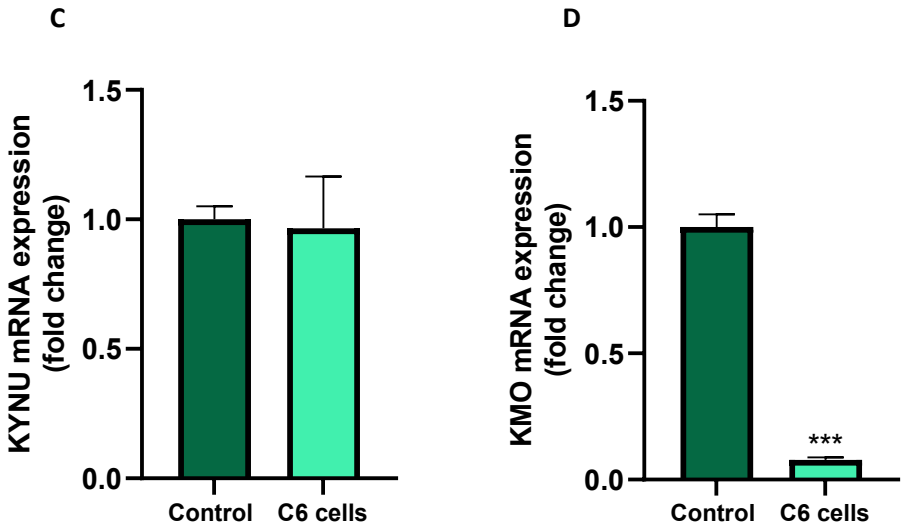

Figure 13: mRNA expression of KP enzymes in primary cortical astrocytes and C6 cells
Primary astrocytes (DIV14) and C6 cells were treated with vehicle (cDMEM) for 24 hours. Cells were harvested for RNA extraction followed by RT-PCR to analyse the expression of the KP enzymes; IDO1 (A), TDO2 (B), KYNU (C) and KMO (D). Data are expressed as mean ± SEM, n=2 wells per treatment group from 1 experiment. ***P<0.001, *P<0.05 vs primary cortical astrocytes (Unpaired t-test).

3.3.2 mRNA expression of KP enzymes in mixed glia, IFNγ exposed mixed glia, and C6 cells

One-way ANOVA of IDO1 mRNA expression showed an effect of treatment [F (2, 3) = 12526, P < 0.0001]. Post hoc comparisons revealed that mRNA expression of IDO1 was higher in C6 cells [P < 0.0001] and in IFNγ exposed mixed glia [P < 0.0001] when compared to untreated mixed glia [Figure 14 A].

One-way ANOVA of TDO2 mRNA expression showed an effect of treatment [F (2, 3) = 39.80, P = 0.0069]. Post hoc comparisons revealed that mRNA expression of TDO2 was higher in C6 cells [P = 0.0021] and in IFNγ exposed mixed glia [P < 0.05] when compared to untreated mixed glia [Figure 14 B].

One-way ANOVA of KYNU mRNA expression showed an effect of treatment [F (2, 3) = 25.70, P = 0.0130]. Post hoc comparisons revealed that mRNA expression of KYNU was lower in C6 cells [P < 0.05] when compared to untreated mixed glia [Figure 14 C].

One-way ANOVA of KMO mRNA expression showed an effect of treatment [F (2, 3) = 56.85, P = 0.0041]. Post hoc comparisons revealed that mRNA expression of KMO was higher in C6 cells [P = 0.0021] when compared to untreated mixed glia [Figure 14 D].

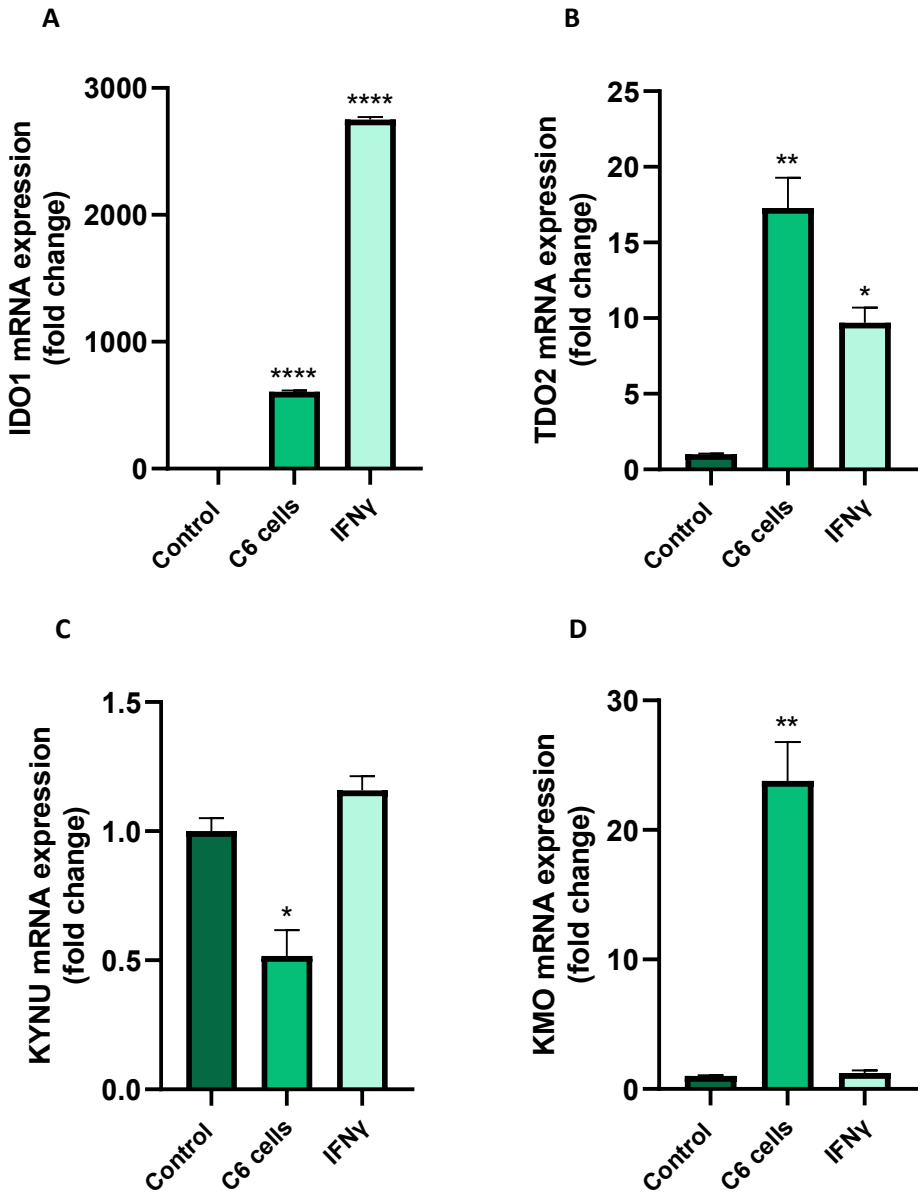

Figure 14: mRNA expression of KP enzymes in mixed glia, C6 cells and IFNγ exposed mixed glia
Mixed glial cultures (DIV14) and C6 cells were treated with vehicle (cDMEM) for 24 hours. Mixed glial cultures were also treated with IFNγ for 24 hours. Cells were harvested for RNA extraction followed by RT-PCR to analyse the expression of the KP enzymes; IDO1 (A), TDO2 (B), KYNU (C) and KMO (D). Data are expressed as mean ± SEM, n=2 wells per treatment group from 1 experiment. ****P<0.0001, **P<0.01, *P<0.05 vs primary mixed glia (Neuman-Keuls post hoc test).

3.4 The effect of conditioned media from C6 glioma cell line on the viability, complexity, and co-localized expression of synaptic proteins in mature primary cortical neuronal culture

3.4.1 The effect of conditioned media from C6 glioma cells on neuronal viability

Unpaired t-test of viability showed no effect of C6 CM on neuronal viability compared to CM transferred from mixed glial cultures following 24- and 48-hours exposure.

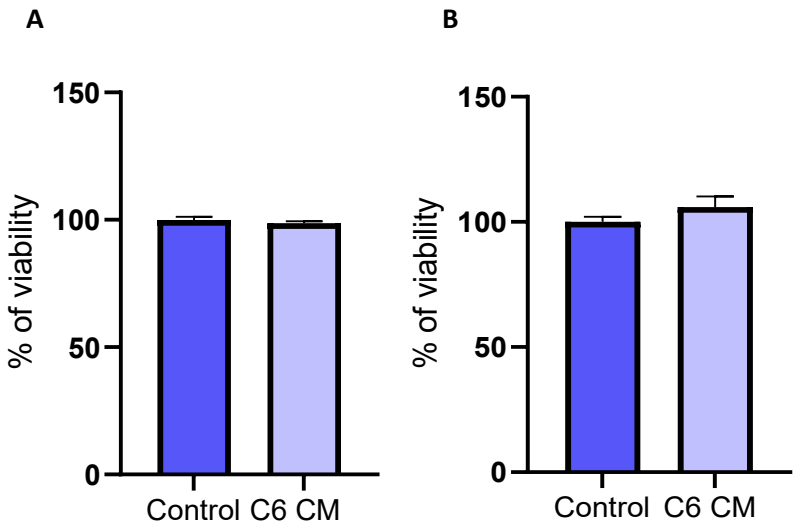

Figure 15: C6 CM does not affect the viability of mature primary cortical neurons
Mature primary cortical neurons (DIV 21) were treated with C6 CM for 24 hours (A) and 48 hours (B). Data are expressed as a mean ± SEM, n=6 replicates per treatment groups from 3 independent experiments (Unpaired t-test).

3.4.2 The effect of conditioned media from C6 glioma cells on neuronal complexity

Transfer of CM from C6 cells to primary cortical neurons provoked a reduction in the number of neuritic branches [$P = 0.0003$], neuritic length [$P < 0.001$] but no effect on the number of primary neurites when compared to mixed glia CM control [Unpaired t-tests, Figure 16 A, B, C].

Two-way ANOVA of the number of neuritic branches at specific distances from the neuronal cell soma showed an effect of distance [$F (1, 156) = 140.6$, $P < 0.0001$], an effect of treatment [$F (25, 156) = 112.9$, $P < 0.0001$] and a treatment x distance interaction [$F (25, 156) = 5.931$, $P < 0.0001$]. Lower neuritic branching at the distances 40-130 µm from the cell soma were observed following transfer of C6 CM compared to CM from mixed glial cultures [Figure 16 D].

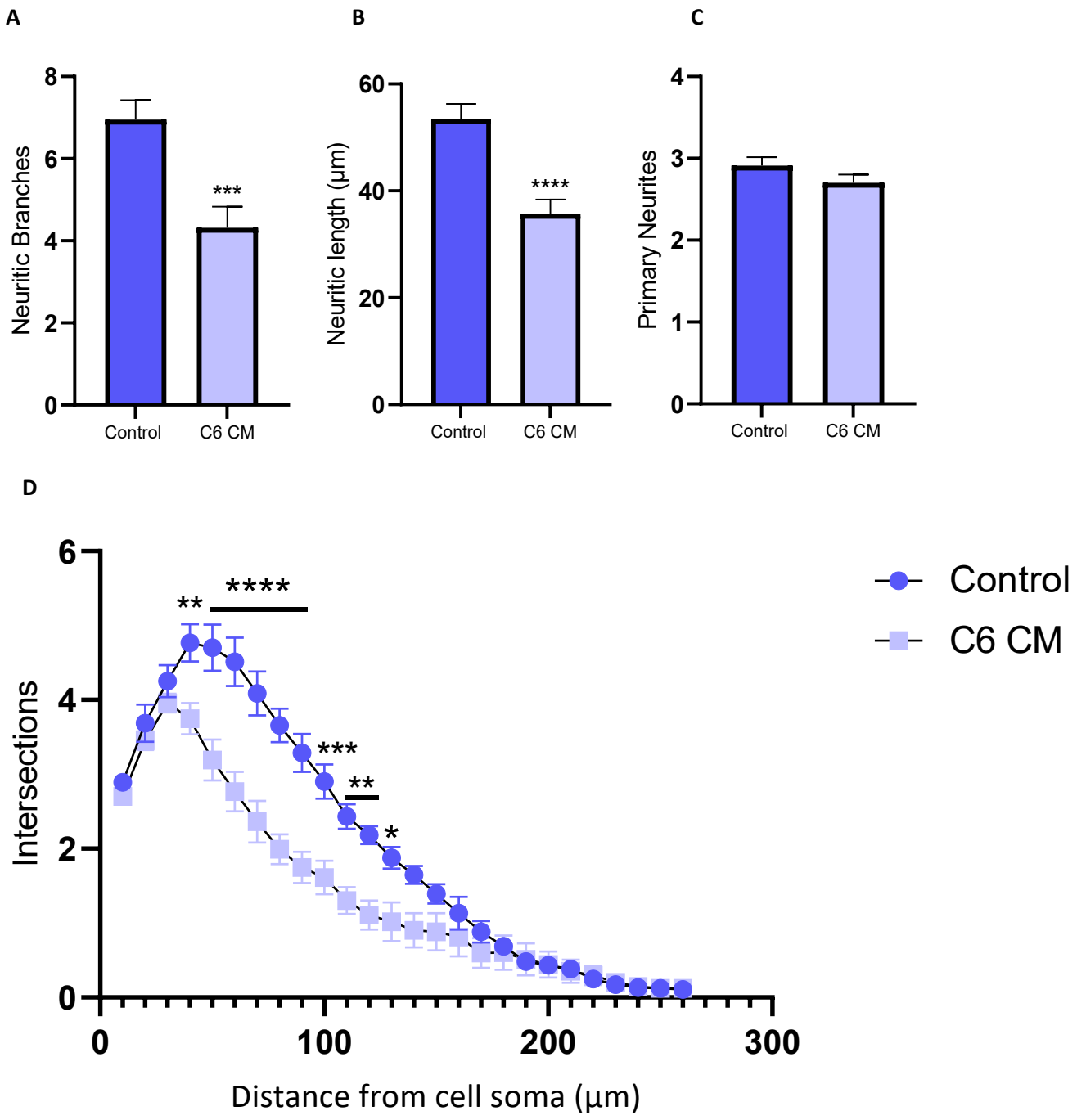
A
B
C
Neuritic Branches
Neuritic length (µm)
Primary Neurites
***
****
Control
C6 CM
D
Intersections
Distance from cell soma (µm)
Control
C6 CM
**
****
***
**
*
0
100
200
300

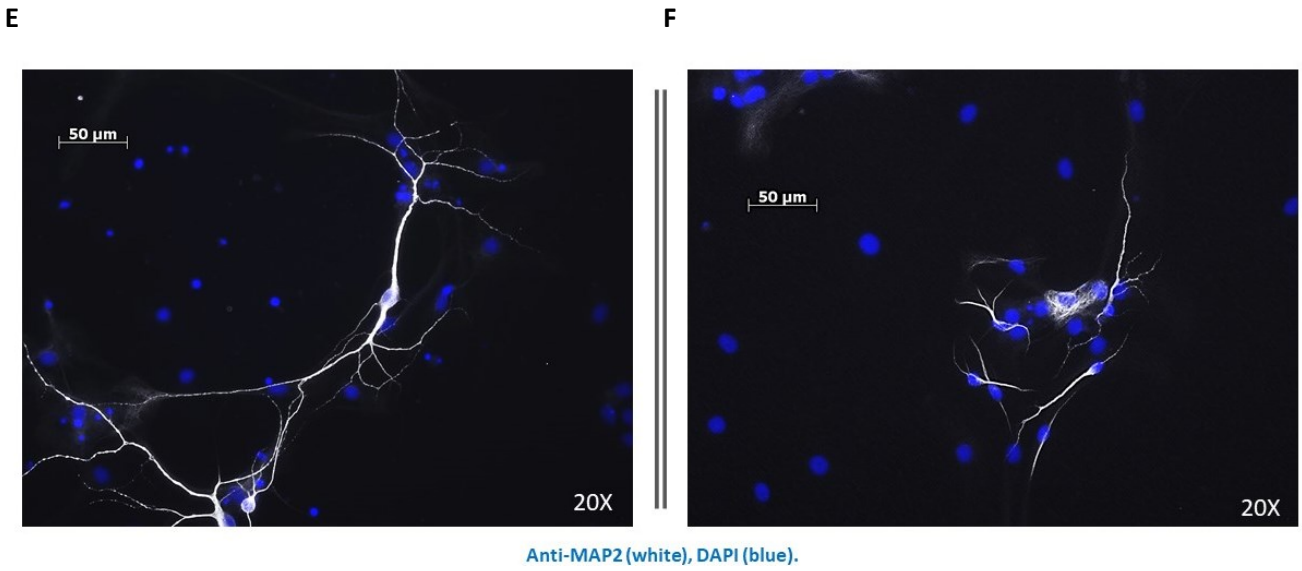

Figure 16: Conditioned media from C6 cell culture reduces the complexity of mature primary cortical neurons
Sholl analysis was performed to determine the number of neuritic branches (A), neuritic length (B), number of primary neurites (C) and the Scholl profile (D). Data are expressed as mean ± SEM, n=6 coverslips per treatment group from 3 independent experiments. ****P<0.0001, ***P<0.001, **P<0.01, *P<0.05 vs CM transferred from primary mixed glia (Unpaired t-test/Neuman-Keuls post hoc test). Representative images of control (E) and C6 CM (F) treatment groups.

3.4.3 The effect of conditioned media from C6 glioma cells on the co-localized expression of synaptic proteins

There was a reduction in the number of synaptophysin, PSD-95 and co-localized puncta following treatment with C6 CM compared to CM transferred from primary mixed glia [P < 0.0001 Figure 17 A, B, C].

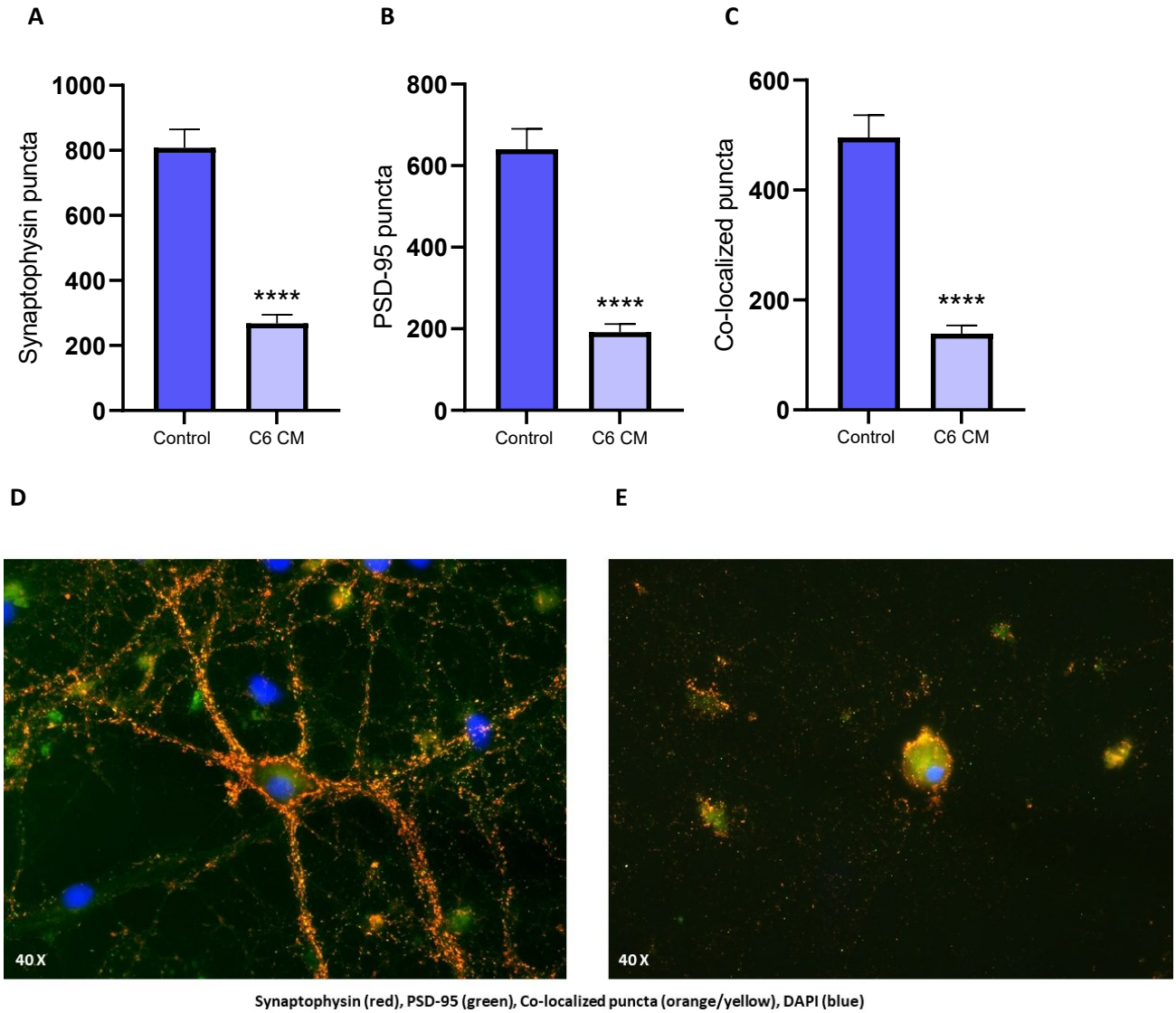

Figure 17: Conditioned media from C6 cells reduces co-localized expression of synaptic proteins in mature primary cortical neurons
Synaptophysin puncta (A), PSD-95 puncta (B) and co-localized puncta (C). Data are expressed as mean ± SEM, n=6 coverslips per treatment group from 3 replicates of 1 experiment. ****P<0.0001 vs CM from mixed glial cultures (Unpaired t-test). Representative images of control (D) and C6 CM (E) treatment groups.

3.5 The effect of conditioned media from C6 glioma cells on the morphology of microglia and astrocytes in primary mixed glial cultures

3.5.1 The effect of conditioned media from C6 glioma cells on microglial morphology and IBA1 immunoreactivity

Cell/soma ratio and cell perimeter were lower in microglial cells upon treatment with C6 CM compared to CM transferred from primary mixed glia [P < 0.0001 Figure 18 A, B]. There was no difference in CTCF between the transfer of the two types of CM.

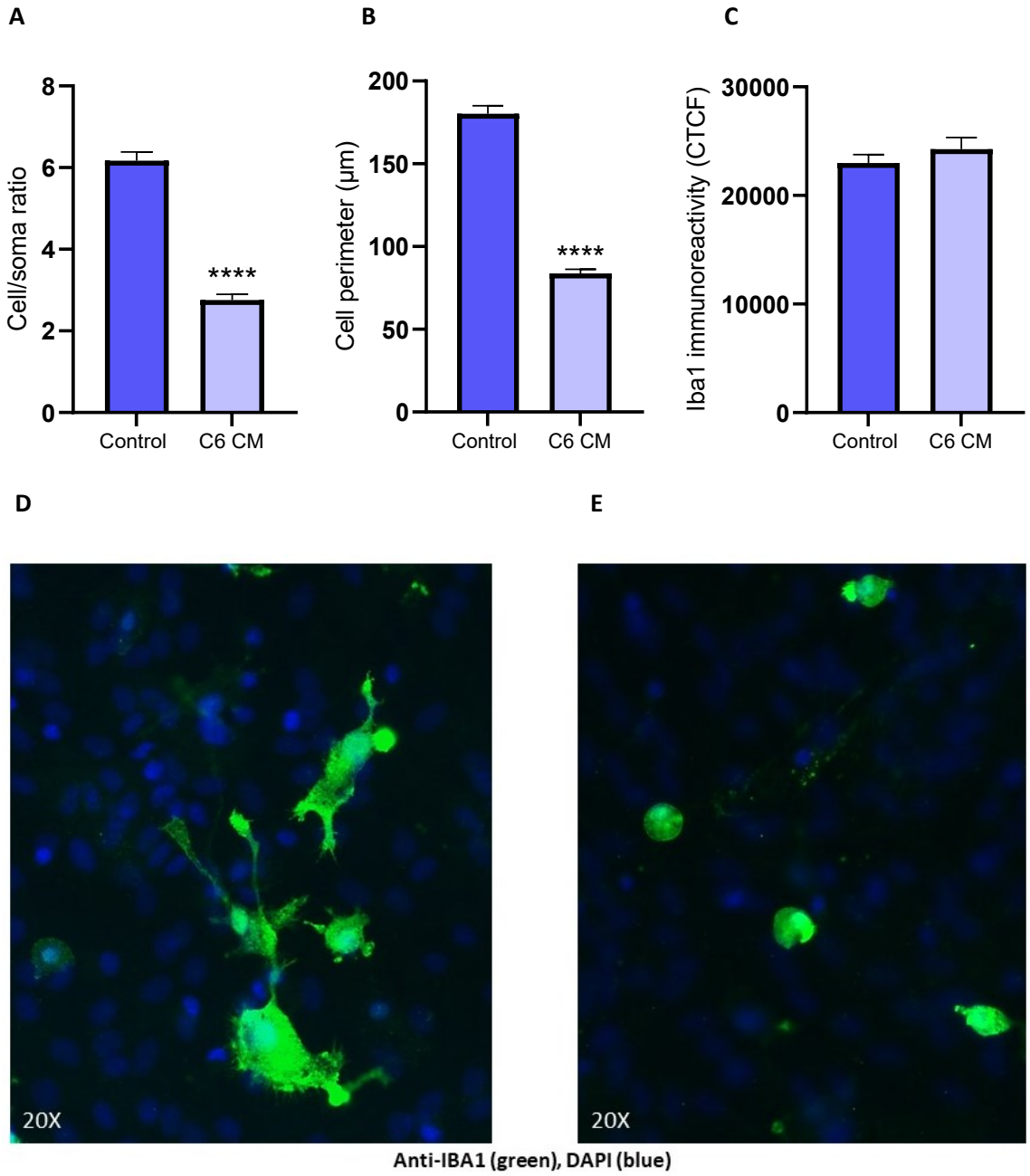

Figure 18: Conditioned media from C6 cells affects morphology of primary microglial cells in mixed glial cultures

Immunocytochemical and cell morphology analyses were performed to quantify cell/soma ratio (A), cell perimeter (B) and Iba1 immunoreactivity (C). Cell/soma ratio was quantified as a ratio of total cell perimeter to cell soma perimeter. A higher cell/soma ratio indicates more ramified microglial morphology. Data are expressed as mean ± SEM, n=6 coverslips per treatment group

from 3 independent experiments. ****P<0.0001 vs control DMEM (Unpaired t-test). Representative images of control (D) and C6 CM (E) treated Iba1+ cells.

3.5.2 The effect of conditioned media from C6 glioma cells on astrocytic morphology and GFAP immunoreactivity

Cell/soma ratio were lower and CTCF higher in astrocytic cells upon treatment with C6 CM compared to transfer of CM from mixed glial cells [P < 0.0001 Figure 19 A, C]. There was no difference in cell perimeter between the two types of CM.

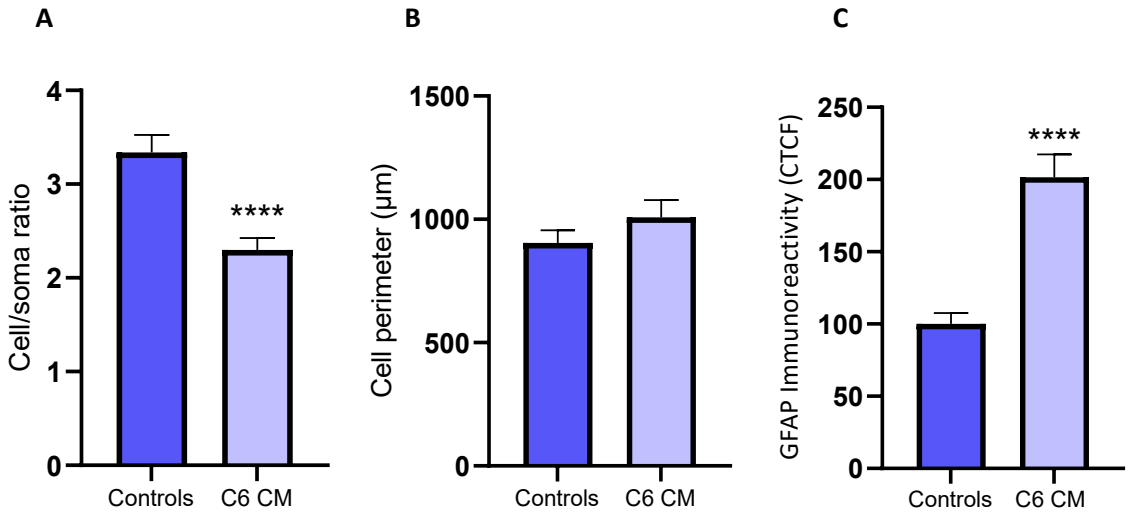

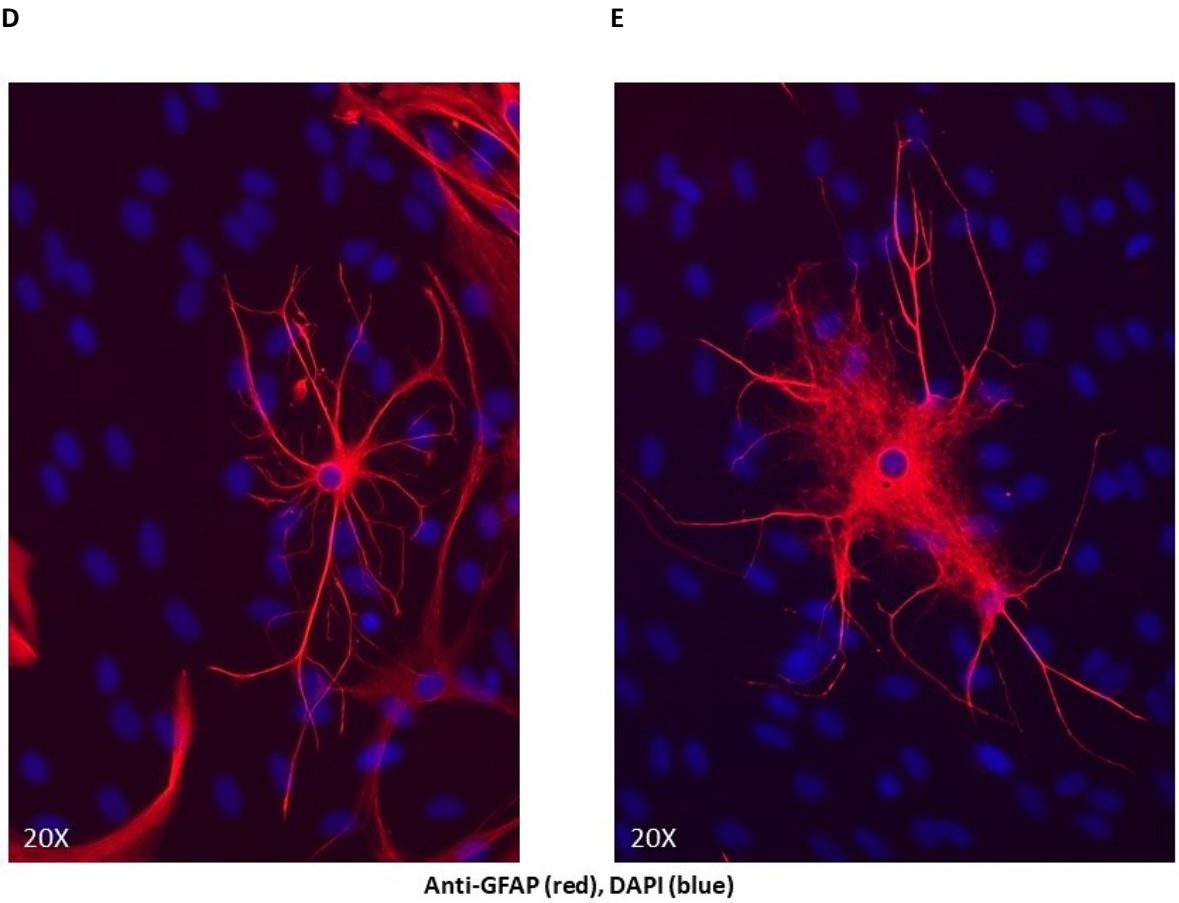

Figure 19: Conditioned media from C6 cells effects cell/soma and GFAP immunoreactivity but not cell perimeter of astrocytes in mixed glial cultures
Immunocytochemical and cell morphology analyses were performed to quantify cell/soma ratio (A), cell perimeter (B) and GFAP immunoreactivity (C). Cell/soma ratio was quantified as a ratio of total cell perimeter to cell soma perimeter. A higher cell/soma ratio indicates more ramified astrocytic morphology. Data are expressed as mean ± SEM, n=6 coverslips per treatment group from 3 independent experiments. ****P<0.0001 vs control DMEM (Unpaired t-test). Representative images of control (D) and C6 CM (E) treated GFAP+ cells.

3.6 The effect of 1-MT on C6 conditioned media induced reductions in complexity and co-localized expression of synaptic proteins in mature primary cortical neuronal cultures

3.6.1 The effect of 1-MT on conditioned media from C6 cells induced reductions in neuronal complexity

One-way ANOVA of neuritic branches showed an effect of treatment [F (2, 214) = 8.115, P = 0.0004]. Post hoc comparisons revealed that 1-MT protected against C6 CM induced reductions in branches when compared to vehicle treated control [Figure 20 A].

One-way ANOVA of neuritic length showed an effect of treatment [F (2, 214) = 10.75, P < 0.0001]. Post hoc comparisons revealed that 1-MT protected against C6 CM induced reductions in length compared to vehicle treated control [Figure 20 B].

One-way ANOVA of primary neurites showed an effect of treatment [F (2, 254) = 62.14, P < 0.0001]. Post hoc comparisons revelaed that 1-MT increases the number of primary neurites when compared to vehicle treated control [P < 0.0001, Figure 20 C].

Two-way ANOVA of the number of neuritic branches at specific distances from the neuronal cell soma showed an effect of distance [F (2, 234) = 13.90, P < 0.0001] and an effect of treatment [F (25, 234) = 20.66, P < 0.001]. Post hoc comparisons revealed that C6 CM reduced neuritic branching at the distances 40-130 µm from the cell soma compared to CM from mixed glia. 1-MT protected against these reductions when compared to vehicle treated controls [Figure 20 D].

Transfer of CM from primary mixed glial cultures treated with 1-MT to primary cortical neurons does not affect neuritic branching, neuritic length or number of primary neurites when compared to transfer of CM from untreated primary mixed glial controls [Figure 20 H, I, J, K].

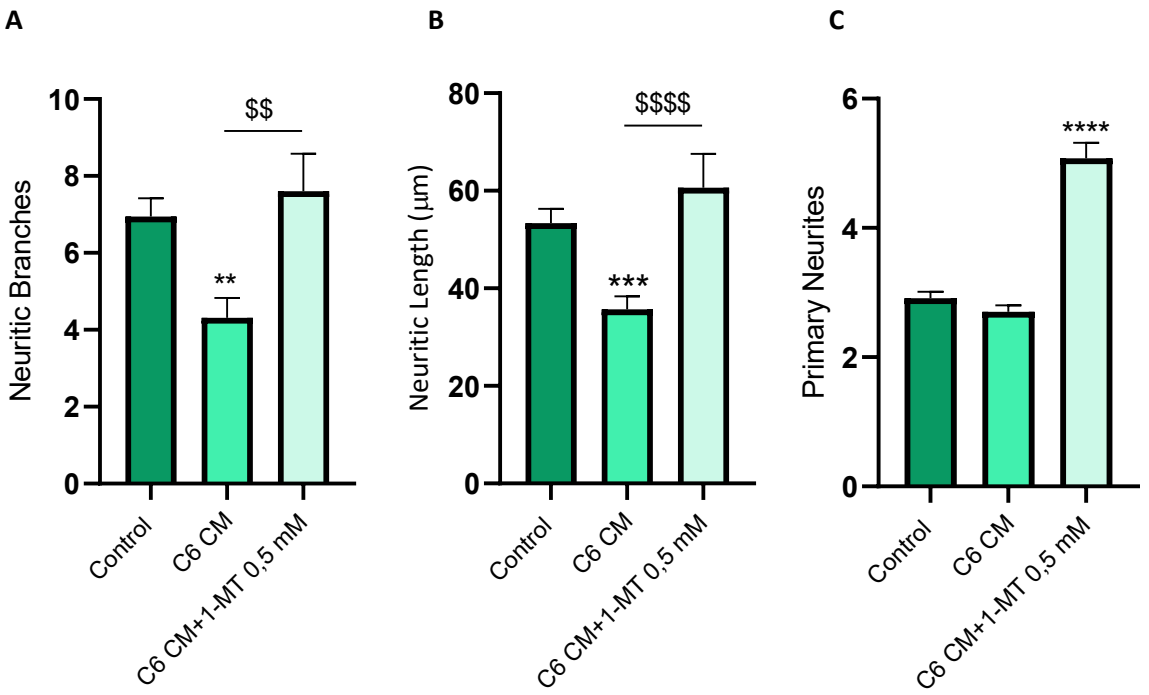

D

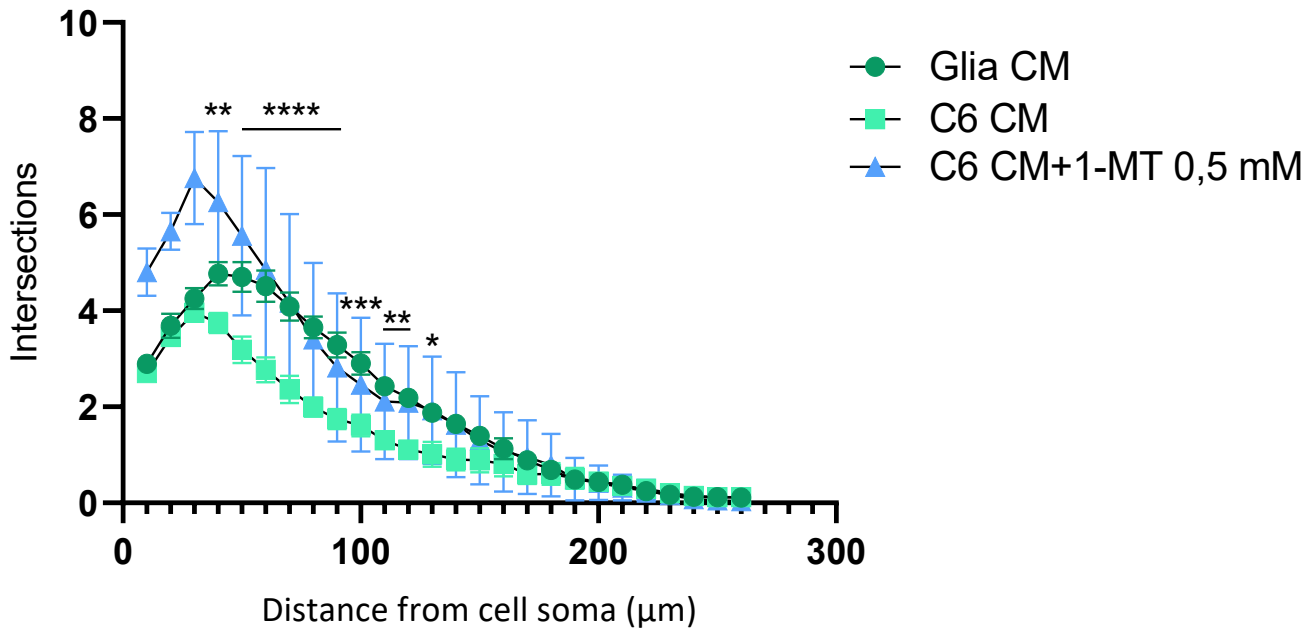

E F G

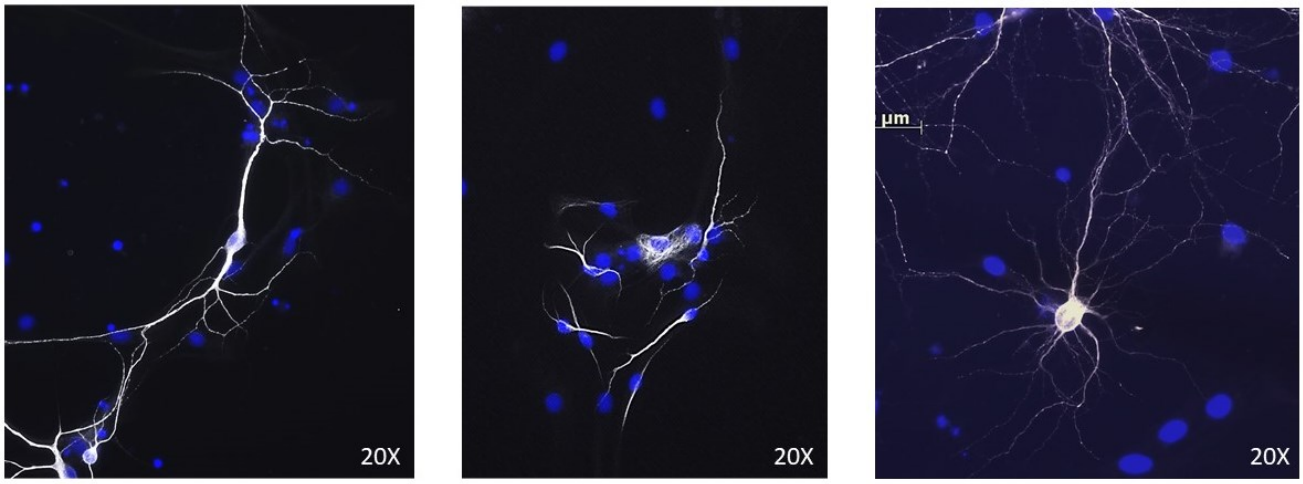

Anti-MAP2 (white), DAPI (blue).

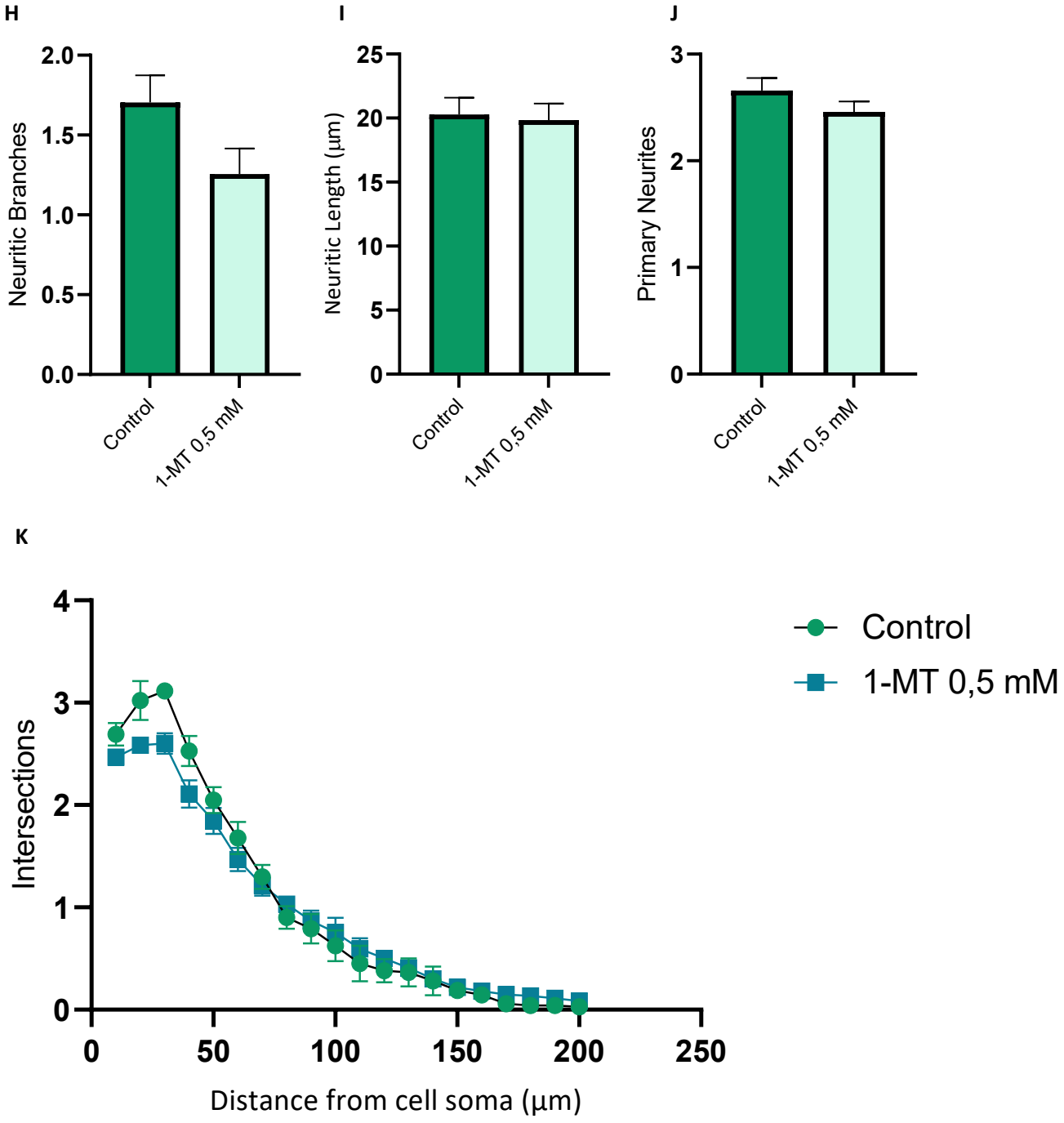

Figure 20: Transfer of CM from C6 and primary mixed glial cultures treated with 1-MT to primary cortical neurons affects neuronal complexity

Sholl analysis was performed to determine number of neuritic branches (A), neuritic length (B), number of primary neurites (C) and the Scholl profile (D). Transfer of CM from primary mixed glial cultures treated with 1-MT to primary cortical neurons does not affect the number of neuritic branches (H), neuritic length (I), number of primary neurites (J) or the Sholl profile (K). Data are expressed as mean ± SEM, n=6 coverslips per treatment group from 3 independent experiments. ****P<0.0001, ***P<0.001, **P<0.01, *P<0.05 vs control CM from mixed glia (Newman-Keuls post hoc test). Representative images of control (E), C6 CM (F), C6 CM+1-MT (G) treatment groups.

3.6.2 The effect of 1-MT on conditioned media from C6 cells induced reductions in co-localized expression of synaptic proteins in mature primary cortical neuronal cultures

Two-way ANOVA of synaptophysin puncta showed an effect of C6 CM [$F(1,267) = 7.865$, $P = 0.0054$], and an interaction with 1-MT [$F(1, 267) = 8.115$, $P = 0.0047$]. Post hoc comparisons revealed a reduction in the number of puncta following treatment with C6 CM compared to transfer of media from primary mixed glial cultures [$P < 0.0001$, Figure 21 A]. Co-treatment with 1-MT protected against C6 CM induced reductions in the number of synaptophysin puncta compared to vehicle treated controls. Transfer of CM from primary mixed glial cultures treated with 1-MT to primary cortical neurons reduced the number of puncta compared to untreated controls [$P < 0.05$], albeit to a lesser extent.

Two-way ANOVA of the number of PSD-95 puncta showed an effect of C6 CM [$F(1, 267) = 11.88$, $P = 0.0007$], and an interaction with 1-MT [$F(1, 267) = 16.38$, $P < 0.0001$]. Post hoc comparisons revealed a reduction in the number of puncta following treatment with C6 CM compared to transfer of media from primary mixed glial cultures [$P < 0.0001$, Figure 21 B]. Co-treatment with 1-MT protected against C6 CM induced reductions in the number of PSD-95 puncta compared to vehicle treated controls.

Two-way ANOVA of the number of co-localized puncta showed an effect of C6 CM [$F(1, 267) = 24.95$, $P < 0.0001$], and an interaction with 1-MT [$F(1, 267) = 8.312$, $P < 0.0043$]. Post hoc comparisons revealed a reduction in the number of puncta following treatment with C6 CM compared to transfer of media from primary mixed glial cultures [$P < 0.0001$, Figure 21 C]. Co-treatment with 1-MT protected against C6 CM induced reductions in the number of co-localized puncta compared to vehicle treated controls.

A

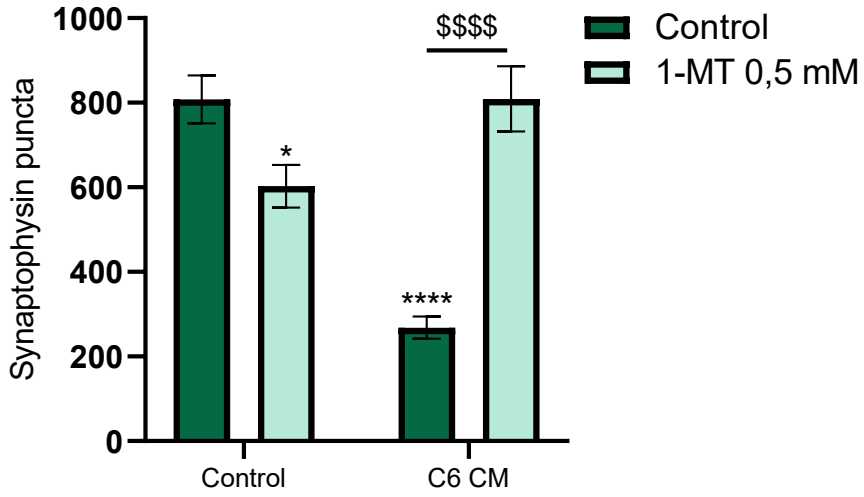
Synaptophysin puncta
1000
800
600
400
200
0
*
****
$$$$
Control
1-MT 0,5 mM
Control
C6 CM

B

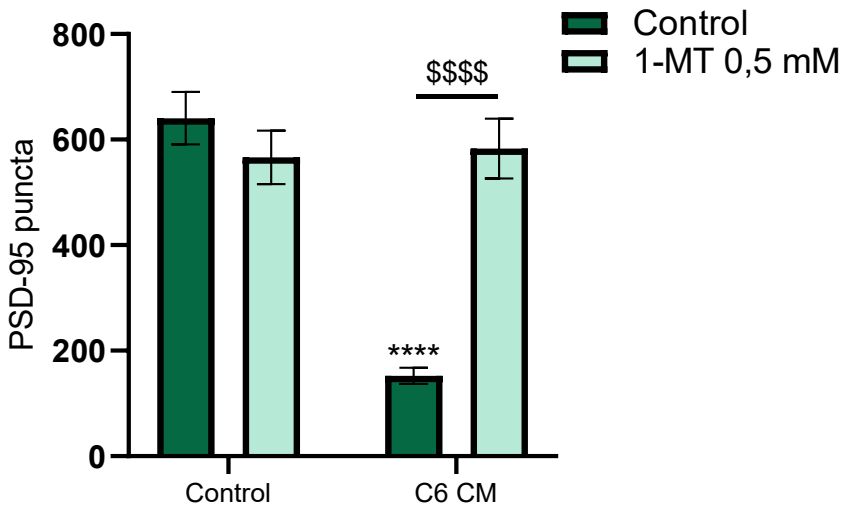
PSD-95 puncta
800
600
400
200
0
****
$$$$
Control
1-MT 0,5 mM
Control
C6 CM

C

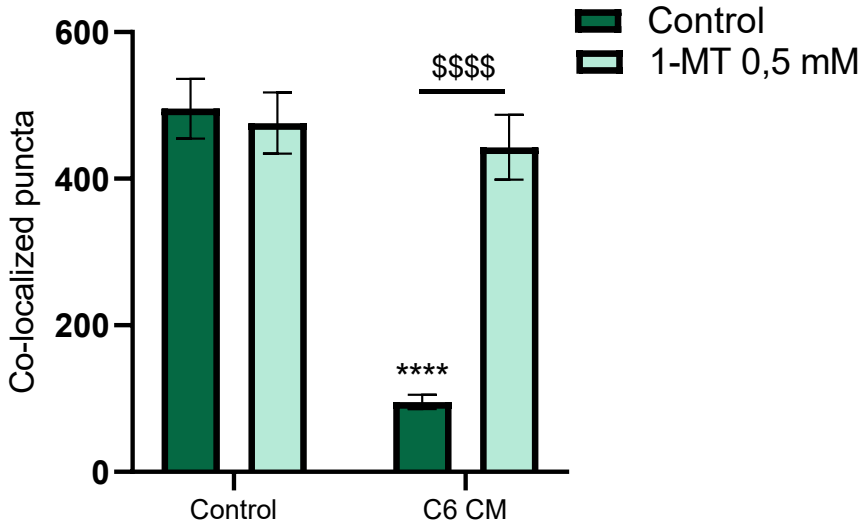
Co-localized puncta
600
400
200
0
****
$$$$
Control
1-MT 0,5 mM
Control
C6 CM

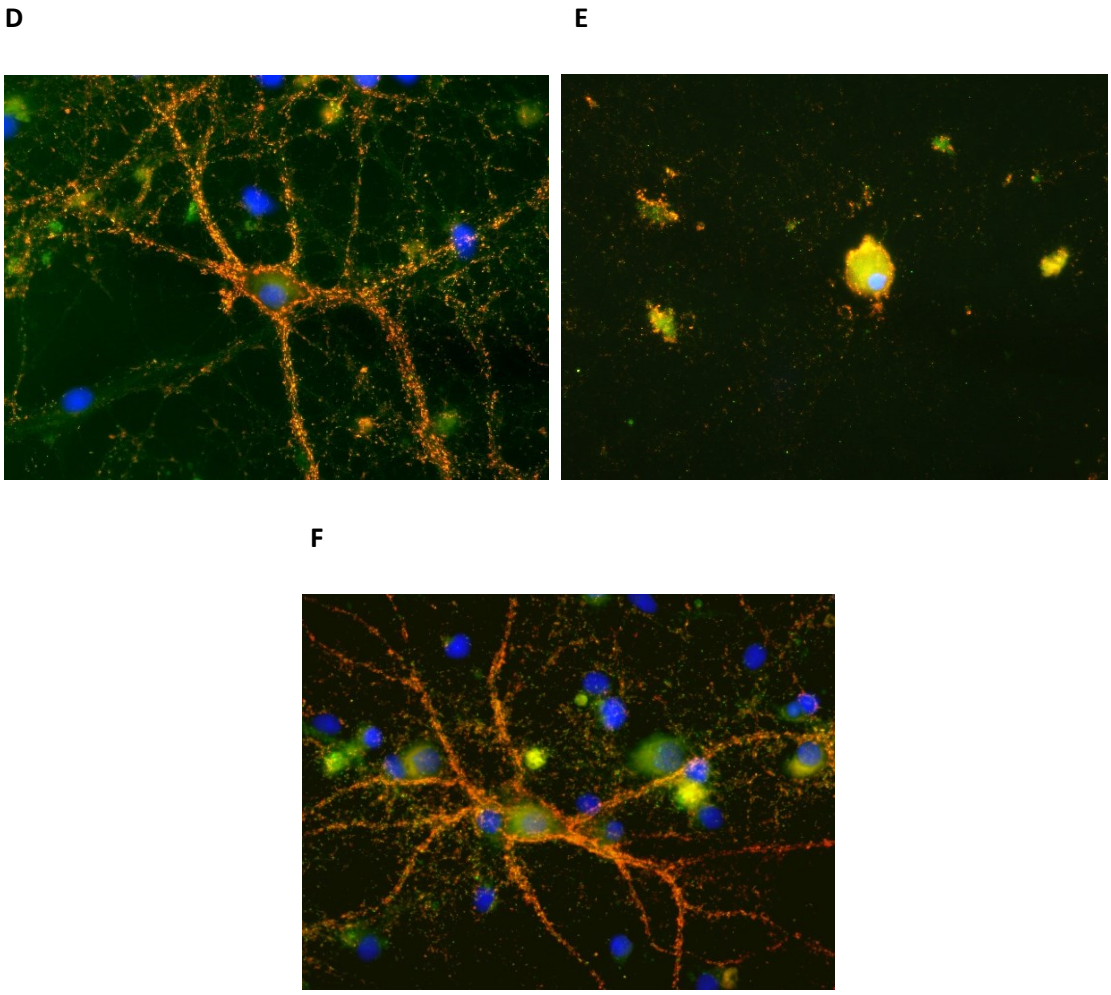

Figure 21: 1-MT protects against reductions in the co-localized expression of synaptic proteins induced by transfer of conditioned media from C6 cells to mature primary cortical neurons
Synaptophysin puncta (A), PSD-95 puncta (B) and co-localized puncta (C). Treatment of mixed glia cultures with 1-MT and transfer of CM to primary cortical neurons reduces the number of synaptophysin puncta [$P < 0.05$] compared to vehicle treated control but does not affect the number of PSD-95 or co-localized puncta. Data are expressed as mean ± SEM, n=6 coverslips per treatment group from 3 replicates of 1 experiment. ****P<0.0001, *P<0.05 vs control CM from mixed glia; $$$$ P<0.0001 vs C6 CM (Newman-Keuls post hoc test). Representative images of control (D), C6 CM (E), C6 CM+1-MT (F) treatment groups. Synaptophysin (red), PSD-95 (green), Co-localized puncta (orange/yellow), DAPI (blue), 40X.

3.7 The effect of 1-MT on C6 conditioned media induced changes in microglial and astrocytic morphology, IBA1 and GFAP immunoreactivity

3.7.1 The effect of 1-MT on conditioned media from C6 cells induced changes in microglia morphology and IBA1 immunoreactivity in mixed glia culture

Two-way ANOVA of cell/soma ratio showed effects of C6 CM [F (1, 664) = 298.2, P < 0.0001], 1-MT [F (1, 664) = 58.22, P < 0.0001], and C6 CM by 1-MT interaction [F (1, 664) = 19.04, P < 0.0001]. Post hoc comparisons revealed a reduction in microglial cell/soma ratio upon treatment with C6 CM compared to CM transferred from mixed glial cultures [P < 0.0001, Figure 22 A]. Co-treatment with 1-MT increased the cell/soma ratio of microglia compared to C6 CM vehicle treated control [P = 0.0332, Figure 22 A]. Cell/soma ratio was increased upon 1-MT treatment compared to DMEM transferred from mixed glial culutures [P < 0.0001, Figure 22 A].

Two-way ANOVA of CTCF showed an effect of 1-MT [F (1, 66) = 88.54, P < 0.0001]. Post hoc comparison revealed a decrease in CTCF following 1-MT treatment of C6 glia and mixed glia compared to vehicle treated controls [P < 0.0001, Figure 22 B].

Two-way ANOVA of cell perimeter showed an effect of C6 CM [F (1, 660) = 257.4, P < 0.0001]. Post hoc comparisons revealed reduction in microglial cell perimeter upon transfer of C6 CM [P < 0.0001, Figure 22 C]. Treatment of C6 cells with 1-MT did not influence this reduction when compared to vehicle treated controls.

A

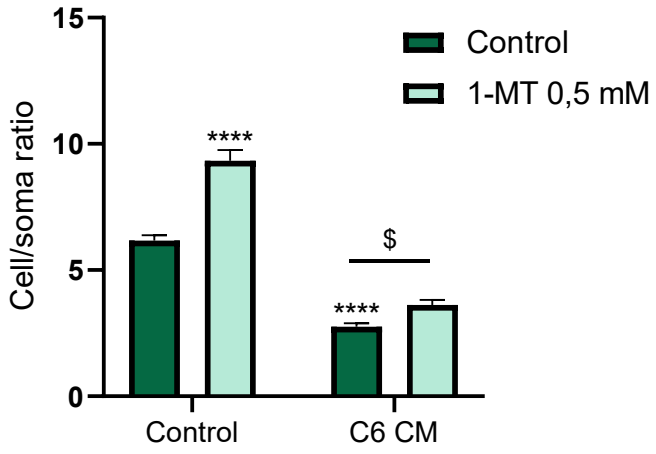

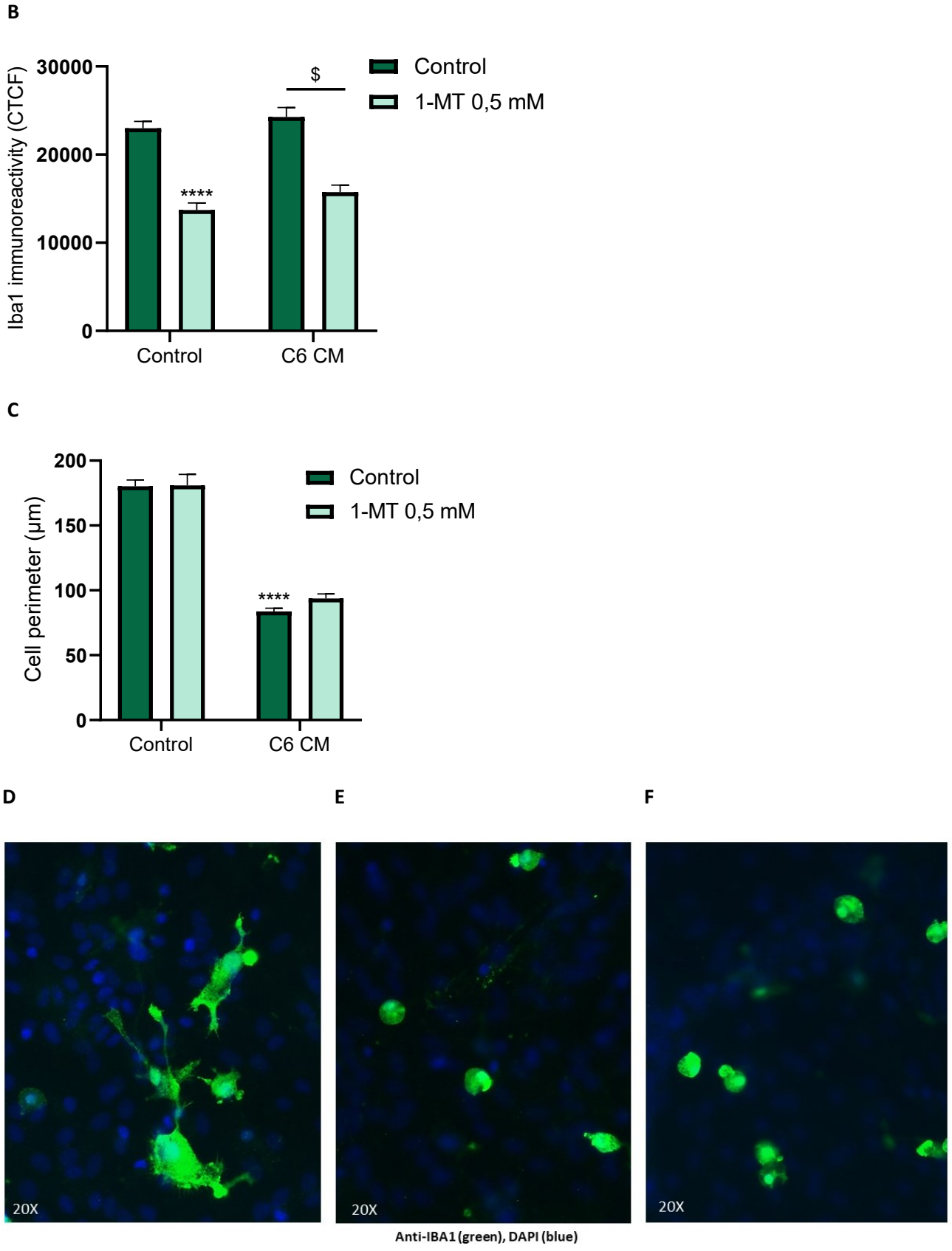

Figure 22: Effect of 1-MT on C6 CM induced changes in the morphology of microglia and immunoreactivity of IBA1 in mixed glia cultures

Immunocytochemical and morphological analyses were performed to quantify cell/soma ratio

(A), cell perimeter (B) and Iba1 immunoreactivity (C). Cell/soma ratio was quantified as a ratio of total cell perimeter to cell soma perimeter. A higher cell/soma ratio indicates more ramified microglial morphology. Data are expressed as mean ± SEM, n=6 coverslips per treatment group from 3 independent experiments. ****P<0.0001 vs control DMEM (Newman-Keuls post hoc test). $ P<0.05 vs C6 CM (Newman-Keuls post hoc test). Representative images of control (D), C6 CM (E), C6 CM+1-MT (F) treatment groups.

3.7.2 The effect of 1-MT on conditioned media from C6 cells induced GFAP immunoreactivity and changes in astrocytic morphology in mixed glia culture

Two-way ANOVA of cell/soma ratio showed an interaction between C6 CM and 1-MT [F (1, 339) = 33.31, P < 0.0001]. Post hoc comparisons revealed a reduction in astrocytic cell/soma ratio upon treatment with C6 CM compared to CM transferred from mixed glia [P < 0.0001, Figure 23 A]. Treatment of C6 cells with 1-MT increased the cell/soma ratio of astrocytes compared to vehicle treated control [P = 0.0002, Figure 23 A]. Cell/soma ratio was decreased upon 1-MT treatment of mixed glial cells compared to vehicle treated control [P < 0.0001, Figure 23 A].

Two-way ANOVA of CTCF showed an effect of C6 CM [F (1, 358) = 14.96, P = 0.0001] and C6 CM with 1-MT interaction [F (1, 358) = 20.55, P < 0.0001]. Post hoc comparisons revealed an increase in GFAP CTCF upon treatment with C6 CM compared to transfer of media from mixed glia [P < 0.0001, Figure 23 B]. Treatment of C6 cells with 1-MT increased CTCF compared to vehicle treated co troll [P < 0.0001, Figure 23 B]. CTCF was increased upon treatment of mixed glia with 1-MT compared to vehicle treated control [P < 0.0001, Figure 23 B].

Two-way ANOVA of cell perimeter showed an effect of 1-MT [F (1, 328) = 98.89, P < 0.0001], and C6 CM with 1-MT interaction [F (1, 328) = 29.10, P < 0.0001]. Treatment of C6 cells with 1-MT increased the cell perimeter when compared to vehicle treated control [P = 0.0332, Figure 23 C]. CTCF was increased upon 1-MT treatment compared to DMEM control [P < 0.0001, Figure 23 C].

A

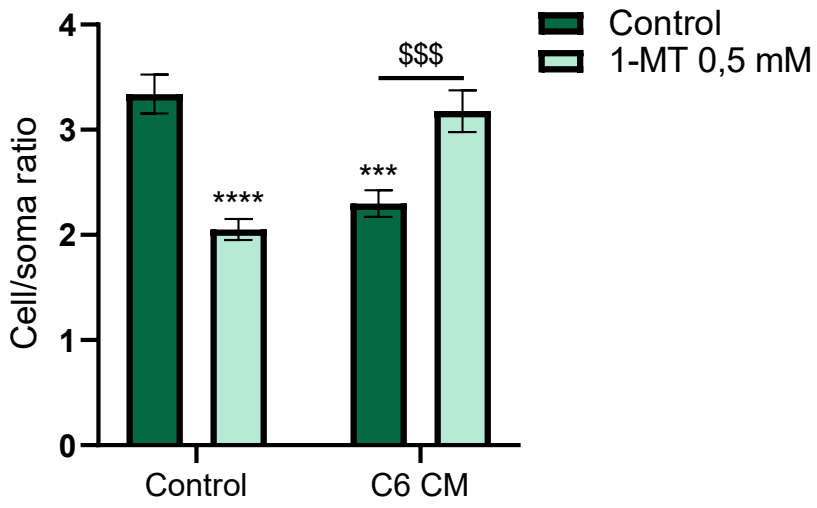
Control
1-MT 0,5 mM
Cell/soma ratio
4
3
2
1
0
****
***
$$$
Control
C6 CM

B

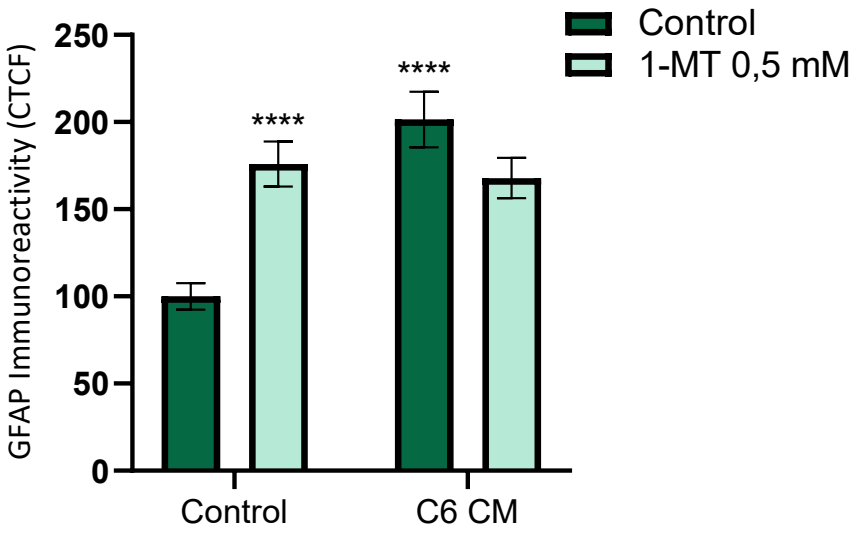
Control
1-MT 0,5 mM
GFAP Immunoreactivity (CTCF)
250
200
150
100
50
0
****
****
Control
C6 CM

C

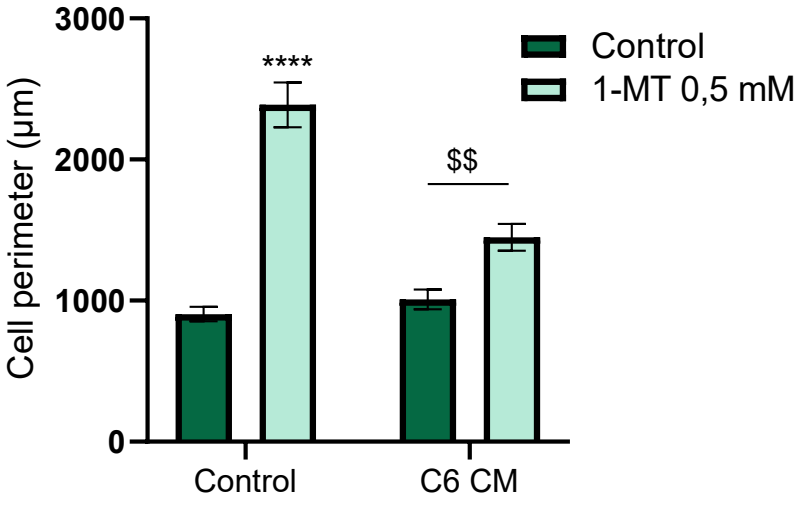
Control
1-MT 0,5 mM
Cell perimeter (µm)
3000
2000
1000
0
****
$$
Control
C6 CM

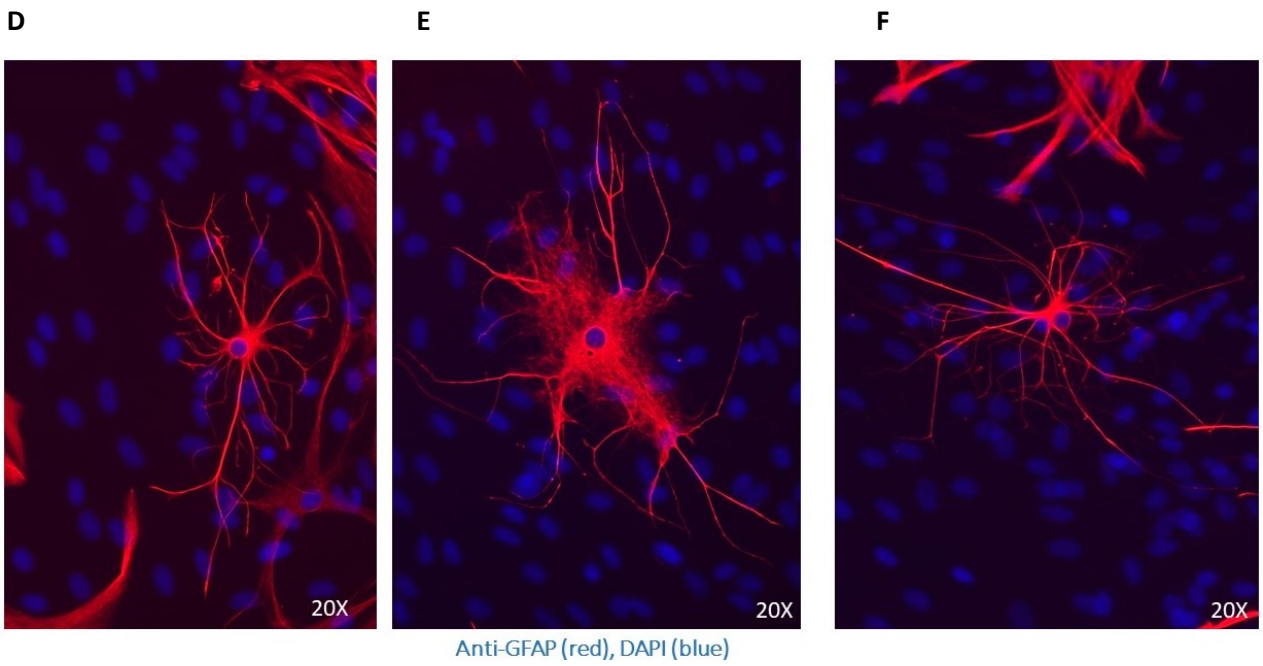

Figure 23: Effect of 1-MT on C6 CM induced changes in the morphology of astrocytes and immunoreactivity of GFAP in mixed glia cultures
Immunocytochemical and morphological analyses were performed to quantify cell/soma ratio (A), cell perimeter (B) and GFAP immunoreactivity (C). Cell/soma ratio was quantified as a ratio of total cell perimeter to cell soma perimeter. A higher cell/soma ratio indicates more ramified astrocytic morphology. Data are expressed as mean ± SEM, n=6 coverslips per treatment group from 3 independent experiments. ****P<0.0001 vs control DMEM (Newman-Keuls post hoc test). $$$ P<0.001, $$ P<0.01 vs C6 CM (Newman-Keuls post hoc test). Representative images of control (D), C6 CM (E), C6 CM+1-MT (F) treatment groups.

3.8 The effect of KYNA on C6 conditioned media induced reductions in neuronal complexity and co-localized expression of synaptic proteins in mature primary cortical neuronal cultures

3.8.1 The effect of direct KYNA treatment on the co-localized expression of synaptic proteins in mature primary cortical neurons

One-way ANOVA of synaptophysin puncta showed an effect of treatment [F (3, 351) = 11.60, P < 0.0001]. Post hoc comparisons revealed that 0.03 µM, 0.1 µM, 0.3 µM direct KYNA treatment induced reductions in the number of synaptophysin puncta when compared to vehicle treated control [Figure 24 A].

One-way ANOVA of PSD-95 puncta showed an effect of treatment [F (3, 339) = 3.256, P = 0.0218]. Post hoc comparisons revealed that 0.03 µM but not 0.1 or 0.3 µM direct KYNA treatment induced reductions in the number of synaptophysin puncta when compared to vehicle treated control [Figure 24 B].

One-way ANOVA of co-localized puncta showed an effect of treatment [F (3, 330) = 5.237, P = 0.0015]. Post hoc comparisons revealed that 0.03 µM, 0.1 µM, 0.3 µM direct KYNA treatment induced reductions in the number of co-localized puncta when compared to vehicle treated control [Figure 24 C].

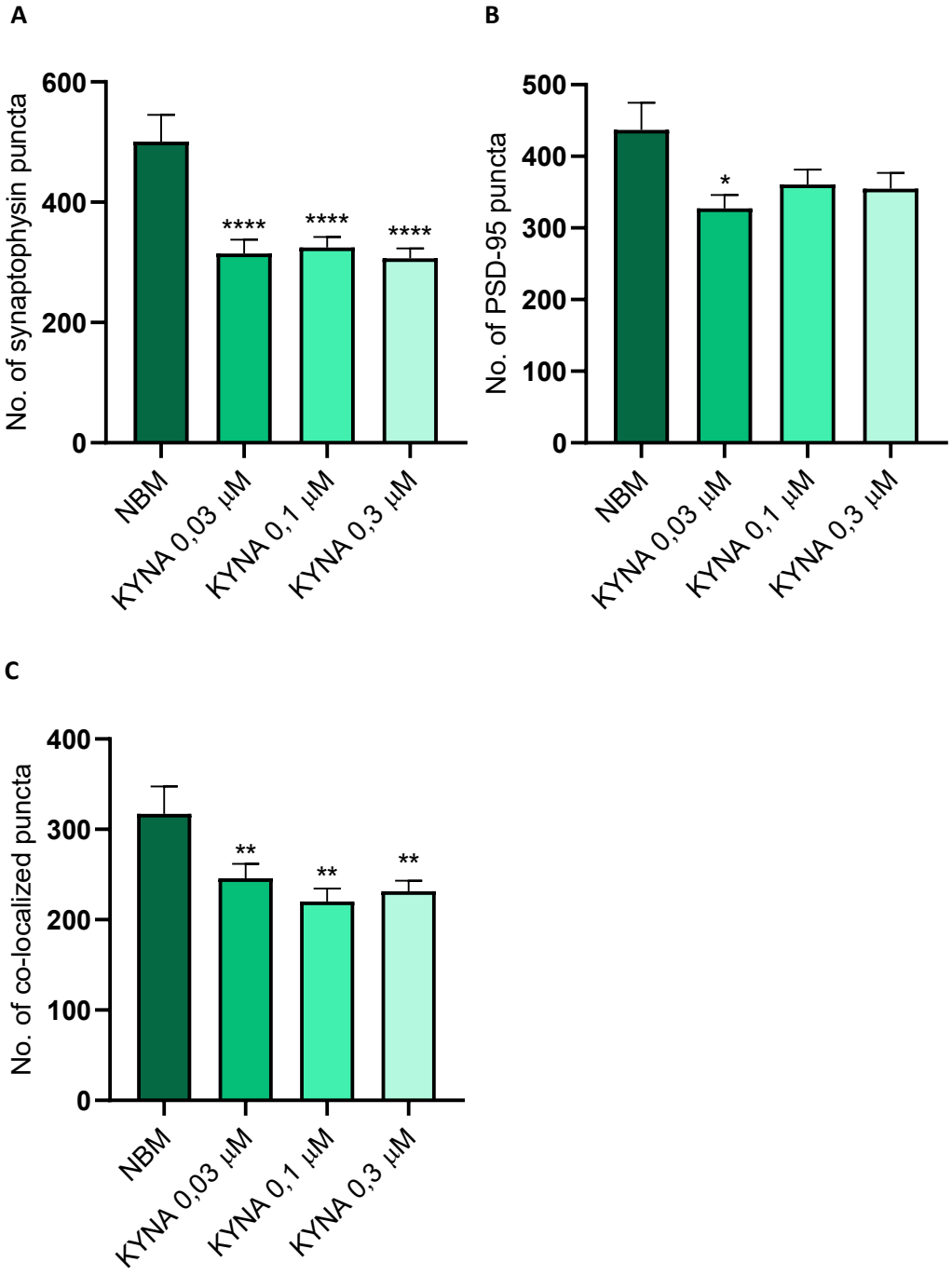

Figure 24: KYNA 0.03 μM, 0.1 μM and 0.3 μM reduce the co-localized expression of synaptic proteins in mature primary cortical neurons
We quantified synaptophysin puncta (A), PSD-95 puncta (B) and co-localized puncta (C). Data are expressed as mean ± SEM, n=6 coverslips per treatment group from 3 independent experiments. ****P<0.0001, **P<0.01, *P<0.05 vs control cNBM (Newman-Keuls post hoc test).

3.8.2 The effect of KYNA on conditioned media from C6 cells induced reductions in neuronal synaptic protein co-localization

One-way ANOVA of synaptophysin puncta showed an effect of treatment [$F(2, 214) = 46.21$, $P < 0.0001$]. Post hoc comparisons revealed a reduction in the number of puncta following treatment with C6 CM compared to mixed glia CM control [$P < 0.0001$, Figure 25 A]. Co-treatment of C6 cells with 0.3 μM KYNA protected against C6 CM induced reductions in the number of synaptophysin puncta compared to vehicle treated controls.

One-way ANOVA of PSD-95 puncta showed an effect of treatment [$F(2, 213) = 45.76$, $P < 0.0001$]. Post hoc comparisons revealed a reduction in the number of puncta following treatment with C6 CM compared to mixed glia CM control [$P < 0.0001$, Figure 25 B]. Co-treatment of C6 cells with 0.3 μM KYNA protected against C6 CM induced reductions in the number of PSD-95 puncta compared to vehicle treated controls.

One-way ANOVA of co-localized puncta showed an effect of treatment [$F(2, 211) = 42.68$, $P < 0.0001$]. Post hoc comparisons revealed a reduction in the number of puncta following treatment with C6 CM compared to mixed glia CM control [$P < 0.0001$, Figure 25 C]. Co-treatment of C6 cells with 0.3 μM KYNA protected against C6 CM induced reductions in the number of co-localized puncta compared to vehicle treated controls.

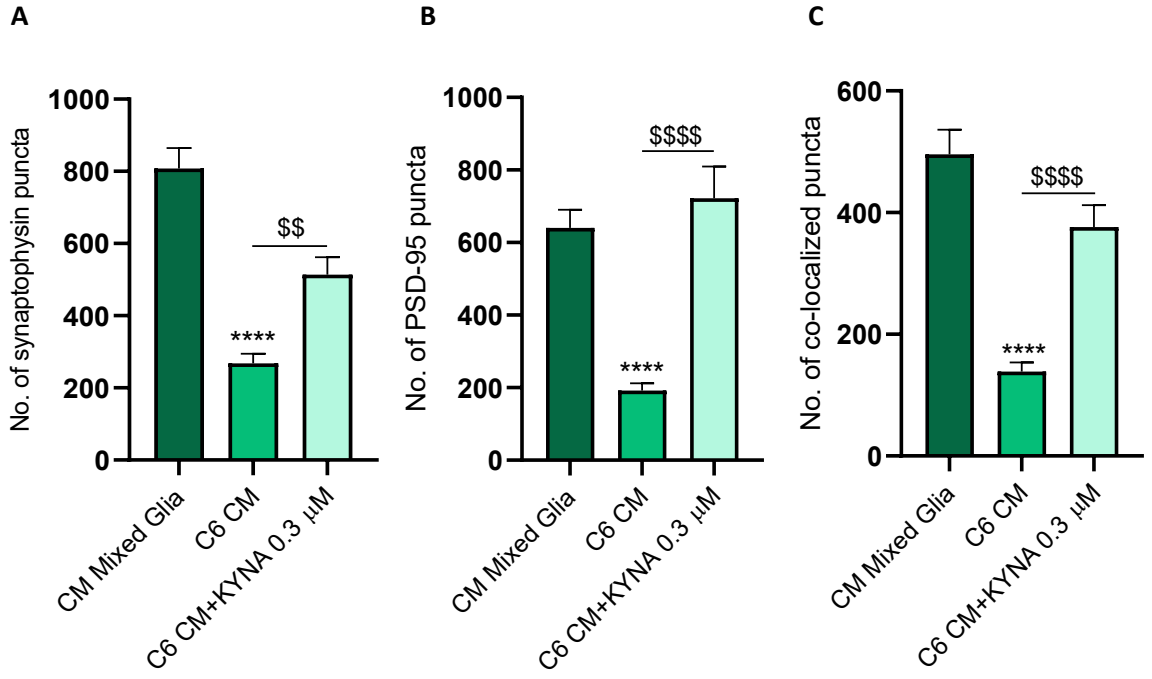
A
B
C
No. of synaptophysin puncta
No. of PSD-95 puncta
No. of co-localized puncta
1000
800
600
400
200
0
$$
$$$$
****
CM Mixed Glia
C6 CM
C6 CM+KYNA 0.3 µM

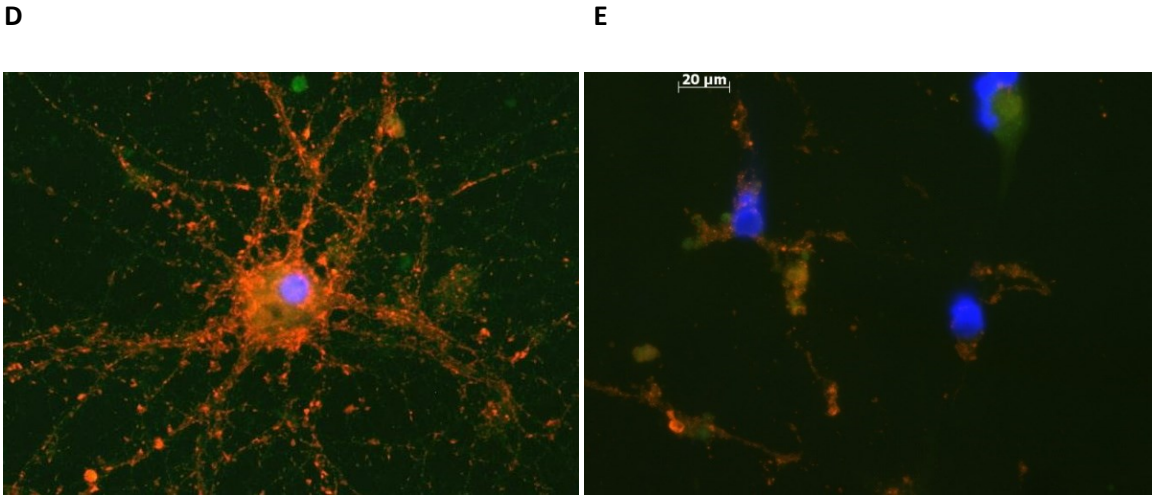
D
E
20 µm

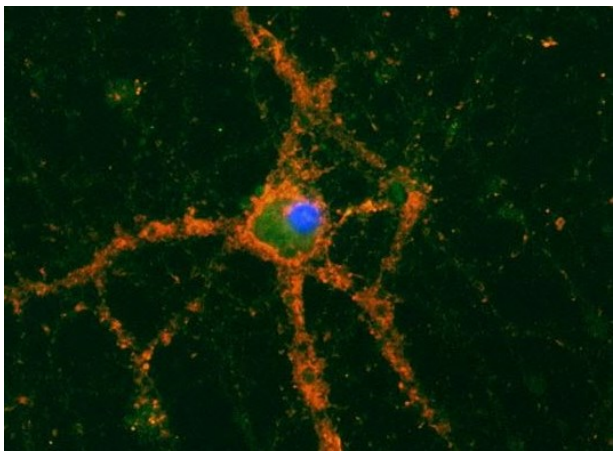
F

Figure 25: KYNA 0.3 µM protects against C6 CM induced reductions in the co-localized expression of synaptic proteins in mature primary cortical neurons
We quantified synaptophysin puncta (A), PSD-95 puncta (B) and co-localized puncta (C). Data are expressed as mean ± SEM, n=6 coverslips per treatment group from one experiment. ****P<0.0001 vs CM from mixed glial culture; $$$$ P<0.0001, $$ P<0.01 vs C6 CM (Newman-Keuls post hoc test). Representative images of control (D), C6 CM (E), C6 CM+1-MT (F) treatment groups.

4 Discussion

4.1 Summary of main findings

The results presented in this thesis provide insight into the mechanisms underlying inflammatory-driven, reactive glial and C6 cells induced neuronal atrophy and synapse loss. These studies align with literature evaluating the role of glial cells in a range of neurodegenerative and neuropsychiatric disorders. Greater understanding of these mechanisms may allow identification of specific targets involved in neuroinflammation and the development of treatments for inflammatory or other CNS conditions, including GBM.

First of all, we have investigated the effects of IFNγ stimulation of primary mixed glia and confirmed that transfer of conditioned media from these cells to mature primary cortical neurons result in the decrease in neuronal integrity, particularly reductions in neuronal complexity and co-localised expression of synaptic markers indicative of synapse loss. We then confirmed the involvement of the KP by using IDO inhibitor, 1-MT, that attenuated changes in neuronal morphology. Furthermore, we have found the increase in mRNA expression of IDO1 and TDO2 in mixed glial culture exposed to IFNγ verifying activation of the KP.

Secondly, we identified that conditioned media from C6 cells induce 1) reductions in neuronal complexity, 2) reductions in the co-localized expression of neuronal markers, 3) transformation of microglia and astrocytes towards the inflammatory phenotype, 4) increased expression of IDO1, TDO2, KMO and decreased expression of KYNU comparing to healthy mixed glia, confirming the involvement of the KP in glioma.

Finally, we have used 1-MT as a KP inhibitory agent to attenuate changes in primary cortical neurons and glia induced by C6 CM. 1-MT has preserved neuronal integrity, particularly protected against neuronal atrophy and synapse loss; the same effect wasn't observed in case of glial changes – 1-MT failed to attenuate changes in astrocytic and microglial morphology.

Additionally, we have tested the effect of three different concentrations of KYNA, 0.03 µM, 0.1 µM, and 0.3 µM, on the complexity of mature primary cortical neurons directly and found that all three concentration of KYNA decreased neuronal complexity. As previous research in our lab suggests that KYNA does protect neurons from glia-associated loss of integrity, we proceeded with KYNA to investigate its effect on C6 CM changes in synapse formation. As expected, KYNA

protected against reductions in co-localized expression of synaptic markers of mature primary cortical neurons.

Overall, the findings of this thesis confirm the involvement of KP in glioma and indicates that inhibition of KP by 1-MT or activation of neuroprotective branch of KP using KYNA provides protection against glioma-associated neuronal atrophy.

4.2 Conditioned media from IFNγ-treated activated glia reduces neuronal complexity and co-localized expression of synaptic proteins *in vitro*

Generally, conditioned media from primary microglia, astrocytes, or mixed glia is considered trophic for neuronal cultures, which is confirmed by the results from our experiments on the co-localized expression of synaptic markers: mature primary neurons treated with NBM possess co-localized synaptic puncta around 300/cell, while neurons treated with conditioned media from mixed glia have 500-600 co-localized puncta/cell.
Activation of glial cells serve primarily a protective and supportive role on neurons, but their excessive activation results in the production of various toxic factors. IFNγ promotes signalling in glial cells that initiates various pro-inflammatory responses which when released promote alterations in neuronal integrity [153]. In particular, the activation of IFNγ signalling in glial cells *in vitro* results in the increased expression and release of TNF-α, IL-1α, and IL-6 [29], all of which are reportedly up-regulated following microglial activation [29,154,155] and known to contribute to neuroinflammation [156].

Previous studies have shown that treatment of microglia with IFNγ resulted in changes in cell morphology and Iba1 immunoreactivity typical of inflammatory-mediated microglial activation [86,157]. IFNγ induced similar effects on astrocytes causing an increase in cellular volume and GFAP immunoreactivity characteristic of cellular hypertrophy [158]. Conditioned media from IFNγ treated glia (microglia, astrocytes and mixed glia) decreased neuronal complexity; however, conditioned media from IFNγ treated microglia induced the greatest reduction inferring that microglia may be the first responders and primary contributors to inflammatory driven neuronal atrophy [159,160]. No effect of direct treatment of IFNγ at a concentration of 10 ng/ml on the viability or complexity of rat primary cortical neurons was previously reported [161]. Here, we demonstrated that the transfer of conditioned media from primary mixed glia cultures treated with IFNγ (10 ng/ml) results in a robust decrease in the complexity and co-localized expression of synaptic proteins in mature rat primary cortical neurons. These results are in line with reports that

activation of IFNγ signalling in glial cells *in vitro* [40] produces a range of pro-inflammatory responses which drive alterations in neuronal integrity. Analysis of MAP2 immunohistochemical staining showed reductions in neuritic length and branching with the number of primary neuritic roots remaining intact. There was a reduction in the number of synaptic puncta: approximately 35% reduction in the number of synaptophysin puncta and more than 50% reduction in the number of PSD-95 puncta, indicating that loss of synapses may be driven by reductions in the expression of both pre- and post-synaptic markers. The effect of conditioned media from IFNγ treated mixed glia, but not when IFNγ is applied directly to neurons, indicates a prominent role of glia in mediating a loss of neuronal complexity.

IFNγ increased mRNA expression of IDO1 and TDO2 in mixed glial culture, indicating induction of the KP. Previous studies have reported that IFNγ stimulation of microglial cultures results in the release of KP metabolites, such as 3-HK, 3-HAA, QUIN and also glutamate which promote oxidative stress and excitotoxicity [151]. However, 1-MT didn't completely protect against loss of neuronal integrity induced by conditioned media from IFNγ treated mixed glia, confirming that KP activation plays a role in inflammatory driven neuronal atrophy, but there are likely other pro-inflammatory mechanisms involved [162].

4.3 Conditioned media from C6 cells does not effect neuronal viability in vitro

Changes in neuronal viability upon exposure to soluble cytokines from glioma has been observed. In the *in-vivo* murine models of glioma brain slices and neurons, the exposure of neurons to glioma cells does not affect neuronal viability within a short period of time (15 min) [163]. However, exposure of neurons to glioma for a longer duration does not spare neuronal viability. In an indirect measure, a loss of visual evoked potentials was seen in glioma bearing mice. The measurement of peak to baseline ratio as a fraction of stimulus elicited and spontaneous activity of neurons show a severe decrease when compared to naive neuronal cultures, further proving the hypothesis that although peritumoral neurons are hyperexcitable, their responses to *applied stimuli* decrease. Furthermore, neurons in the glioma microenvironment fail to evoke responses to varying visuals. Exposures to different contrasts of lights produced attenuated potentials in neurons of the glioma environment, proving that the effect of glioma on neuronal viability and function may be highly significant [164]. A possible mechanism of loss of neuronal viability could be through the impairment of neuronal integrity mediated by Activated Transcription Factor 4 [165].

In contrary, our results indicate that exposure of mature primary cortical neurons to conditioned media from C6 glioma cells for 24 or 48 hours does not effect neuronal viability. The longer

exposure to C6 CM (5-7 days [164,165]) may alter neuronal viability, however, it was not within the scope of this study to investigate that. At the moment, there is a lack of evidence to suggest that soluble glioma factors can cause neuronal mortality without cell-cell contact or to speculate a time dependent neuronal viability deterioration.

4.4 Conditioned media from C6 cells induces neuronal atrophy in mature neurons *in vitro*

Previous studies on various *in vitro* glioma cell lines, but not C6 cell line, have demonstrated a robust reduction in neuritic branching and length, and neuronal degeneration with phosphorylated tau pathology [164,166]. In particular, Vannini et al. (2016) demonstrated shrunken appearance, reduced branching and length of neurons upon examining post mortem tissue of mice with the transplanted GL261 glioblastoma cell line [164]. Lim et al. (2018), utilizing A172, HS683, U87, U373, and T98G glioma cell lines as well as with the U87 glioma mouse model, transgenic tau mice and human glioblastoma tissue, have showed that the glioblastoma-secretome activates tau pathology and identified the responsible protein as glioblastoma-secreted CD44 – a cell surface glycoprotein involved in cell to cell interactions [166]. Immunofluorescence analysis of AT8, which is used to stain for paired helical filaments (late stage of tau aggregation), revealed a 25-fold increase of AT8-positive neurons in the cortex of U87 injected mice and a 16-fold increase in the tumor region [166].

In this *in vitro* study, we demonstrated that the transfer of conditioned media from C6 cells results in neuronal damage. In line with the literature, neurons upon exposure to peritumoral factors appear shrunken, with severed processes, decreased neuritic length and axonal degeneration (Figure 26). Surprisingly, there was no effect on neuronal viability (CCK-8 assay). Alterations in neuronal complexity result in metabolic abnormalities, excitotoxicity and frequent firing rates, as has been described by recent studies [164,166]. Neuronal shrinkage observed upon treatment of neurons with conditioned media from C6 cells is indicative of neuronal atrophy in the TME.

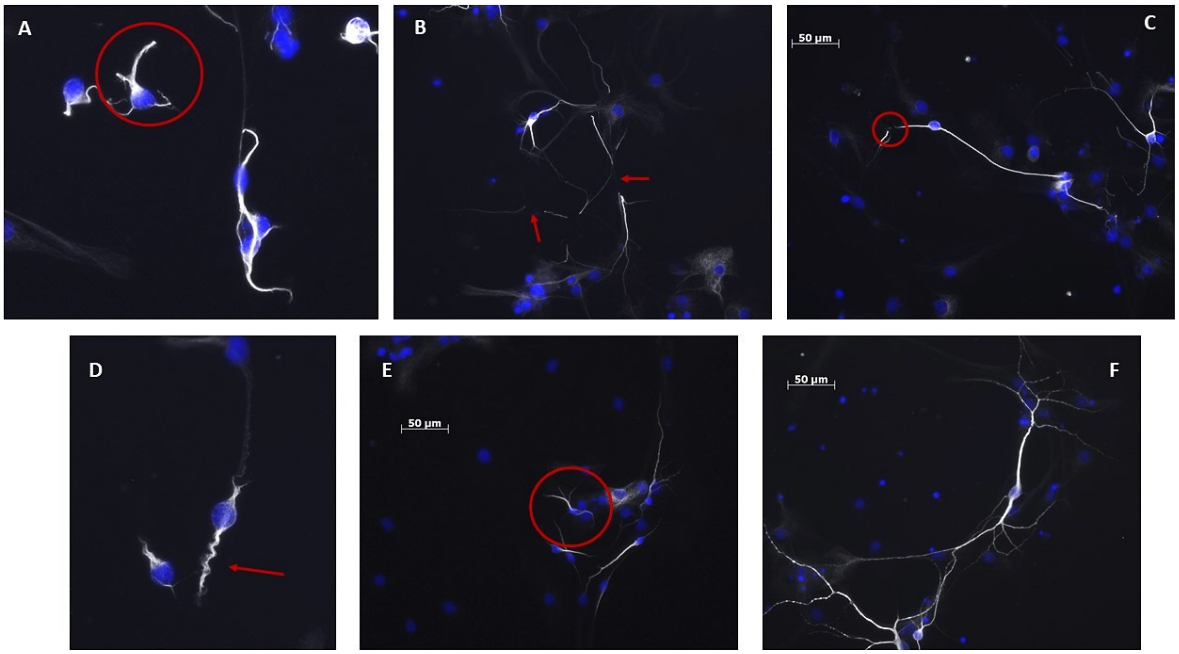

Figure 26: Conditioned media from C6 cells reduced the complexity of mature primary cortical neurons (DIV 21)

A – circle indicates axonal degeneration; B, C – arrows and circle indicate severed neuronal processes; D – arrow indicates shrunken neurons; E – circle indicate a neuron with reduced neuritic length; F – control. Anti-MAP2 (white), DAPI (blue). 20X

Wainwright et al. (2012), analyzing the IDO mRNA expression in human glioma tissues, revealed a positive correlation between IDO expression and poor prognosis; elevated IDO expression was also observed more often in high-grade gliomas [140]. These results were supported by another study, where high IDO expression was linked to shorter survival time of GBM patients [167]. Recent study has also reported increased IDO1 and IDO2 mRNA expression when compared with human fetal and adult astrocytes *in vitro*, and increased KYN/TRYP and decreased KYNA/KYN ratios in the plasma of GBM patients comparing to healthy controls. In addition, both TRYP and KYN levels decreased 48 hours and 10 weeks upon tumor resection [142].

In line with the literature, we demonstrated that mRNA expression of IDO1 was greater in C6 cells when compared to primary astrocytes or primary mixed glia, and mRNA expression of KMO when compared to mixed glia. However, when compared to primary astrocytes, C6 cells exhibited lower expression of KMO. This could indicate that in the absence of microglia, astrocytes upregulate their expression of KMO.

4.5 Conditioned media from C6 cells induces a loss of synaptic markers in mature primary cortical neurons *in vitro*

The impact of the glioma microenvironment on the co-localized expression of synaptic markers indicative of synapse formation is poorly explored to date. Recent studies observed increased cortical excitability in the glioma-infiltrated brain by human intraoperative electrocorticography [168]. Others reported neural network hyperexcitability and seizure onset – both are features of glioma pathophysiology [169]. In several studies, Venkatesh et al. suggested that increased neuronal activity promotes glioma tumor proliferation [168,170,171]. Lai et al. (2018), utilizing a mouse GBM model with stereotaxically injected GMB sphere cells, demonstrated citric cycle activation and glutamine synthesis during tumor infiltration *in vivo*, whereas N-acetyl aspartate, glutamate and gamma-aminobutyric acid concentrations were decreased resulting in decreased neurotransmission [172]. A recent study has reported decreased synapse formation in an *in vivo* Drozophila glioma model: glioma expressed protein Frizzled1, that serves as a receptor of neuronal protein Wingless, is suggested to be implicated in loss of synapses, as the depletion of Wingless from neurons by glioma interrupts neuronal Wingless-Frizzled1 signalling [173]. These findings indicate that crosstalk between glioma tumours and surrounding neuronal cells is a key contributor to malignant growth.

We demonstrated that conditioned media transferred from C6 cells reduced the number of synaptophysin puncta by approximately 75% and PSD-95 puncta by 60%. In contrast to conditioned media from IFNγ treated mixed glia, conditioned media from C6 cells had a greater effect on the co-localized expression of synaptic proteins, with synaptophysin protein being affected to a greater extent. This effect may be due to neuronal hyperexcitability as described in studies to date, however, further research is required to confirm the impact of the loss of synaptic proteins.

4.6 Treatment with the KP inhibitor 1-MT attenuates conditioned media from IFNγ treated mixed glia and C6 cells induced reductions in neuronal complexity and co-localization of synaptic markers in primary cortical neurons

Kynurenine pathway enzymes are overexpressed in GBM. Upregulated expression of these enzymes has been related to severity of gliomas and patient survival. Moreover, in an orthotopic GL261 cell tumor model was shown that brain tumors possessing high IDO levels increased the recruitment of immunosuppressive Tregs and decreased the frequency of CD68+ T cells

compared with IDO-deficient brain tumors [174]. Another study, including 75 gliomas, showed higher expression of IDO in malignant gliomas compared with low-grade gliomas. Moreover, stronger IDO expression was associated with shortened survival time in GBM patient [167]. Additionally, it has been reported that glioma cells have increased mRNA expression of IDO1 and IDO2 compared with human fetal astrocytes and human adult astro- cytes cultures as well as decreased Kats mRNA expression, and these expression enhanced when cells were stimulated with IFNγ [142]; the same work also reported increased Kyn/Trp ratios and decreased Kyna/Kyn ratios in the plasma of glioblastoma patients compared with healthy people [142]. This is in line with our findings where mRNA expression of IDO1 and TDO2 is increased in C6 glioma cells and IFNγ stimulated mixed glia. Therefore, significantly increased expression of IDO in cancer cells and in the tumor microenvironment has arisen as a promising target for GBM treatment, based on the inhibition of IDO as a potential therapy for cancer patients. Among the first strategies, is the systemic administration of 1-MT, a competitive inhibitor of the IDO, which delayed tumor development in a murine model of Lewis lung carcinoma [175]. Subsequently, it was described that the expression of IDO in immunogenic cells (P815B) avoided their rejection by preimmunized mice, an effect that was associated with the inhibition of specific T cell response [176]. This effect was partially reversed when preimmunized mice were administered with 1-MT [176]. Due to the results observed in animal models, 1-MT has been tested and approved on phase I clinical trials in patients with solid and solid metastatic neoplasms, lung, ovarian, Fallopian tube, and breast cancer showing disease stabilization in most cases [177,178].

Thus, the use of IDO inhibitors and microglial elimination in combination with classical chemotherapy and radiotherapy in GBM murine models, as well as the clinical trials that have tested 1-MT in different kinds of solid and metastatic tumors has shown promising results for targeting IDO and the KP against GBM.

Previous studies reported a preventive effect of 1-MT on reduced neuronal complexity upon pre-treatment of IFNγ-stimulated immortalized BV-2 microglia and transfer of conditioned media from BV-2 cells to primary cortical neurons. The results of this thesis concur with prior findings, demonstrating that 1-MT protects mature primary cortical neurons from loss of neuronal complexity, reduction in the number of synaptic markers and their co-localized expression induced by conditioned media from IFNγ treated mixed glia and conditioned media from C6 cells. Treatment with 1-MT leads to protection from reduced neuritic length and number of branches after exposure to conditioned media from C6 cells, but in contrast, protected only neuritic branching after exposure to conditioned media from IFNγ stimulated mixed glia. These results indicate that additional pro-inflammatory mechanisms in IFNγ induced

neuronal atrophy are likely to be involved. As IFNγ receptors are expressed on most of glial cells [54,179,180], it is expected that other cell death pathways such as MAPK-driven pathways and gene regulatory pathways mediated by transcription factors such as interferon regulatory factor 1 (IRF1) and IRF8 [181] are activated in addition to the KP. As reactive glia are also known to produce nitric oxide which inhibits cellular respiration and results in rapid glutamate release and excitotoxicity [182] it is reasonable to expect that NO may have also contributed to the observed reductions in neuronal complexity.

In both cases, treatment with 1-MT conserved the ability of neuronal cells to form synapses by preventing a reduction in synaptophysin, PSD-95 puncta, and their co-localization. A reduction in the expression of synaptic markers and loss of neuronal complexity are likely to disable synaptic processes within neuronal networks.

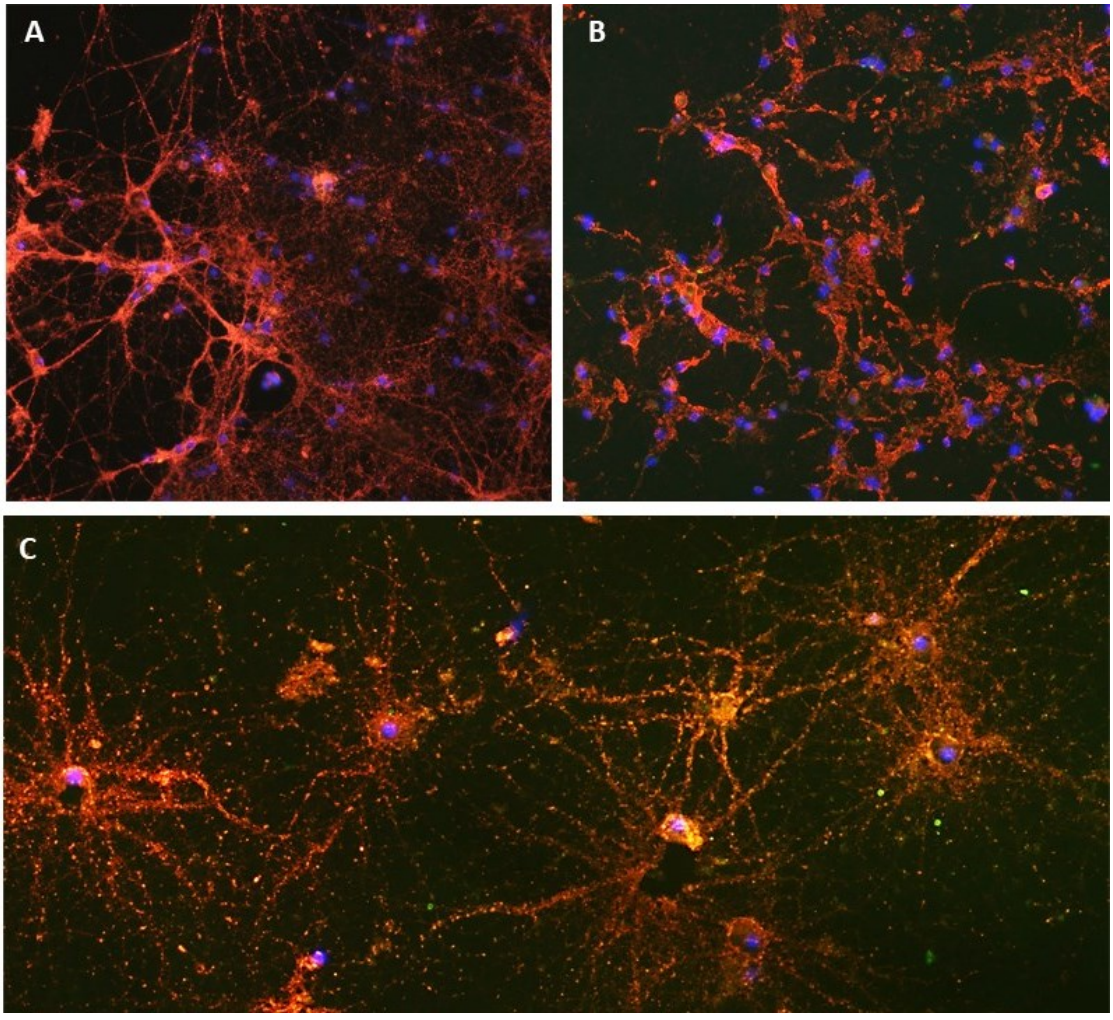

Figure 27: 1-MT protects against conditioned media from C6 cells induced reduction in the co-localized expression of synaptic markers in primary cortical neurons

This figure shows neuronal networks on control (A), C6 CM (B) and C6 CM + 1-MT (C) treatment groups at 10X magnification. Neurons are interconnected on A and C, but the network is disrupted in B. Anti-synaptophysin (red), Anti-PSD-95 (green), co-localized puncta (orange).

4.7 Conditioned media from C6 cells induces microglial and astrocytic cell transformation in mixed glial culture. Effect of 1-MT

Reactive glial-mediated neurotoxicity remains underexplored despite the numerous studies conducted in the field. Astrocytes and microglia can differentiate and change their morphology upon exposure to various triggering stimuli via complex signalling mechanisms capable of producing both neurotoxic and neuroprotective factors. As glial cells are key components of the brain's immune system, it was of our great interest to investigate the effect of peritumoral factors (conditioned media from C6 cells) on the morphology of healthy glial cells as determined by IBA1 immunoreactivity for microglial cells and GFAP immunoreactivity for astrocytes.

Previous studies exploring astrocytic morphology have reported equivocal results: analysis of post mortem murine or human glioma tissues show swollen and large cell bodies [183,184], long, dense and branched processes [184–186], with some of them directed towards glioma [185], hypertrophic morphology with short and thick processes [186], no change in morphology [187] or mixture of different astrocytic phenotypes in the tissue [186].

Mixed glial culture utilized in the current experiments didn't show uniformity of astrocytic phenotype across treatment groups. We identified four astrocytic phenotypes that may also represent four stages of astrocytic cell transformation (Figure 28).

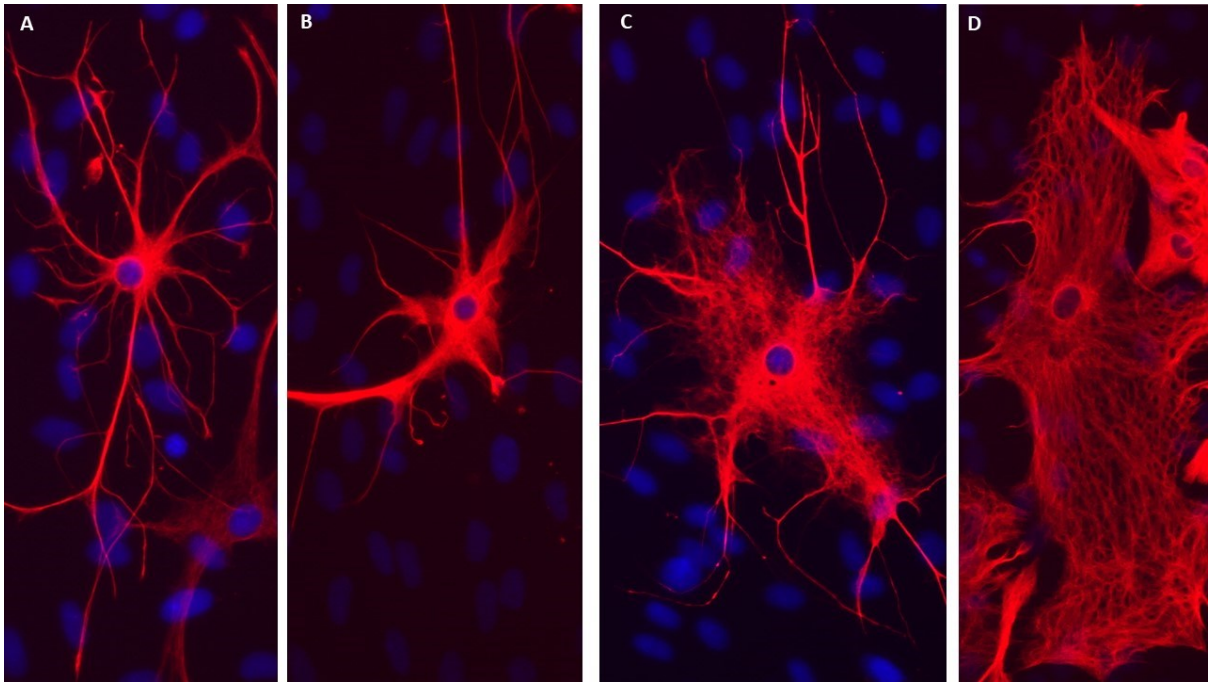

Figure 28: Astrocytic phenotypes across mixed glial cultures
Anti-GFAP (red), DAPI (blue). 20X.

The cells on figure 28 A exhibits small cell bodies and long branched processes, cells C and B are intermediate stages, and cell D is a hypertrophic swollen astrocyte with very short to no processes.

Nonetheless, we observed a significant difference in some aspects of astrocytic morphology following exposure to conditioned media from C6 cells: a reduced astrocytic cell/soma ratio, indicating cell body enlargement, and an increase in GFAP immunoreactivity, indicating induction of GFAP expression. Increased expression of GFAP is associated with astrocytic activation and astrogliosis [188]. In fact, the increase in GFAP mRNA expression was observed in response of astrocytes to IFNγ, NO or LPS *in vitro* and *in vivo* [188–190].

It is well known that microglia exhibit amoeboid morphology upon activation by inflammatory or other pathogen or disease associated molecular patterns [9,12,14,16,51,180,191]. Indeed, recent *in vitro, in vivo* and *ex-vivo* studies of glioma models demonstrate amoeboid and swollen microglial morphology with short to no processes. In line with the literature, in this investigation, microglia exhibited a robust reduction in the cell area, cell/soma ratio and cell perimeter, as apparent from Figure 29, but no difference in the intensity of IBA1 immunoreactivity was observed.

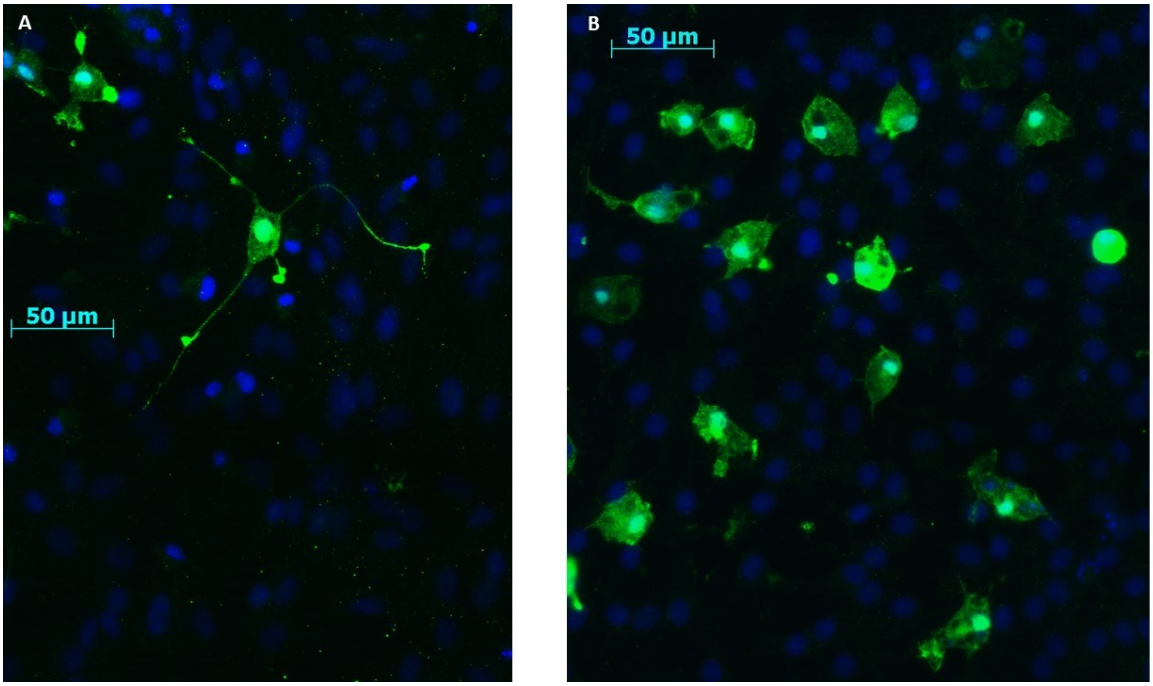

Figure 29: Conditioned media from C6 cells induce microglia transformation into amoeboid phenotype
A – control; B – conditioned media from C6 cells. Anti-IBA1 (green), DAPI (blue). 40X.

As 1-MT was able to protect against conditioned media from C6 cells induced reduction in astrocytic cell/soma ratio but not against other alterations in glial morphology, we suggest that the KP plays a minor role and that different mechanisms underlying glial cell activation are involved. Moreover, the KP may be activated as a consequence of glial cell activation.

Treatment of mixed glial cultures with 1-MT alone resulted in a) increase in microglial cell/soma ratio and decrease in IBA1 immunoreactivity and b) decrease in astrocytic cell/soma ratio and increase in GFAP immunoreactivity. These results indicate that inhibiting the KP under physiological conditions may result in changes in glia morphology, directing microglia to a resting, ramified state and astrocytes to a hypertrophic state.

4.8 Treatment of C6 cells with KYNA protects against conditioned media from C6 cells induced reductions in the co-localized expression of synaptic markers

KYNA is reported to be a neuroprotective KP metabolite [192–194]. KYNA is also the only endogenous antagonist to NMDA receptors known so far; it inhibits the α7-nicotinic receptors, showing anticonvulsant effects on murine models as well as in human patients [195]. Recently, it was found that KYNA is a free radical scavenger of superoxide anion, hydroxyl radical, and

peroxynitrite. KYNA is also considered as an endogenous antioxidant as it is able to reduce oxidative damage [196]. Furthermore, it has been shown that KYNA binds selectively to GPR35 receptor [142]; Kyna-mediated activation of GPR35 leads to intracellular Ca2+ influx, inositol phosphate production, attenuating LPS-induced TNF-α release and reducing acetic acid-induced pain [142,197]. As KYNA is unable to cross the BBB, systemic l-kynurenine administration has been used to show the protective effect of KYNA in 6-hydroxidopamine-induced Parkinson disease models, hippocampal β-amyloid, and glutamate toxicity [198,199].

Taking into consideration the potential influence of endogenous and exogenous sources of KYNA and the process of its excretion on the overall KYNA level in physiological fluids, measurements of this compound in cancer tissue and its surrounding seem to be the most relevant. The majority of studies revealed the elevated KYNA level in tumours in comparison to healthy tissue [196]. However, decreased concentration of KYNA in renal cell carcinoma might be associated with loss of filtration properties by cancer tissue [195]. Importantly, the possible relationship between KYNA content and type of biopsy specimen has not been investigated so far.

We previously reported that KYNA attenuates reductions in the complexity of mature primary cortical neurons and co-localized expression of synaptic markers following transfer of conditioned media from IFNγ treated mixed glia, as well as from IFNγ treated BV-2 microglia [128,162]. Direct treatment of mature primary cortical neurons albeit with higher concentrations of KYNA (0.03, 0.1 and 0.3 µM) however results in a reduction of synaptophysin, PSD-95 puncta and their co-localization. This indicates a dual action of KYNA: well-described neuroprotective metabolite but also potentially damaging to neurons at higher concentrations. Disrupting a sensitive balance of KP metabolites (raising KYNA) or enzymes under physiological conditions is likely directing the KP towards the neurotoxic branch, hence the decrease in the co-localization of synaptic proteins.

A recent study reported that KYNA applied to human GBM T89G cells inhibited their proliferation at micro- and millimolar concentrations, that were non-toxic to neurons [200]. On the other hand, KYNA promoted glioma cell proliferation through Fibroblast Growth Factor-1 release [201]. In this investigation, KYNA was able to protect against conditioned media from C6 cells induced reductions in the co-localized expression of synaptic proteins. These results indicate that KP metabolites may be differentiated for their protective and potentially damaging effects on neurons and that increasing KYNA, on the neuroprotective branch of the KP has the potential to reduce the deleterious effects of excitotoxic and oxidative metabolites such as QUIN, 3-HAA and 3-HK, associated with the neurotoxic branch. Further research will need to be carried out to

clarify the role of individual metabolites and whether these might be targeted to protect neurons within the TME.

4.9 Conclusions

The results of this thesis highlight a role of neuronal-glial interaction and KP in driving activated glia-associated changes in neuronal integrity, such as neuronal atrophy and synapse loss. The results described also provide new insights into malignancy-associated changes: altered neuronal and glial morphology. Having established the effect of KP inhibition on IFNγ-induced reactive glia-associated reduction in neuronal complexity and synapse formation *in vitro*, we further assessed a role for KP in mediating glioma-neuronal interactions with the C6 cell line. We demonstrated that treatment with the IDO1 inhibitor protected against conditioned media from C6 cells-induced reduction in neuronal complexity, synaptic protein co-localization, and partially astrocytic activation and transformation. In addition, we showed that treatment of C6 cells with KYNA protects against conditioned media from C6 cells induced reductions in neuronal complexity and ability to form synapses, indicative of the protective properties of KYNA.

These findings collectively indicate an important role for KP activation in mediating C6 glioma induced reductions in neuronal complexity and synapse formation and suggest that the KP might be targeted to protect against inflammatory-associated changes in neuronal integrity and astrocytic morphology.

Limitations

The use of *in vitro* primary brain cell cultures provides numerous advantages including but not limited to technique simplicity, ability to study specific cell types in a well-defined controlled environment, consistency and reproducibility of the results, etc. However, they don't always represent a complex interconnected system found in animal or human brain. The disadvantages of cell culture techniques are a) high sensitivity to small changes in the experimental conditions, which was reported to affect neuronal outgrowth [202], b) bacteria and fungi contamination with failure to follow strict aseptic practices, c) cross-contamination with other cell types as well as d) inter-culture variability. The use of cell lines, in turn, present a risk of genotyping, phenotyping variations, genetic drift and heterogeneity over an extended period of time of repeated passaging of the cells. One of the alternatives to primary cell culture and cell lines is a co-culture or 3D cell spheres representing a more natural environment. The co-culture of patient-derived

low-passage glioma-initiating stem cells with primary neurons, astrocytes and microglia was successfully utilized to investigate the crosstalk between glioma and healthy brain cells [203]. This approach can be adapted to co-culture C6 cells with primary rat cortical neurons, astrocytes, microglia and mixed glia to verify the results presented in this study of the effect of conditioned media from C6 cells.

Sholl analysis used to analyze neuronal complexity in this study fails to fully represent *in vivo* neuronal systems and differentiation of basic morphological structures, such as axon and dendrites, as the imaged neurons have to be isolated from each other in order to enable the use of this technique. Similarly to Sholl analysis, the technique utilized to analyze pre- and post-synaptic markers and their co-localized expression requires isolated neuron imaging. The assay is also limited to identifying mostly excitatory and unstable synapses [150].

Future directions

In this study, we investigated the viability of neuronal cells *in vitro* using CCK-8 assay. Still, it is necessary to confirm the results using MTT, lactate dehydrogenase release or Alamar blue assays, as they are based on a different principles of viability detection. It is also of interest to test astrocytic and microglial cell viability upon treatment with conditioned media from C6 cells.

To expand our understanding of the impact of C6 cells on healthy brain cells, *in vivo* work should be carried out to verify *in vitro* findings. The use of *in vivo* glioma cell model with C6 cells injected into the brain is appropriate [204]. We could then examine the impact that tumor has on healthy brain cells by analyzing neuronal complexity and neurite outgrowth by Ca^{2+} imaging [205] or transfection of neurons with green fluorescent protein [206], and analyzing synapse formation by two-photon excitation laser scanning microscopy [207]. In that way, we would overcome the limitations of Sholl analysis and *in vitro* approaches to determine expression of co-localized synaptic markers adapted from Eroglu et al. (2010).

The protective effects of 1-MT and KYNA have to be confirmed in the *in vivo* studies as well. Overall additional *in vitro* and *in vivo* work will help to further understand the role of the kynurenine pathway in glioma-induced neuronal atrophy, loss of synapses and the effect on morphology of healthy glial cells. mRNA expression of KP enzymes such as IDO, TDO, KMO, KATs and KYNU in mixed glia, astrocytes and microglia upon transfer of conditioned media from C6 cells should be confirmed *in vivo*. The activation of the neurotoxic part of the kynurenine pathway results in the production of most biologically active KP metabolite QUIN. Its concentration in the brain is usually maintained at nanomolar; however, inflammation increases

its levels dramatically [208]. We previously demonstrated that activation of glial cells in mixed glial culture induced by IFNγ results in the induction of the KP with increased concentrations of QUIN, KYN, KYNA in the conditioned media of mixed glial cultures [162]. The complexity of neurons is severely affected by direct treatment with QUIN or by transfer of conditioned media from IFNγ treated mixed glia, and the resulting neuronal atrophy may be attenuated by the application of KYNA [162]. In this investigation, we have demonstrated the protective effect of KYNA on the reductions in the co-localized expression of synaptic markers induced by conditioned media from C6 cells. As we previously showed that direct treatment of primary cortical neurons with KYNA *in vitro* increases their complexity and outgrowth [162], we hypothesize that KYNA will have similar protective effects on reductions in the complexity of primary cortical neurons treated with conditioned media from C6 cells. Additional *in vitro* work has to be done to more fully elucidate the effects of KYNA on neuronal complexity *in vitro.*

O'Farrell et al. (2017) showed that reductions in neuronal viability and complexity induced by IFNγ treated BV-2 microglia were prevented by co-treatment of neurons with the NMDA receptor antagonist, MK-801 [128]. We suggest that MK-801, together with 1-MT, can also preserve neuronal integrity, protect from a loss of complexity, outgrowth and co-localized expression of synaptic proteins.

O'Farrell et al. (2017) also reported that treatment of IFNγ stimulated BV-2 cells with the synthetic glucocorticoid dexamethasone attenuated neuronal atrophy induced by transfer of conditioned media from IFNγ treated BV-2 microglia [128]. Steroid use is also common in pre- and post-operative treatment of brain cancers, such as glioblastoma, mainly to reduce glioma-associated vasogenic edema and to prevent increased intracranial pressure [209]. It would be of great interest to investigate if dexamethasone has a similar protective effect on reductions of neuronal complexity and co-localized expression of synaptic markers induced by transfer of conditioned media from C6 cells.

Publications

Kate O'Reilly, Katherine O'Farrell, Oivind Midttun, Yuliia Rakovets, Jennifer David -Bercholz, Andrew Harkin. (2021) Kynurenic Acid Protects Against Reactive Glial-associated Reductions in the Complexity of Primary Cortical Neurons. *J Neuroimmune Pharmacol*. Published online 2021. doi:10.1007/s11481-020-09976-x.

References

1. DeFelipe J, Jones EG. Santiago Ramón y Cajal and methods in neurohistology. *Trends Neurosci*. 1992;15(7):237-246. doi:10.1016/0166-2236(92)90057-F

2. Azevedo FAC, Carvalho LRB, Grinberg LT, et al. Equal numbers of neuronal and nonneuronal cells make the human brain an isometrically scaled-up primate brain. *J Comp Neurol*. 2009;513(5):532-541. doi:10.1002/cne.21974

3. Crossman AR, Neary D. Neuroanatomy: An illustrated colour text. Edinburgh: Churchill Livingstone. Published online 2010.

4. Kevenaar JT, Hoogenraad CC. The axonal cytoskeleton: From organization to function. *Front Mol Neurosci*. 2015;8(AUGUST):1-12. doi:10.3389/fnmol.2015.00044

5. Südhof TC, Malenka RC. Understanding Synapses: Past, Present, and Future. *Neuron*. 2008;60(3):469-476. doi:10.1016/j.neuron.2008.10.011

6. Dent EW, Baas PW. Microtubules in neurons as information carriers. *J Neurochem*. 2014;129(2):235-239. doi:10.1111/jnc.12621

7. Turrin NP, Rivest S. Molecular and cellular immune mediators of neuroprotection. *Mol Neurobiol*. 2006;34(3):221-242. doi:10.1385/MN:34:3:221

8. Gehrmann J, Matsumoto Y, Kreutzberg GW. Microglia: Intrinsic immuneffector cell of the brain. *Brain Res Rev*. 1995;20(3):269-287. doi:10.1016/0165-0173(94)00015-H

9. Olah M, Biber K, Vinet J, W.G.M. Boddeke H. Microglia Phenotype Diversity. *CNS Neurol Disord - Drug Targets*. 2011;10(1):108-118. doi:10.2174/187152711794488575

10. Nimmerjahn A, Kirchhoff F, Helmchen F. Resting Microglial Cells Are Highly Dynamic Surveillants of Brain Parenchyma in vivo. *Science (80-)*. 2005;308:1314-1318.

11. Gomez-Nicola D, Perry VH. Microglial dynamics and role in the healthy and diseased brain: A paradigm of functional plasticity. *Neuroscientist*. 2015;21(2):169-184. doi:10.1177/1073858414530512

12. Kettenmann H, Hanisch U-K, Noda M, Verkhratsky A. Physiology of microglia. *Physiol Rev*. 2011;91(2):461-553. doi:10.1152/physrev.00011.2010

13. Aloisi F. Immune function of microglia. *Glia*. 2001;36(2):165-179. doi:10.1002/glia.1106

14. Thored P, Heldmann U, Gomes-Leal W, et al. Long-term accumulation of microglia with proneurogenic phenotype concomitant with persistent neurogenesis in adult subventricular zone after stroke. *Glia*. 2009;57(8):835-849. doi:10.1002/glia.20810

15. Zhou T, Huang Z, Sun X, et al. Microglia polarization with M1/M2 phenotype changes in rd1 mouse model of retinal degeneration. *Front Neuroanat*. 2017;11(September):1-11. doi:10.3389/fnana.2017.00077

16. Ma Y, Wang J, Wang Y, Yang GY. The biphasic function of microglia in ischemic stroke. *Prog Neurobiol*. 2017;157:247-272. doi:10.1016/j.pneurobio.2016.01.005

17. Park HJ, Oh SH, Kim HN, Jung YJ, Lee PH. Mesenchymal stem cells enhance α-synuclein clearance via M2 microglia polarization in experimental and human parkinsonian disorder. *Acta Neuropathol*. 2016;132(5):685-701. doi:10.1007/s00401-016-1605-6

18. Gao HM, Liu B, Hong JS. Critical role for microglial NADPH oxidase in rotenone-induced degeneration of dopaminergic neurons. *J Neurosci*. 2003;23(15):6181-6187. doi:10.1523/jneurosci.23-15-06181.2003

19. Qin L, Liu Y, Wang T, et al. NADPH Oxidase Mediates Lipopolysaccharide-induced Neurotoxicity and Proinflammatory Gene Expression in Activated Microglia. *J Biol Chem*. 2004;279(2):1415-1421. doi:10.1074/jbc.M307657200

20. Wu J, Yang S, Xi G, Fu G, Keep RF, Hua Y. Minocycline reduces intracerebral hemorrhage-induced brain injury. *Neurol Res*. 2009;31(2):183-188. doi:10.1179/174313209X385680

21. Kigerl KA, Gensel JC, Ankeny DP, Alexander JK, Donnelly DJ, Popovich PG. Identification of two distinct macrophage subsets with divergent effects causing either neurotoxicity or regeneration in the injured mouse spinal cord. *J Neurosci*. 2009;29(43):13435-13444. doi:10.1523/JNEUROSCI.3257-09.2009

22. Fagan SC, Waller JL, Nichols FT, et al. Minocycline to Improve Neurologic Outcome in Stroke (MINOS): A dose-finding study. *Stroke*. 2010;41(10):2283-2287. doi:10.1161/STROKEAHA.110.582601

23. Colombo E, Farina C. Astrocytes: Key Regulators of Neuroinflammation. *Trends Immunol*. 2016;37(9):608-620. doi:10.1016/j.it.2016.06.006

24. Farina C, Aloisi F, Meinl E. Astrocytes are active players in cerebral innate immunity. *Trends Immunol*. 2007;28(3):138-145. doi:10.1016/j.it.2007.01.005

25. Perea G, Navarrete M, Araque A. Tripartite synapses: astrocytes process and control synaptic information. *Trends Neurosci*. 2009;32(8):421-431. doi:10.1016/j.tins.2009.05.001

26. Sofroniew M V., Vinters H V. Astrocytes: Biology and pathology. *Acta Neuropathol*. 2010;119(1):7-35. doi:10.1007/s00401-009-0619-8

27. Belanger M, Magistretti PJ. The role of astroglia in neuroprotection. *Dialogues Clin Neurosci*. 2009;11(3):281-296.

28. Cordiglieri C, Farina C. Astrocytes Exert and Control Immune Responses in the Brain. *Curr Immunol Rev*. 2010;6(3):150-159. doi:10.2174/157339510791823655

29. Liddelow SA, Guttenplan KA, Clarke LE, et al. Neurotoxic reactive astrocytes are induced by activated microglia. *Nature*. 2017;541(7638):481-487. doi:10.1038/nature21029

30. Zamanian JL, Xu L, Foo LC, et al. Genomic analysis of reactive astrogliosis. *J Neurosci*. 2012;32(18):6391-6410. doi:10.1523/JNEUROSCI.6221-11.2012

31. Liberto CM, Albrecht PJ, Herx LM, Yong VW, Levison SW. Pro-regenerative properties of cytokine-activated astrocytes. *J Neurochem*. 2004;89(5):1092-1100. doi:10.1111/j.1471-4159.2004.02420.x

32. Lambertsen KL, Clausen BH, Babcock AA, et al. Microglia protect neurons against ischemia by synthesis of tumor necrosis factor. *J Neurosci*. 2009;29(5):1319-1330. doi:10.1523/JNEUROSCI.5505-08.2009

33. Jimenez S, Baglietto-Vargas D, Caballero C, et al. Inflammatory response in the hippocampus of PS1M146L/APP 751SL mouse model of Alzheimer's disease: Age-dependent switch in the microglial phenotype from alternative to classic. *J Neurosci*. 2008;28(45):11650-11661. doi:10.1523/JNEUROSCI.3024-08.2008

34. Felger JC, Lotrich FE. Inflammatory cytokines in depression: Neurobiological mechanisms and therapeutic implications. *Neuroscience*. 2013;246:199-229. doi:10.1016/j.neuroscience.2013.04.060

35. Crain JM, Nikodemova M, Watters JJ. Microglia express distinct M1 and M2 phenotypic markers in the postnatal and adult central nervous system in male and female mice. *J Neurosci Res*. 2013;91(9):1143-1151. doi:10.1002/jnr.23242

36. Krause DL, Müller N. Neuroinflammation, microglia and implications for anti-inflammatory treatment in Alzheimer's disease. *Int J Alzheimers Dis*. 2010;2010. doi:10.4061/2010/732806

37. Boche D, Perry VH, Nicoll JAR. Review : Activation patterns of microglia and their identification in the human brain. Published online 2013:3-18. doi:10.1111/nan.12011

38. Nguyen VT, Benveniste EN. Critical role of tumor necrosis factor-α and NF-κB in interferon-γ-induced CD40 expression in microglia/macrophages. *J Biol Chem*. 2002;277(16):13796-13803. doi:10.1074/jbc.M111906200

39. Harm AS, Cao S, Rowse AL, et al. MHCII is required for α-Synuclein-induced activation of microglia, CD4 T cell proliferation, and dopaminergic neurodegeneration. *J Neurosci*. 2013;33(23):9592-9600. doi:10.1523/JNEUROSCI.5610-12.2013

40. Hashioka S, Klegeris A, Schwab C, Yu S, McGeer PL. Differential expression of interferon-γ receptor on human glial cells in vivo and in vitro. *J Neuroimmunol*. 2010;225(1-2):91-99. doi:10.1016/j.jneuroim.2010.04.023

41. Yan Z, Gibson SA, Buckley JA, Qin H, Benveniste EN. Role of the JAK/STAT signaling pathway in regulation of innate immunity in neuroinflammatory diseases. *Clin Immunol*. 2018;189:4-13. doi:10.1016/j.clim.2016.09.014

42. Sun D, Ding A. MyD88-mediated stabilization of interferon-c-induced cytokine and chemokine mRNA. 2006;7(4):375-381. doi:10.1038/ni1308

43. Finco TS, Baldwin AS. Mechanistic aspects of NF-κB regulation: The emerging role of phosphorylation and proteolysis. *Immunity*. 1995;3(3):263-272. doi:10.1016/1074-7613(95)90112-4

44. Shabab T, Khanabdali R, Moghadamtousi SZ, Kadir HA, Mohan G. Neuroinflammation pathways: a general review. *Int J Neurosci*. 2017;127(7):624-633. doi:10.1080/00207454.2016.1212854

45. Stone KP, Kastin AJ, Pan W. NFκB is an unexpected major mediator of interleukin-15 signaling in cerebral endothelia. *Cell Physiol Biochem*. 2011;28(1):115-124. doi:10.1159/000331720

46. Shih RH, Wang CY, Yang CM. NF-kappaB signaling pathways in neurological inflammation: A mini review. *Front Mol Neurosci*. 2015;8(DEC):1-8. doi:10.3389/fnmol.2015.00077

47. O'Shea JJ, Plenge R. JAK and STAT Signaling Molecules in Immunoregulation and Immune-Mediated Disease. *Immunity*. 2012;36(4):542-550. doi:10.1016/j.immuni.2012.03.014

48. Benveniste EN, Liu Y, McFarland BC, Qin H. Involvement of the Janus kinase/signal transducer and activator of transcription signaling pathway in multiple sclerosis and the animal model of experimental autoimmune encephalomyelitis. *J Interf Cytokine Res*. 2014;34(8):577-588. doi:10.1089/jir.2014.0012

49. Tsai MC, Chen WJ, Tsai MS, Ching CH, Chuang JI. Melatonin attenuates brain contusion-

induced oxidative insult, inactivation of signal transducers and activators of transcription 1, and upregulation of suppressor of cytokine signaling-3 in rats. *J Pineal Res*. 2011;51(2):233-245. doi:10.1111/j.1600-079X.2011.00885.x

50. Nicolas CS, Amici M, Bortolotto ZA, et al. The role of JAK-STAT signaling within the CNS. *Jak-Stat*. 2013;2(1):e22925. doi:10.4161/jkst.22925

51. Akhmetzyanova E, Kletenkov K, Mukhamedshina Y, Rizvanov A. Different Approaches to Modulation of Microglia Phenotypes After Spinal Cord Injury. *Front Syst Neurosci*. 2019;13(August):1-12. doi:10.3389/fnsys.2019.00037

52. Ta T, Onur H, Schilling S, Chausse B, Lewen A, Hollnagel J. Priming of microglia with IFN- γ slows neuronal gamma oscillations in situ. Published online 2019:1-6. doi:10.1073/pnas.1813562116

53. Browne TC, McQuillan K, McManus RM, O'Reilly J-A, Mills KHG, Lynch MA. IFN-γ Production by Amyloid β–Specific Th1 Cells Promotes Microglial Activation and Increases Plaque Burden in a Mouse Model of Alzheimer's Disease. *J Immunol*. 2013;190(5):2241-2251. doi:10.4049/jimmunol.1200947

54. Papageorgiou IE, Lewen A, Galow L V., et al. TLR4-activated microglia require IFN-γ to induce severe neuronal dysfunction and death in situ. *Proc Natl Acad Sci U S A*. 2016;113(1):212-217. doi:10.1073/pnas.1513853113

55. De Weerd NA, Nguyen T. The interferons and their receptors-distribution and regulation. *Immunol Cell Biol*. 2012;90(5):483-491. doi:10.1038/icb.2012.9

56. Downen M, Amaral TD, Hua LL, Zhao ML, Lee SC. Neuronal death in cytokine-activated primary human brain cell culture: Role of tumor necrosis factor-α. *Glia*. 1999;28(2):114-127. doi:10.1002/(SICI)1098-1136(199911)28:2<114::AID-GLIA3>3.0.CO;2-O

57. Bezzi P, Domercq M, Brambilla L, et al. CXCR4-activated astrocyte glutamate release via TNFa: Amplification by microglia triggers neurotoxicity. *Nat Neurosci*. 2001;4(7):702-710. doi:10.1038/89490

58. Sheng WS, Hu S, Feng A, Rock RB. Reactive oxygen species from human astrocytes induced functional impairment and oxidative damage. *Neurochem Res*. 2013;38(10):2148-2159. doi:10.1007/s11064-013-1123-z

59. Chao CC, Hu S, Sheng WS, Bu D, Bukrinsky MI, Peterson PK. Cytokine-stimulated astrocytes damage human neurons via a nitric oxide mechanism. *Glia*. 1996;16(3):276-284. doi:10.1002/(SICI)1098-1136(199603)16:3<276::AID-GLIA10>3.0.CO;2-X

60. Hashioka S, McGeer E, Miyaoka T, Wake R, Horiguchi J, McGeer P. Interferon-γ-Induced Neurotoxicity of Human Astrocytes. *CNS Neurol Disord - Drug Targets*. 2015;14(2):251-256. doi:10.2174/1871527314666150217122305

61. Ostrom QT, Gittleman H, Farah P, et al. CBTRUS statistical report: Primary brain and central nervous system tumors diagnosed in the United States in 2006-2010. *Neuro Oncol*. 2013;15(SUPPL.2). doi:10.1093/neuonc/not151

62. Ohgaki H, Kleihues P. Genetic pathways to primary and secondary glioblastoma. *Am J Pathol*. 2007;170(5):1445-1453. doi:10.2353/ajpath.2007.070011

63. Ohgaki H, Kleihues P. Genetic profile of astrocytic and oligodendroglial gliomas. *Brain Tumor Pathol*. 2011;28(3):177-183. doi:10.1007/s10014-011-0029-1

64. Louis DN, Perry A, Reifenberger G, et al. The 2016 World Health Organization

Classification of Tumors of the Central Nervous System: a summary. *Acta Neuropathol*. 2016;131(6):803-820. doi:10.1007/s00401-016-1545-1

65. IJzerman-Korevaar M, Snijders TJ, de Graeff A, Teunissen SCCM, de Vos FYF. Prevalence of symptoms in glioma patients throughout the disease trajectory: a systematic review. *J Neurooncol*. 2018;140(3):485-496. doi:10.1007/s11060-018-03015-9

66. Waziri A. Glioblastoma-Derived Mechanisms of Systemic Immunosuppression. *Neurosurg Clin N Am*. 2010;21(1):31-42. doi:10.1016/j.nec.2009.08.005

67. Tang B, Wu W, Wei X, Li Y, Ren G, Fan W. Activation of glioma cells generates immune tolerant NKT cells. *J Biol Chem*. 2014;289(50):34595-34600. doi:10.1074/jbc.M114.614503

68. Dhodapkar KM, Cirignano B, Chamian F, et al. Invariant natural killer T cells are preserved in patients with glioma and exhibit antitumor lytic activity following dendritic cell-mediated expansion. *Int J Cancer*. 2004;109(6):893-899. doi:10.1002/ijc.20050

69. Brandenburg S, Müller A, Turkowski K, et al. Resident microglia rather than peripheral macrophages promote vascularization in brain tumors and are source of alternative pro-angiogenic factors. *Acta Neuropathol*. 2016;131(3):365-378. doi:10.1007/s00401-015-1529-6

70. Watters JJ, Schartner JM, Badie B. Microglia function in brain tumors. *J Neurosci Res*. 2005;81(3):447-455. doi:10.1002/jnr.20485

71. Hathout L, Pope WB, Lai A, Nghiemphu PL, Cloughesy TF, Ellingson BM. Radial expansion rates and tumor growth kinetics predict malignant transformation in contrast-enhancing low-grade diffuse astrocytoma. *CNS Oncol*. 2015;4(4):247-256. doi:10.2217/cns.15.16

72. Galeffi F, A. Turner D. Exploiting Metabolic Differences in Glioma Therapy. *Curr Drug Discov Technol*. 2014;9(4):280-293. doi:10.2174/157016312803305906

73. Ye ZC, Rothstein JD, Sontheimer H. Compromised glutamate transport in human glioma cells: Reduction- mislocalization of sodium-dependent glutamate transporters and enhanced activity of cystine-glutamate exchange. *J Neurosci*. 1999;19(24):10767-10777. doi:10.1523/JNEUROSCI.19-24-10767.1999

74. Ye ZC, Sontheimer H. Glioma cells release excitotoxic concentrations of glutamate. *Cancer Res*. 1999;59(17):4383-4391.

75. Buckingham SC, Campbell SL, Haas BR, et al. Glutamate release by primary brain tumors induces epileptic activity. *Nat Med*. 2011;17(10):1269-1274. doi:10.1038/nm.2453

76. Campbell SL, Buckingham SC, Sontheimer H. Human glioma cells induce hyperexcitability in cortical networks. *Epilepsia*. 2012;53(8):1360-1370. doi:10.1111/j.1528-1167.2012.03557.x

77. John Lin CC, Yu K, Hatcher A, et al. Identification of diverse astrocyte populations and their malignant analogs. *Nat Neurosci*. 2017;20(3):396-405. doi:10.1038/nn.4493

78. Zhang J, Sarkar S, Cua R, Zhou Y, Hader W, Wee Yong V. A dialog between glioma and microglia that promotes tumor invasiveness through the CCL2/CCR2/interleukin-6 axis. *Carcinogenesis*. 2012;33(2):312-319. doi:10.1093/carcin/bgr289

79. Zhang L, Alizadeh D, van Handel M, Kortylewski M, Yu H, Badie B. Stat3 inhibition activates tumor macrophages and abrogates glioma growth in mice. *Glia*. 2009;57(13):1458-1467. doi:10.1002/glia.20863

80. Morimura T, Neuchrist C, Kitz K, et al. Monocyte subpopulations in human gliomas: expression of Fc and complement receptors and correlation with tumor proliferation. *Acta Neuropathol*. 1990;80(3):287-294. doi:10.1007/BF00294647

81. Roggendorf W, Strupp S, Paulus W. Distribution and characterization of microglia/macrophages in human brain tumors. *Acta Neuropathol*. 1996;92(3):288-293. doi:10.1007/s004010050520

82. Desbaillets I, Tada M, De Tribolet N, Diserens A -C, Hamou M -F, Van Meir EG. Human astrocytomas and glioblastomas express monocyte chemoattractant protein-1 (MCP-1) in vivo and in vitro. *Int J Cancer*. 1994;58(2):240-247. doi:10.1002/ijc.2910580216

83. Pyonteck SM, Akkari L, Schuhmacher AJ, et al. CSF-1R inhibition alters macrophage polarization and blocks glioma progression. *Nat Med*. 2013;19(10):1264-1272. doi:10.1038/nm.3337

84. Sielska M, Przanowski P, Wylot B, et al. Distinct roles of CSF family cytokines in macrophage infiltration and activation in glioma progression and injury response. *J Pathol*. 2013;230(3):310-321. doi:10.1002/path.4192

85. Henrik Heiland D, Ravi VM, Behringer SP, et al. Tumor-associated reactive astrocytes aid the evolution of immunosuppressive environment in glioblastoma. *Nat Commun*. 2019;10(1). doi:10.1038/s41467-019-10493-6

86. Zhang Y, Sloan SA, Clarke LE, et al. Purification and Characterization of Progenitor and Mature Human Astrocytes Reveals Transcriptional and Functional Differences with Mouse. *Neuron*. 2016;89(1):37-53. doi:10.1016/j.neuron.2015.11.013

87. Benda P, Lightbody J, Sato G, Levine L. Differentiated Rat Glial Cell Strain in Tissue Culture Published by : American Association for the Advancement of Science Stable URL : http://www.jstor.org/stable/1724233. 1968;161(3839):370-371.

88. Auer R, Rice G, Hinton G, Amacher L, Gilber J. Cerebellar astrocytoma with benign histology and malignant clinical course. *J Neurosurg*. 1981;54:128-132.

89. Doblas S, He T, Saunders D, et al. Glioma morphology and tumor-induced vascular alterations revealed in seven rodent glioma models by in vivo magnetic resonance imaging and angiography. *J Magn Reson Imaging*. 2010;32(2):267-275. doi:10.1002/jmri.22263

90. Gieryng A, Pszczolkowska D, Bocian K, et al. Immune microenvironment of experimental rat C6 gliomas resembles human glioblastomas. *Sci Rep*. 2017;7(1):1-14. doi:10.1038/s41598-017-17752-w

91. Nagano N, Sasaki H, Aoyagi M, Hirakawa K. Invasion of experimental rat brain tumor: early morphological changes following microinjection of C6 glioma cells. *Acta Neuropathol*. 1993;86(2):117-125. doi:10.1007/BF00334878

92. Grobben B, De Deyn PP, Slegers H. Rat C6 glioma as experimental model system for the study of glioblastoma growth and invasion. *Cell Tissue Res*. 2002;310(3):257-270. doi:10.1007/s00441-002-0651-7

93. Doblas S, He T, Saunders D, et al. In vivo characterization of several rodent glioma models by 1H MRS. *NMR Biomed*. 2012;25(4):685-694. doi:10.1002/nbm.1785

94. Guo P, Hu B, Gu W, et al. Platelet-derived growth factor-B enhances glioma angiogenesis by stimulating vascular endothelial growth factor expression in tumor endothelia and by

promoting pericyte recruitment. *Am J Pathol*. 2003;162(4):1083-1093. doi:10.1016/S0002-9440(10)63905-3

95. Heimberger AB, Suki D, Yang D, Shi W, Aldape K. The natural history of EGFR and EGFRvIII in glioblastoma patients. *J Transl Med*. 2005;3:1-6. doi:10.1186/1479-5876-3-38

96. Zhang Y, Pan C, Wang J, et al. Genetic and immune features of resectable malignant brainstem gliomas. *Oncotarget*. 2017;8(47):82571-82582. doi:10.18632/oncotarget.19653

97. Valable S, Barbier EL, Bernaudin M, et al. In vivo MRI tracking of exogenous monocytes/macrophages targeting brain tumors in a rat model of glioma. *Neuroimage*. 2007;37(SUPPL. 1):47-58. doi:10.1016/j.neuroimage.2007.05.041

98. Valable S, Lemasson B, Farion R, Beaumont M, Segebarth C. Assessment of blood volume, vessel size, and the expression of angiogenic factors in two rat glioma models: a longitudinal in vivo and ex vivo study. *NMR Biomed*. 2008;20(3):304-325. doi:10.1002/nbm

99. Assadian S, Aliaga A, Del Maestro RF, Evans AC, Bedell BJ. FDG-PET imaging for the evaluation of antiglioma agents in a rat model. *Neuro Oncol*. 2008;10(3):292-299. doi:10.1215/15228517-2008-014

100. Karmakar S, Foster Olive M, Banik NL, Ray SK. Intracranial stereotaxic cannulation for development of orthotopic glioblastoma allograft in Sprague-Dawley rats and histoimmunopathological characterization of the brain tumor. *Neurochem Res*. 2007;32(12):2235-2242. doi:10.1007/s11064-007-9450-6

101. Shen G, Shen F, Shi Z, et al. Identification of cancer stem-like cells in the C6 glioma cell line and the limitation of current identification methods. *Vitr Cell Dev Biol - Anim*. 2008;44(7):280-289. doi:10.1007/s11626-008-9115-z

102. Clark MJ, Homer N, O'Connor BD, et al. U87MG decoded: The genomic sequence of a cytogenetically aberrant human cancer cell line. *PLoS Genet*. 2010;6(1). doi:10.1371/journal.pgen.1000832

103. Pontén J, Macintyre EH. Long term culture of normal and neoplastic human glia. *Acta Pathol Microbiol Scand*. 1968;74(4):465-486. doi:10.1111/j.1699-0463.1968.tb03502.x

104. Yi GZ, Liu YW, Xiang W, et al. Akt and β-catenin contribute to TMZ resistance and EMT of MGMT negative malignant glioma cell line. *J Neurol Sci*. 2016;367:101-106. doi:10.1016/j.jns.2016.05.054

105. Diao W, Tong X, Yang C, Zhang F, Bao C, Chen H. Behaviors of Glioblastoma Cells in in Vitro Microenvironments. *Sci Rep*. 2019;(November 2018):1-9. doi:10.1038/s41598-018-36347-7

106. Yu KK, Taylor JT, Pathmanaban ON, et al. High content screening of patient-derived cell lines highlights the potential of non-standard chemotherapeutic agents for the treatment of glioblastoma. Published online 2018:1-17.

107. Allen M, Bjerke M, Edlund H, Nelander S, Westermark B. Origin of the U87MG glioma cell line: Good news and bad news. *Sci Transl Med*. 2016;8(354). doi:10.1126/scitranslmed.aaf6853

108. Jin K, Teng L, Shen Y, He K, Xu Z, Li G. Patient-derived human tumour tissue xenografts in immunodeficient mice: A systematic review. *Clin Transl Oncol*. 2010;12(7):473-480.

doi:10.1007/s12094-010-0540-6

109. Hidalgo M, Amant F, Biankin A V, et al. Patient Derived Xenograft Models : An Emerging Platform for Translational Cancer Research. *Cancer Discov*. 2015;4(9):998-1013. doi:10.1158/2159-8290.CD-14-0001.Patient

110. Fei XF, Zhang Q Bin, Dong J, et al. Development of clinically relevant orthotopic xenograft mouse model of metastatic lung cancer and glioblastoma through surgical tumor tissues injection with trocar. *J Exp Clin Cancer Res*. 2010;29(1):1-8. doi:10.1186/1756-9966-29-84

111. Kim KM, Shim JK, Chang JH, et al. Failure of a patient-derived xenograft for brain tumor model prepared by implantation of tissue fragments. *Cancer Cell Int*. 2016;16(1):1-6. doi:10.1186/s12935-016-0319-0

112. Kang SG, Cheong JH, Huh YM, Kim EH, Kim SH, Chang JH. Potential use of glioblastoma tumorsphere: Clinical credentialing. *Arch Pharm Res*. 2015;38(3):402-407. doi:10.1007/s12272-015-0564-0

113. Lee J, Kotliarova S, Kotliarov Y, et al. Tumor stem cells derived from glioblastomas cultured in bFGF and EGF more closely mirror the phenotype and genotype of primary tumors than do serum-cultured cell lines. *Cancer Cell*. 2006;9(5):391-403. doi:10.1016/j.ccr.2006.03.030

114. Chen R, Nishimura MC, Bumbaca SM, et al. A Hierarchy of Self-Renewing Tumor-Initiating Cell Types in Glioblastoma. *Cancer Cell*. 2010;17(4):362-375. doi:10.1016/j.ccr.2009.12.049

115. Günther HS, Schmidt NO, Phillips HS, et al. Glioblastoma-derived stem cell-enriched cultures form distinct subgroups according to molecular and phenotypic criteria. *Oncogene*. 2008;27(20):2897-2909. doi:10.1038/sj.onc.1210949

116. Wakimoto H, Mohapatra G, Kanai R, et al. Maintenance of primary tumor phenotype and genotype in glioblastoma stem cells. *Neuro Oncol*. 2012;14(2):132-144. doi:10.1093/neuonc/nor195

117. Amarouch A, Mazeron JJ. Radiotherapy plus concomitant and adjuvant Temozolomide for glioblastoma. *Cancer/Radiotherapie*. 2005;9(3):196-197. doi:10.1016/j.canrad.2005.05.001

118. Lee CY. Strategies of temozolomide in future glioblastoma treatment. *Onco Targets Ther*. 2017;10:265-270. doi:10.2147/OTT.S120662

119. Zhang H, Gao S. Temozolomide/PLGA microparticles and antitumor activity against Glioma C6 cancer cells in vitro. *Int J Pharm*. 2007;329(1-2):122-128. doi:10.1016/j.ijpharm.2006.08.027

120. Reithmeier T, Graf E, Piroth T, Trippel M, Pinsker MO, Nikkhah G. BCNU for recurrent glioblastoma multiforme: Efficacy, toxicity and prognostic factors. *BMC Cancer*. 2010;10:1-8. doi:10.1186/1471-2407-10-30

121. Shapira-Furman T, Serra R, Gorelick N, et al. Biodegradable wafers releasing Temozolomide and Carmustine for the treatment of brain cancer. *J Control Release*. 2019;295(December 2018):93-101. doi:10.1016/j.jconrel.2018.12.048

122. Xing WK, Shao C, Qi ZY, Yang C, Wang Z. The role of Gliadel wafers in the treatment of newly diagnosed GBM: A meta-analysis. *Drug Des Devel Ther*. 2015;9:3341-3348. doi:10.2147/DDDT.S85943

123. Baumgartner R, Forteza MJ, Ketelhuth DFJ. The interplay between cytokines and the Kynurenine pathway in inflammation and atherosclerosis. *Cytokine*. 2017;122(May 2017):154148. doi:10.1016/j.cyto.2017.09.004

124. Schwarcz R, Stone TW. The kynurenine pathway and the brain: Challenges, controversies and promises. *Neuropharmacology*. 2017;112:237-247. doi:10.1016/j.neuropharm.2016.08.003

125. Bishnupuri KS, Alvarado DM, Khouri AN, et al. IDO1 and kynurenine pathway metabolites activate PI3K-Akt signaling in the neoplastic colon epithelium to promote cancer cell proliferation and inhibit apoptosis. *Cancer Res*. 2019;79(6):1138-1150. doi:10.1158/0008-5472.CAN-18-0668

126. Adams S, Braidy N, Bessesde A, et al. The kynurenine pathway in brain tumor pathogenesis. *Cancer Res*. 2012;72(22):5649-5657. doi:10.1158/0008-5472.CAN-12-0549

127. Zinger A, Barcia C, Herrero MT, Guillemin GJ. The involvement of neuroinflammation and Kynurenine pathway in Parkinson's disease. *Parkinsons Dis*. 2011;2011. doi:10.4061/2011/716859

128. O'Farrell K, Fagan E, Connor TJ, Harkin A. Inhibition of the kynurenine pathway protects against reactive microglial-associated reductions in the complexity of primary cortical neurons. *Eur J Pharmacol*. 2017;810(July):163-173. doi:10.1016/j.ejphar.2017.07.008

129. Cervantes G, Arellano N, Ortega D, Esquivel D. Role of Kynurenine Pathway in Glioblastoma. *Intech*. Published online 2016:13. doi:http://dx.doi.org/10.5772/57353

130. Mándi Y, Vécsei L. The kynurenine system and immunoregulation. *J Neural Transm*. 2012;119(2):197-209. doi:10.1007/s00702-011-0681-y

131. Vécsei L, Szalárdy L, Fülöp F, Toldi J. Kynurenines in the CNS: Recent advances and new questions. *Nat Rev Drug Discov*. 2013;12(1):64-82. doi:10.1038/nrd3793

132. Braidy N, Guillemin GJ, Grant R. Effects of kynurenine pathway inhibition on NAD + metabolism and cell viability in human primary astrocytes and neurons. *Int J Tryptophan Res*. 2011;4(1):29-37. doi:10.4137/IJTR.S7052

133. Bostian ACL, Eo RL. Aberrant Kynurenine Signaling Modulates DNA Replication Stress Factors and Promotes Genomic Instability in Gliomas. Published online 2016. doi:10.1021/acs.chemrestox.6b00255

134. Heyes MP, Saito K, Milstien S, Schiff SJ. Quinolinic acid in tumors , hemorrhage and bacterial infections of the central nervous system in children. Published online 1995.

135. Sahm F, Oezen I, Opitz CA, et al. The Endogenous Tryptophan Metabolite and NAD + Precursor Quinolinic Acid Confers Resistance of Gliomas to Oxidative Stress The Endogenous Tryptophan Metabolite and NAD þ Precursor Quinolinic Acid Confers Resistance of Gliomas to Oxidative Stress. Published online 2013:3225-3234. doi:10.1158/0008-5472.CAN-12-3831

136. Hiroaki Y, Katsuji T, Ryotaro Y, Osamu H. Interferon enhances tryptophan metabolism by inducing pulmonary indoleamine 2 , 3-dioxygenase : Its possible occurrence in cancer patients. 1986;83(September):6622-6626.

137. Soliman H, Mediavilla-Varela M, Antonia S. Indoleamine 2,3-Dioxygenase: Is It an Immune Supressor? *Cancer J*. 2010;1616(4). doi:10.1097/PPO.0b013e3181eb3343.Indoleamine

138. Muller AJ, DuHadaway JB, Donover PS, Sutanto-Ward E, Prendergast GC. Inhibition of

indoleamine 2,3-dioxygenase, an immunoregulatory target of the cancer suppression gene Bin1, potentiates cancer chemotherapy. *Nat Med*. 2005;11(3):312-319. doi:10.1038/nm1196

139. Zhai L, Ladomersky E, Lauing KL, et al. Infiltrating T cells increase IDO1 expression in glioblastoma and contribute to decreased patient survival. *Clin Cancer Res*. 2017;23(21):6650-6660. doi:10.1158/1078-0432.CCR-17-0120

140. Wainwright DA, Balyasnikova I V., Chang AL, et al. IDO expression in brain tumors increases the recruitment of regulatory T cells and negatively impacts survival. *Clin Cancer Res*. 2012;18(22):6110-6121. doi:10.1158/1078-0432.CCR-12-2130

141. Muller A, Mandik-Nayak L, Prendergast, C G. Beyond immunosuppression: reconsidering indoleamine 2,3-dioxygenase as a pathogenic element of chronic inflammation. *Immunotheraphy*. 2014;2(3):293-297. doi:10.2217/imt.10.22.Beyond

142. Adams S, Teo C, McDonald KL, et al. Involvement of the kynurenine pathway in human glioma pathophysiology. *PLoS One*. 2014;9(11):1-28. doi:10.1371/journal.pone.0112945

143. McNamee EN, Griffin ÉW, Ryan KM, et al. *Noradrenaline Acting at β-Adrenoceptors Induces Expression of IL-1β and Its Negative Regulators IL-1ra and IL-1RII, and Drives an Overall Anti-Inflammatory Phenotype in Rat Cortex*. Vol 59.; 2010. doi:10.1016/j.neuropharm.2010.03.014

144. Day JS, O'Neill E, Cawley C, et al. Noradrenaline acting on astrocytic β2-adrenoceptors induces neurite outgrowth in primary cortical neurons. *Neuropharmacology*. 2014;77:234-248. doi:10.1016/j.neuropharm.2013.09.027

145. Ishiyama M, Tominaga H, Shiga M, Sasamoto K, Ohkura Y, Ueno K. A combined assay of cell viability and in Vitro cytotoxicity with a highly water-soluble tetrazolium salt, neutral red and crystal violet. *Biol Pharm*. 1996;19(11):1518-1520.

146. Ishiyama M, Miyazono Y, Sasamoto K, Ohkura Y, Ueno K. A highly water-soluble disulfonated tetrazolium salt as a chromogenic indicator for NADH as well as cell viability. *Talanta*. 1997;44(7):1299-1305. doi:10.1016/S0039-9140(97)00017-9

147. Jo HY, Kim Y, Park HW, et al. The Unreliability of MTT Assay in the Cytotoxic Test of Primary Cultured Glioblastoma Cells. *Exp Neurobiol*. 2015;24(3):235-245. doi:10.5607/en.2015.24.3.235

148. Sholl DA. Dendritic organization in the neurons of the visual and motor cortices of the cat. *J Anat*. 1953;87(4):387-406. http://www.ncbi.nlm.nih.gov/pubmed/13117757%0Ahttp://www.pubmedcentral.nih.gov/articlerender.fcgi?artid=PMC1244622

149. Gutierrez H, Davies AM. A fast and accurate procedure for deriving the Sholl profile in quantitative studies of neuronal morphology. *J Neurosci Methods*. 2007;163(1):24-30. doi:10.1016/j.jneumeth.2007.02.002

150. Ippolito DM, Eroglu C. Quantifying synapses: An immunocytochemistry-based assay to quantify synapse number. *J Vis Exp*. 2010;(45):2-9. doi:10.3791/2270

151. O'Farrell K. The impact of pharmacological modulation of the NMDA-R/NO signalling pathway on neuronal complexity in vitro. Published online 2015.

152. Guillemin GJ, Braidy N, Grant R, Brew BJ, Adams S, Jayasena T. Synthesis and Cell Death in Human Primary Astrocytes and Neurons. *Int J Tryptophan Res*. 2009;2:61-69.

https://www.ncbi.nlm.nih.gov/pmc/articles/PMC3195228/pdf/ijtr-2-2009-061.pdf

153. Roy ER, Wang B, Wan YW, et al. Type I interferon response drives neuroinflammation and synapse loss in Alzheimer disease. *J Clin Invest*. 2020;130(4):1912-1930. doi:10.1172/JCI133737

154. Czeh M, Gressens P, Kaindl AM. The yin and yang of microglia. *Dev Neurosci*. 2011;33(3-4):199-209. doi:10.1159/000328989

155. Norden DM, Trojanowski PJ, Villanueva E, Navarro E, Godbout JP. Sequential activation of microglia and astrocyte cytokine expression precedes increased iba-1 or GFAP immunoreactivity following systemic immune challenge. *Glia*. 2016;64(2):300-316. doi:10.1002/glia.22930

156. Jensen CJ, Massie A, De Keyser J. Immune players in the CNS: The astrocyte. *J Neuroimmune Pharmacol*. 2013;8(4):824-839. doi:10.1007/s11481-013-9480-6

157. Luo XG, Chen S Di. The changing phenotype of microglia from homeostasis to disease. *Transl Neurodegener*. 2012;1:1-13. doi:10.1186/2047-9158-1-9

158. Pekny M, Pekna M. Astrocyte reactivity and reactive astrogliosis: Costs and benefits. *Physiol Rev*. 2014;94(4):1077-1098. doi:10.1152/physrev.00041.2013

159. Bilbo BS, Ph D, Stevens B, Ph D. Microglia : The Brain ' s First Responders. 2017;(November):1-14.

160. Cătălin B, Cupido A, Iancău M, Valeria Albu C, Kirchhoff F. Microglia: First responders in the central nervous system. *Rom J Morphol Embryol*. 2013;54(3):467-472.

161. O'Reilly K. A study of glial associated changes in the complexity of primary cortical neurons Supervised by. Published online 2020.

162. O'Reilly K, O'Farrell K, Midttun O, Rakovets Y, David -Bercholz J, Harkin A. Kynurenic Acid Protects Against Reactive Glial-associated Reductions in the Complexity of Primary Cortical Neurons. *J Neuroimmune Pharmacol*. Published online 2021. doi:10.1007/s11481-020-09976-x

163. Xu WL, Wang Y, Wu J, Li GY. Quantitative analysis of U251MG human glioma cells invasion in organotypic brain slice co-cultures. *Eur Rev Med Pharmacol Sci*. 2016;20(11):2221-2229.

164. Vannini E, Olimpico F, Middei S, et al. Electrophysiology of glioma: a Rho GTPase-activating protein reduces tumor growth and spares neuron structure and function. *Neuro Oncol*. 2016;0(April):1-10. doi:10.1093/neuonc/now114

165. Chen Z, Ross JL, Hambardzumyan D. Intravital 2-photon imaging reveals distinct morphology and infiltrative properties of glioblastoma-associated macrophages. *Proc Natl Acad Sci U S A*. 2019;116(28):14254-14259. doi:10.1073/pnas.1902366116

166. Lim S, Kim D, Ju S, et al. Glioblastoma-secreted soluble CD44 activates tau pathology in the brain. *Exp Mol Med*. Published online 2018. doi:10.1038/s12276-017-0008-7

167. Mitsuka K, Kawataki T, Satoh E, Asahara T, Horikoshi T, Kinouchi H. Expression of Indoleamine 2,3-Dioxygenase and Correlation With Pathological Malignancy in Gliomas. 2013;72(6):1031-1039. doi:10.1227/NEU.0b013e31828cf945

168. Venkatesh S, Morishita W, Geraghty AC, et al. Electrical and synaptic integration of glioma into neural circuits. *Nature*. 2019;573. doi:10.1038/s41586-019-1563-y

169. Huang-hobbs E, Cheng Y, Beechar VB, et al. PIK3CA variants selectively initiate brain hyperactivity during gliomagenesis. *Nature*. 2019;(December 2018). doi:10.1038/s41586-020-1952-2

170. Venkatesh HS, Johung TB, Mallick P, et al. Neuronal Activity Promotes Glioma Growth through Article Neuronal Activity Promotes Glioma Growth through Neuroligin-3 Secretion. *Cell*. Published online 2015:1-14. doi:10.1016/j.cell.2015.04.012

171. Venkatesh HS, Tam LT, Woo PJ, et al. Targeting neuronal activity-regulated neuroligin-3 dependency in high-grade glioma. *Springer Nat*. Published online 2017. doi:10.1038/nature24014

172. Marta L, Irene V, Bernard L, et al. In vivo characterization of brain metabolism by 1H MRS, 13C MRS and 18FDG PET reveals significant glucose oxidation of invasively growing glioma cells. *Int J Cancer*. Published online 2018.

173. Marta P, Venkataramani V, Fahey-lozano N, et al. Glioblastoma cells vampirize WNT from neurons and trigger a JNK / MMP signaling loop that enhances glioblastoma progression and neurodegeneration. *PLOS Biol*. Published online 2019:1-45. doi:10.1371/journal.pbio.3000545

174. Wainwright DA, Balyasnikova I V, Chang AL, et al. IDO expression in brain tumors increases the recruitment of regulatory T cells and negatively impacts survival. *Clin Anat*. 2013;18(22):6110-6121. doi:10.1158/1078-0432.CCR-12-2130.IDO

175. Friberg M, Jennings R, Alsarraj M, et al. Indoleamine 2,3-dioxygenase contributes to tumor cell evasion of T cell-mediated rejection. *Int J Cancer*. 2002;101(2):151-155. doi:10.1002/ijc.10645

176. Uyttenhove C, Pilotte L, Théate I, et al. Evidence for a tumoral immune resistance mechanism based on tryptophan degradation by indoleamine 2,3-dioxygenase. *Nat Med*. 2003;9(10):1269-1274. doi:10.1038/nm934

177. Vacchelli E, Aranda F, Eggermont A, et al. Trial watch: IDO inhibitors in cancer therapy. *Oncoimmunology*. 2014;3(10):e957994-1-e957994-10. doi:10.4161/21624011.2014.957994

178. Iversen TZ, Engell-Noerregaard L, Ellebaek E, et al. Long-lasting disease stabilization in the absence of toxicity in metastatic lung cancer patients vaccinated with an epitope derived from indoleamine 2,3 dioxygenase. *Clin Cancer Res*. 2014;20(1):221-232. doi:10.1158/1078-0432.CCR-13-1560

179. Hashioka S, Klegeris A, Schwab C, McGeer PL. Interferon-γ-dependent cytotoxic activation of human astrocytes and astrocytoma cells. *Neurobiol Aging*. 2009;30(12):1924-1935. doi:10.1016/j.neurobiolaging.2008.02.019

180. Lively S, Schlichter LC. Microglia responses to pro-inflammatory stimuli (LPS, IFNγ+TNFα) and reprogramming by resolving cytokines (IL-4, IL-10). *Front Cell Neurosci*. 2018;12(July):1-19. doi:10.3389/fncel.2018.00215

181. Stark GR, Darnell JE. The JAK-STAT Pathway at Twenty. *Immunity*. 2012;36(4):503-514. doi:10.1016/j.immuni.2012.03.013

182. Bal-Price A, Moneer Z, Brown GC. Nitric oxide induces rapid, calcium-dependent release of vesicular glutamate and ATP from cultured rat astrocytes. *Glia*. 2002;40(3):312-323. doi:10.1002/glia.10124

183. J. S. Ultrastructural pathology of dendritic spines in epitumorous human cerebral cortex. *Acta Neuropathol*. 1987;73:77-85.

184. Ovrea ALSIŞ, Ca ADBIBOŞ, Eorgiu CAG, et al. The diagnostic value of immunohistochemistry and silver impregnation techniques for characterization of normal , reactive and tumoral astrocytes. *RJME*. 2014;55:525-538.

185. Chekhonin VP, Baklaushev VP, Yusubalieva GM, Pavlov KA, Ukhova O V, Gurina OI. Modeling and Immunohistochemical Analysis of C6 Glioma In Vivo. 2007;(2):501-509.

186. Mariko N, Seiki Y, Saito T, et al. GFAP-Positive Neoplastic Astrocytes in Spontaneous Oligodendrogliomas and Mixed Gliomas of Rats. *Toxicol Pathol*. 2013;41:653-661. doi:10.1177/0192623312463987

187. Gagliano N, Costa F, Cossetti C, et al. Glioma-astrocyte interaction modifies the astrocyte phenotype in a co-culture experimental model. *Oncol Rep*. 2009;22:1349-1356. doi:10.3892/or

188. Brahmachari S, Fung YK, Pahan K. Induction of Glial Fibrillary Acidic Protein Expression in Astrocytes by Nitric Oxide. *J Neurosci*. 2006;26(18):4930-4939. doi:10.1523/JNEUROSCI.5480-05.2006

189. Parrott JM, Redus L, Connor JCO. Kynurenine metabolic balance is disrupted in the hippocampus following peripheral lipopolysaccharide challenge. *J Neuroinflammation*. Published online 2016:1-15. doi:10.1186/s12974-016-0590-y

190. Chin M, Lim C, Maubach G, Zhuo L. Glial Fibrillary Acidic Protein Splice Variants in Hepatic Stellate Cells - Expression and Regulation. *Mol Cells*. 2008;(May 2014).

191. Chitnis T, Weiner HL. CNS inflammation and neurodegeneration. *J Clin Invest*. 2017;127(10):3577-3587. doi:10.1172/JCI90609

192. Garc L, Francisca P. Absence of Aryl Hydrocarbon Receptors Increases Endogenous Kynurenic Acid Levels and Protects Mouse Brain Against Excitotoxic Insult and Oxidative Stress. 2015;1433(April):1423-1433. doi:10.1002/jnr.23595

193. Badawy AA. Kynurenine Pathway of Tryptophan Metabolism : Regulatory and Functional Aspects. Published online 2017. doi:10.1177/1178646917691938

194. Anderson G, Maes M. Interactions of Tryptophan and Its Catabolites With Melatonin and the Alpha 7 Nicotinic Receptor in Central Nervous System and Psychiatric Disorders : Role of the Aryl Hydrocarbon Receptor and Direct Mitochondria Regulation. Published online 2017. doi:10.1177/1178646917691738

195. Walczak K, Zurawska M, Kiś J, et al. Kynurenic acid in human renal cell carcinoma: Its antiproliferative and antimigrative action on Caki-2 cells. *Amino Acids*. 2012;43(4):1663-1670. doi:10.1007/s00726-012-1247-5

196. Mor A, Tankiewicz-Kwedlo A, Krupa A, Pawlak D. Role of Kynurenine Pathway in Oxidative Stress during Neurodegenerative Disorders. *Cells*. 2021;10(7):1-30. doi:10.3390/cells10071603

197. Fotopoulou C, Sehouli J, Pschowski R, et al. Systemic changes of tryptophan catabolites via the indoleamine-2,3- dioxygenase pathway in primary cervical cancer. *Anticancer Res*. 2011;31(8):2629-2635.

198. Berthon C, Fontenay M, Corm S, et al. Metabolites of tryptophan catabolism are elevated in sera of patients with myelodysplastic syndromes and inhibit hematopoietic progenitor

amplification. *Leuk Res*. 2013;37(5):573-579. doi:10.1016/j.leukres.2013.02.001

199. Sagan D, Kocki T, Patel S, Kocki J. Utility of kynurenic acid for non-invasive detection of metastatic spread to lymph nodes in non-small cell lung cancer. *Int J Med Sci*. 2015;12(2):146-153. doi:10.7150/ijms.7541

200. Zgrajka W, Stoma F, Walczak K, et al. Kynurenic acid inhibits proliferation and migration of human glioblastoma T98G cells. *Pharmacol reports*. 2014;66:130-136. doi:10.1016/j.pharep.2013.06.007

201. Serio C Di, Cozzi A, Angeli I, et al. Kynurenic Acid Inhibits the Release of the Neurotrophic Fibroblast Growth Factor (FGF) -1 and Enhances Proliferation of Glia Cells , in vitro. 2005;25(6). doi:10.1007/s10571-005-8469-y

202. Blackmore MG, Moore DL, Smith RP, Goldberg JL, Bixby L, Lemmon VP. Regulators of Axon Growth. 2011;44(1):43-54. doi:10.1016/j.mcn.2010.02.002.High

203. Wei Z, Kale S, Fatimy R El, Rabinovsky R, Krichevsky AM. Co-cultures of Glioma Stem Cells and Primary Neurons , Astrocytes , Microglia , and Endothelial Cells for Investigation of Intercellular Communication in the Brain. *Front Mol Neurosci*. 2019;13(April):1-8. doi:10.3389/fnins.2019.00361

204. Stacker SA, Wilks F. Inhibition of Growth of C6 Glioma Cells in Vivo by Expression of Antisense Vascular Endothelial Growth Factor Sequence'. Published online 2008.

205. Verstraelen P, Pintelon I. Pharmacological Characterization of Cultivated Neuronal Networks : Relevance to Synaptogenesis and Synaptic Connectivity. Published online 2014. doi:10.1007/s10571-014-0057-6

206. Feng G, Mellor RH, Bernstein M, et al. Imaging Neuronal Subsets in Transgenic Mice Expressing Multiple Spectral Variants of GFP. 2000;28:41-51.

207. Okabe S. Fluorescence imaging of synapse dynamics in normal circuit maturation and in developmental disorders. 2017;93(7):483-497.

208. Lugo-huitrón R, Muñiz PU, Pineda B, Pedraza-chaverrí J, Ríos C, Cruz VP. Quinolinic Acid : An Endogenous Neurotoxin with Multiple Targets. 2013;2013.

209. Cenciarini M, Valentino M, Belia S, et al. Dexamethasone in Glioblastoma Multiforme Therapy : Mechanisms and Controversies. *Front Mol Neurosci*. 2019;12(March):1-13. doi:10.3389/fnmol.2019.00065